Analytic Model Derivation Of Microfluidic Flow For MEMS Virtual-Reality CAD

ANALYTIC MODEL DERIVATION OF MICROFLUIDIC FLOW FOR MEMS VIRTUAL-REALITY CAD

MANISAH AUMEERALLY
Masters of Information Technology,
Bachelor of Science,
Certificate in Education

16 Dec 2004

Submitted in fulfilment of the requirements of the degree of

Doctor of Philosophy

School of Information and Communication Technology
Faculty of Engineering and Information Communication Technology
Griffith University, Gold Coast Campus
Queensland, Australia

Principal Supervisor: Dr Renate Sitte
Co-supervisors: Dr Philip Tanner
Dr Ruben Gonzalez

ABSTRACT

This thesis derives a first approximation model that will describe the flow of fluid in microfluidic devices such as in microchannels, microdiffusers and micronozzles using electrical network modelling. The important parameter that is of concern is the flow rates of these devices. The purpose of this work is to contribute to the physical component of our interactive Virtual Reality (VR)-prototyping tool for MEMS, with emphasis on fast calculations for interactive CAD design. Current calculations are too time consuming and not suitable for interactive CAD with dynamic animations. This work contributes to and fills the need for the development of MEMS dynamic visualisation, showing the movement of fluid within microdevices in time scale.

Microfluidic MEMS devices are used in a wide range of applications, such as in chemical analysis, gene expression analysis, electronic cooling system and inkjet printers. Their success lies in their microdimensions, enabling the creation of systems that are considerably minute yet can contain many complex subsystems. With this reduction in size, the advantages of requiring less material for analysis, less power consumption, less wastage and an increase in portability becomes their selling point. Market size is in excess of US$50 billion in 2004, according to a study made by Nexus. New applications are constantly being developed leading to creation of new devices, such as the DNA and the protein chip. Applications are found in pharmaceuticals, diagnostic, biotechnology and the food industry. An example is the outcome of the mapping and sequencing of the human genome DNA in the late 1990's leading to greater understanding of our genetic makeup. Armed with this knowledge, doctors will be able to treat diseases that were deemed untreatable before, such as diabetes or cancer. Among the tools with which that can be achieved include the DNA chip which is used to analyse an individual's genetic makeup and the Gene chip used in the study of cancer.

With this burgeoning influx of new devices and an increase in demand for them there is a need for better and more efficient designs. The MEMS design process is time consuming and costly. Many calculations rely on Finite Element Analysis, which has slow and time consuming algorithms, that make interactive CAD unworkable. This is because the iterative algorithms for calculating the animated images showing the ongoing proccess as they occur, are too slow. Faster computers do not solve the void of efficient algorithms, because with faster computer also comes the demand for a fasters response. A 40 – 90 minute FEA calculation will not be replaced by a faster computer in the next decades to an almost instant response. Efficient design tools are required to shorten this process. These interactive CAD tools need to be able to give quick yet accurate results. Current CAD tools involve time consuming numerical analysis technique which requires hours of numerous iterations for the device structure design followed by more calculations to achieve the required output specification. Although there is a need for a detailed analysis, especially in solving for a particular aspect of the design, having a tool to quickly get a first approximation will greatly shorten the guesswork involved in determining the overall requirement.

The underlying theory for the fluid flow model is based on traditional continuum theory and the Navier-Stokes equation is used in the derivation of a layered flow model in which the flow region is segmented into layered sections, each having different flow rates. The flow characteristics of each sections are modeled as electrical components in an electrical circuit. Matlab 6.5 (Matlab^{TM}) is used for the modelling aspect and Simulink is used for the simulation.

TABLE OF CONTENTS

LIST OF FIGURES

LIST OF TABLES

ACKNOWLEDGEMENT

I wish to thank and acknowledge the assistance and contributions of several people without whom this thesis would not be possible.

First and foremost, I wish to thank Dr Philip Tanner for his assistance and guidance in helping me with the revision of this thesis. I am most grateful for his effort in obtaining the software I needed and to his meticulous attention to detail when reviewing this thesis. Thanks to my supervisor Dr Renate Sitte who provided her invaluable guidance for the work throughout my PhD candidature. Our meetings were a tremendous help and she provided assistance in every aspect of my work, above and beyond her duties. Thanks also due to Mr Greg Cranitch, the Head of the School of IT, for his advice. Thanks to the other postgraduates Zhaoyi Li and Ken Udono, whom I share the research lab with and who are always there to listen to me when I needed someone to talk to or to help me with alternative views.

Finally I wish to thank my dear husband, Reza, for his confidence in my capability, who pushes me to greater achievement, who so patiently supported me throughout the hard times of my work. Thanks to my boys, Imran and Zaid for their faith and pride in their mom and helping me with the chores.

STATEMENT OF ORIGINALITY

This work has not previously been submitted for a degree or diploma in any university. To the best of my knowledge and belief, the thesis contains no material previously published or written by another person except where due reference is made in the thesis itself.

……..

Manisah Aumeerally

ACRONYMS

AHDL	analog hardware description language
BEM	boundary element method
CAD	computer-aided design
CFD	computational fluid dynamics
EHD	electrohydrodynamic
EOF	electroosmotic flow
FEM	finite element method
FPW	flexural plate wave
FVM	finite volume method
FZK	Forschungszentrum Karlsruhe (Research Center Karlsruhe)
IC	integrated circuit
ITO	indium tin oxide
LIGA	lithography, galvanoforming, moulding
MAGDA	MEMS animated graphical design aid
MEMS	Micro-electromechanical system
MHD	magnetohydrodynamic
MST	Microsystem
ODE	ordinary differential equation
PDE	partial differential equation
PDMS	polydimethylsiloxane
PMMA	polymethylmethacrylate
Re	Reynolds number
RL	resistor-inductor
RLC	resistor-inductor-capacitor
rpm	revolutions per minute
SMA	shape memory alloy
VHDL	virtual hardware description language
VR	virtual reality
μTAS	micro-total analysis system

NOTATION

a	radius
$A,\ A_1,\ A_2$	area
b	width
C	capacitance
d,D	diameter
D_h	hydraulic diameter
e	charge
f	force
$\vec{g}$	gravitational acceleration vector
h	height
$h_f,\ h_m$	head loss
i	current
$k_1,\ k_2$	constants
ℓ	length
L	inductance
m	mass
$\vec{n}$	unit vector
r	radial coordinate, radius of channel
$r,\ r_1,\ r_2,\ r_o$	radius of channel
$p,\ p_1,\ p_2$	hydrostatic pressure
P	perimeter
Q	volumetric flow rate
R	equivalent resistance
R_i	position
$\vec{R}_i$	position vector
Re	Reynolds number
$\vec{s}$	streamline coordinate

t	time
u, υ, w	x, y, z components of velocity in Cartesian coordinates
Vol	volume
$\forall$	control volume
$d\forall$	elemental volume
V_t	voltage
V	velocity
$\vec{V}$	velocity vector
V_r, V_θ, V_z	radial, tangential and axial velocity components
V	average velocity
Z	impedance

Greek

α	aperture angle
β	$r_o/r_i + 1$
ε	compression ratio
μ_D	diffuser efficiency
ρ	density of fluid
σ	complex-frequency variable
λ	$= \alpha L_d / r_o$
μ	absolute viscosity of fluid
ν	kinematic viscosity of fluid
τ	transient time

CHAPTER 1: INTRODUCTION

Richard Feynman in his famous speeches "There's Plenty of Room at the Bottom" (1959) and "Infinitesimal Machinery" (1983), envisioned a world of miniaturised systems. He talked about making the computers enormously smaller in order to get them to work faster. He also suggested making miniaturised machines, although at the time, he had no idea what the utility of such machines would be (Senturia 1994). By the end of 1983, about three million micromachined silicon pressure sensors were sold and it is predicted that over 125 million units/year will be sold over the next decade. These sensors were mainly used initially in the automotive industry for better fuel economy while reducing pollution, a requirement that was necessitated by the gasoline crisis of the early 1970s (Bryzek 1996). New products for new application area are constantly being introduced, the market size for established products for 2004 is over US$50 billion. This figure is expected to increase to US$60 billion by 2005, with emerging products adding it up a further 10% (Nexus Market Analysis 2002).

Micro electromechanical systems (MEMS) technology developed in the early 1980s (Fluitman 1996) as an extension of and at about the same time as microelectronics technology, though not at the same pace as the latter which began developing rapidly since the 1960's and is now a mature field. A breakthrough in MEMS technology occurred in 1987 with the fabrication of the first movable micromechanical parts, a microactuator, using surface-micromachining technology, a technology borrowed from microelectronics (Bao and Wang 1996). In the USA, the IEEE Micro Robots and Teleoperators Workshop held in 1987 led to regular MEMS Workshops. In Europe, the invention of scanning tunnelling and the atomic force microscopes as well as the LIGA technology, a spin-off development from nuclear physics research inspired MST. LIGA is the German acronym for "Lithographie, Galvanoformung, Abformung" (lithography, galvanoforming, moulding). The first Micro Mechanics Europe Workshop was in Twente in 1989 followed by the first MST Workshop in Berlin in 1990. In Japan, the Micro Machine Research Society was founded in 1988 and in 1991 the Ministry of International Trade and Industry,

MITI, created and sponsored research and development via its Micromachine Centre (Fluitman 1996).

Microfluidics refers to the study of the flow of fluid in microscale dimensions such as in microchannels and MEMS devices like the micropump, micromixer, microvalves and microsystems containing these devices. Its applications includes the inkjet printers, micrototal analysis system or μTAS for chemical analysis, biochip for gene analysis, portable fuel cell and electronic cooling systems.

The design stage of the development of a micro electromechanical systems (MEMS) device is crucial to its fabrication. It is important to shorten the very expensive device prototyping stage. Computer-aided design (CAD) tools help to accelerate this process and provide a cost-effective method in the prediction and optimisation of device characteristics. Microelectronics or integrated-circuit (IC) technology began its rapid development since the 1960's and is now a mature industry. MEMS technology developed in the early 1980s is an extension of this technology, though not at the same pace as the latter. IC design tools are highly sophisticated, having been developed over four computer generations, they are capable of creating complex designs that incorporates millions of gates. However, design tools for MEMS are lagging behind.

Chapters 1 to 4 are the introductory material of this thesis. Chapter 1 consists of an introduction, the aim of this research and its context. Chapter 2 deals with the background of the research area, MEMS CAD tools as well as MEMS devices in general and microfluidic devices in particular. Chapter 3 will expand on the problem statement, hypothesis and solution of chapter 1 in more detail. Chapter 4 will discuss the basic theory that is applied for the analysis in this research. Chapter 5 and 6 contains the modelling aspect of the thesis, with chapter 5 showing how the layered flow model is derived while chapter 6 the derivation of the electrical model. Chapter 7 provides the simulation aspect, discussing the behaviour of the fluid at the entrance of the microchannel and in an expanding and contracting microchannel, ie diffuser and nozzle. The results of the simulation is shown in chapter 8, where comparison is made with experimental data and theoretical analysis. Finally the conclusion will be presented in chapter 9.

1.1 AIM OF RESEARCH

The principal objective of this research is to determine the volumetric flow rate of several types of microfluidic device components, in terms of their geometrical parameters. These components include straight walls microchannels with circular and square cross-section and diverging and converging microchannels, also known as diffusers and nozzles. The emphasis is on obtaining their throughput as a function of geometries, because they are the starting point of the design. The parameter chosen is the volume flow rate of these components.

Secondly, this study aims to develop a technique that provides for quick first order approximation of the throughput for the purpose of visualising the flow of the fluid in an animated display. This technique is to be compared to FEM for accuracy.

The main objective of my research is to create either an analytical or semi-analytical model that will produce a quick first approximation or simulation of the behaviour of fluid flowing in microfluidic devices, namely the microchannel, microdiffuser and micronozzle for the purpose of visualising this flow. The parameter of concern is their flow rates. The technique chosen must be able to provide a reasonable accuracy as compared to existing software and yet can be easily implemented by using a desktop.

SCOPE: The model becomes part of the physical component of the School of Information Technology Simulation and Modelling groups' project undertaking, the VR CAD known as MEMS Animated Graphic Design Aid (MAGDA). The results obtained from the physical component are used as inputs for an interactive animated display. My project deals with the development of the physical models only. It does not include laboratory experimentation. Other components of the CAD which include the design and implementation of the user interface, the visualization and the control and interaction models, are not part of my research.

1.2 CONTEXT

The purpose of the MAGDA project is to create a CAD system specifically for the design of MEMS devices, presenting them as 3D visualisation with animation. The MAGDA CAD consists of four components; the user interface, the physical models, the visualisations and the control and interaction modules, as shown in Figure 1-1 below.

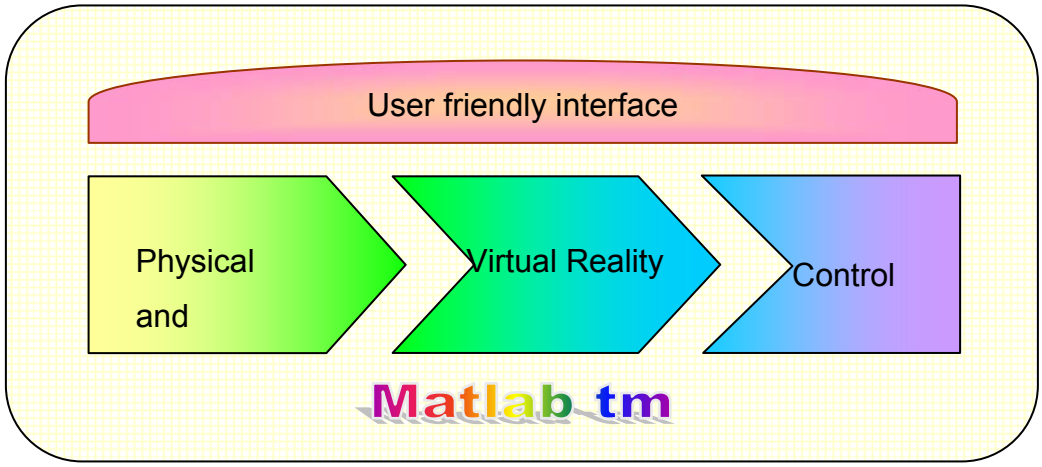

Figure 1-1 MEMS VR CAD structure

The user interface, shown in Figure 1-2, was created by (Kellermann et al 2003). It consists of several windows, one of which is the drawing board where the user can design a device within the constraints set by the system. The design on the drawing board is produced in layers mimicking the production process. The layers are then "assembled" into a MEMS, and this is then virtually "powered" and the working MEMS is displayed in time scaled animation. It is for these animations that the fast analytical models (fluidic flow and others) are required.

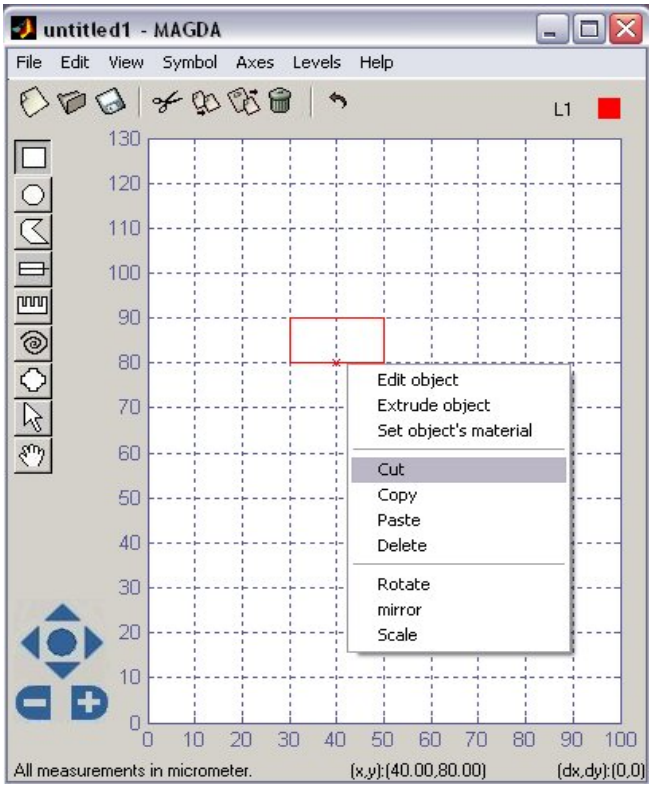

Figure 1-2 The MEMS Animated Graphical Design Aid (MAGDA) drawing board. (Kellermann et al 2003)

Once the design is created and the required throughput is specified, the movement can be visualised. The physical model component takes the specification from the user through the interface module, does the necessary calculations and passes these to the visualisation component after which the movement is displayed. The MAGDA software allows for a 3D mesh view and a rendered dynamic visualisation of the device design as in Figure 1-3, which shows an example device, the tactile sensor.

The physical model is implemented in Matlab 6.5 and Simulink™. My duty in this project is to calculate the dynamics of the system being designed for the 3D animated visualisation, though not on sensors, but on fluid flow in the devices. My contribution is in the physically based modelling of the flow and not on the visual artworks themselves.

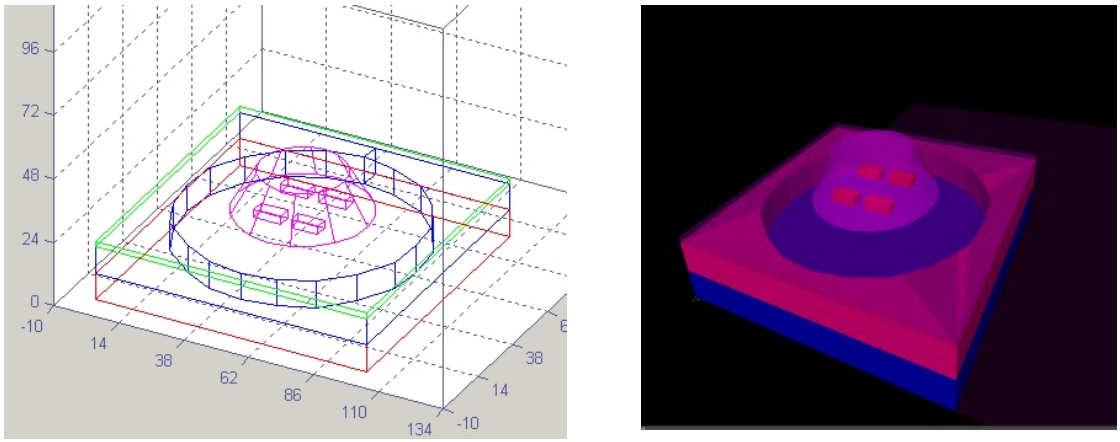

Figure 1-3 Using MAGDA to visualise a tactile sensor (a) 3D mesh view (b) rendered view (Kellermann et al 2003)

1.2.1 OVERVIEW OF PROBLEM STATEMENT

The design of a MEMS device takes a substantial amount of time and effort. Though it gives great insight into the detail working of a design, numerical modelling using techniques such as finite element method, further prolong this process. For finite element analysis, meshing has to be carried out once the device drawing is done. Boundary conditions are applied and the solution iterated many number of times. Sometimes it is possible that convergence does not occur and at other times the value obtained may not meet the required specification, so the whole process has to be repeated. It is the aim of this project to develop a technique that will considerably shorten this process by producing a quick first approximation of the required volumetric flow rate. From this first approximation, one can obtain a 3D view and animation of the device and its working principle.

1.2.2 OVERVIEW OF PROPOSED SOLUTION

In order to develop a fast model the flow in the microdevices, block-diagram description or lumped-element circuit models will be used. Analytical models will be used where possible or semi-analytical as opposed to numerical technique which is more time consuming. The finite element analysis software component in ANSYS will be used for comparison. Since the simulator software should be able to run on a PC and provide a solution within a reasonable time frame, only the essential physical behaviour of the device will be used so that rapid calculations can be carried out, within the limits of reasonable accuracy as a first approximation. The work in this thesis is limited by the type of devices that can be used. Validation of the models is necessary and as a result, only devices with available data from the literature can and will be used.

1.3 RESEARCH CONTRIBUTION

This research contributes towards the development for a MEMS interactive, animated VR prototyping, which in turn contributes to faster, easier design of MEMS. The work in this thesis contributes towards:

- fast calculations for the visualisation of fluid flow in microdevices
- the derivation of the flow model in terms of the movement of layers of fluid
- the application of electrical networks in the simulation of the movement of these layers of fluid
- the application of the above concepts to steady, laminar fluid flow in microchannels, nozzles and diffusers
- the application of the above concepts to unsteady, laminar starting flow in microchannels.

The work reported in chapters 5, 6, and 7, and other parts resulted in the following publications: [1,2,3,4,5]

CHAPTER 2: BACKGROUND

This chapter discusses the background material for the thesis. It begins with a brief description of MEMS, some examples of microfluidic MEMS devices and the basic techniques employed in the fabrication of such devices. Then it proceeds on to a discussion of modelling and simulation techniques in general and those used in current literature. Finally a review of challenges in CAD tools for the design of microfluidic MEMS is given.

2.1 MICRO-ELECTRO-MECHANICAL SYSTEMS (MEMS)

MEMS, the term used in USA, is also known as Microsystem Technology (MST) in Europe and micromachine technology in Japan (Trimmer 1997) (Fujita 1997) (Fukuda and Menz 1998). There is generally no accepted definition of the term MEMS or MST. However, quite a number of researchers adopt the concept of MST or MEMS as the integration of microsensors, microactuators and microelectronics, using special MST/MEMS techniques. The techniques include surface-micromachining technology and batch fabrication, among others (Fatikow and Rembold 1997) (Fujita 1997). In US and Europe, MEMS development is approached from micro- electronics technology while in Japan, it is from precision mechanics (Fukuda and Menz 1998).

A distinctive feature of MEMS technology is miniaturisation. There is no general consensus on the dimensions, though most are of the opinion that it is within the micrometer range. Simply downsizing from macroscopic machines is not possible because of scaling effect. This is due to the fact that the types of forces that are dominant in miniaturised devices are different from those that are dominant in macro-scale devices. For large-scale systems, inertial effects have a greater influence while surface effects influence smaller-scale systems. Being small, micromachines are able to produce small forces only. In order to perform on a large scale, several devices are required. Miniaturisation alone is insufficient, multiplicity is another essential feature of MEMS. For the many moving

elements to work together, microelectronics need to be incorporated in the system (Trimmer 1997).

2.2 MICROFLUIDIC MEMS DEVICES

Microfluidic devices such as microchannels, micronozzles, micropumps, micromixers and microvalves involve the flow of fluid. These devices are often the components of an integrated microfluidic chip or "lab on a chip", forming part of a miniaturised chemical analysis system, a micro total analysis system or a micro dosing system as in (Ikuta et al 2000), (Koch et al 1999), (Guenat et al 2001) and (Nguyen et al 1998).

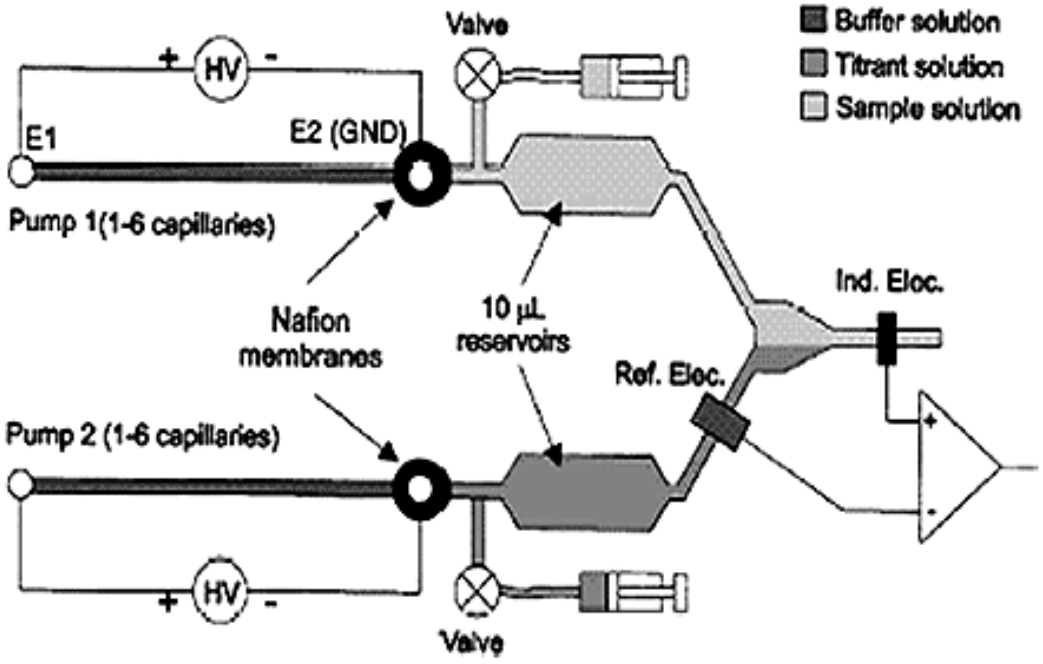

Figure 2-1 A micro total analysis system (µTAS) suited for continuous volumetric nanotitrations from (Woias 2001).

Figure 2-1 above shows a schematic diagram of a micro total analysis system for volumetric nanotitrations. It is made up of two electroosmotic nanopumps, a sensor unit, microchannels and a micromixer where the chemical reaction takes place. This unit is able to achieve typical flow rates ranging from 2 to 65 nl/s.

2.2.1 MICROVALVES

Microvalves are used to rectify fluidic flows, used in pairs in directing fluid flow in and out of a micropump or individually in a microchannel. Microvalves can be either static or dynamic. Static microvalves are mostly mechanical check valves consisting of a micromachined orifice and a deflectable sealing element. This sealing element can be a plate, a ring mesa, a cantilever or a float. Dynamic microvalves have micronozzles and microdiffusers functioning as valves. These are known as dynamic passive valves. Their flux rectification properties occur only at higher flow velocities, i.e. at non-laminar flow (Woias 2001). Refer to Figure 2-2 below.

Figure 2-2 Schematic diagrams of the check valves (Woias 2001)

The diffuser is a flow channel that has gradually expanding cross-section. When used in the opposite direction with converging cross-section it is called a nozzle. Diffusers can have circular or rectangular cross-sections and are called conical and flat-walled diffusers, respectively. Figure 2-3 illustrates the two types of diffusers used as microvalves (Olsson 1998). The microdiffuser valves are relatively simpler to fabricate since they have no moving parts. Another advantage of this absence of moving parts is a reduction of clogging due to particles in the fluid. For a micropump employing these valves, their advantages include high pump performance in terms of pressure head and flow rate and its ability to pump a wide variety of fluids. Its disadvantage, however, is that it does not have an effective self-block mechanism. An overpressure build-up at the outlet can cause a significant reverse flow. Early design of diffuser micropumps are sensitive to gas bubbles and cavitation, which is the formation of vapour resulting from a pressure drop below

vapour pressure (Andersson et al 2001).

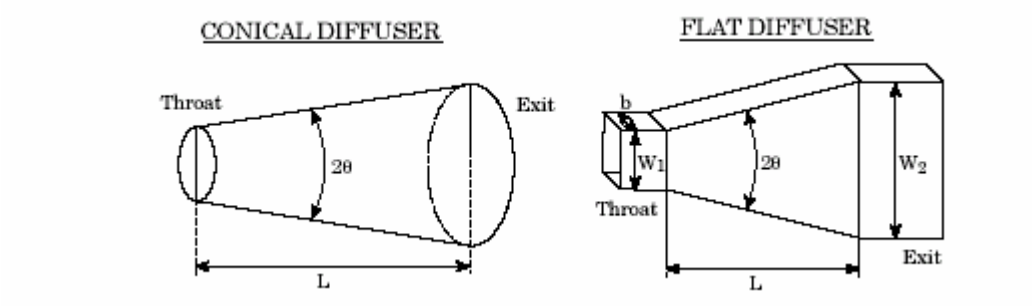

Figure 2-3 Conical and flat diffuser used as microvalves.(Olsson 1998)

Another type of valve is the no-moving parts valves (NMPV), which has fixed geometry as used in the pump in (Gamboa et al 2005). These valves develop a different pressure drop in the forward and reverse flow directions due to shape rather than mechanical moving parts. Figure 2-4 shows a fixed-geometry valve pump with Tesla-type valve.

(a) (b)

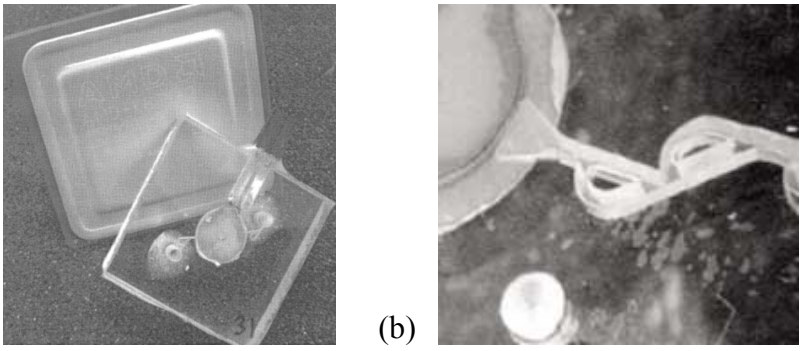

(c)

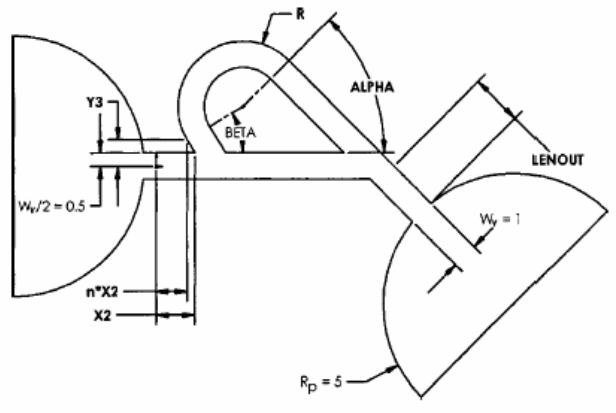

Figure 2-4 (a) A 10 mm pump chamber with 300-µm-wide optimized Tesla valves. (b)

Enlarged view of the Tesla valve. (c) Schematic diagram of the Tesla valve. (Gamboa et al 2005).

2.2.2 MICROMIXERS

A mixer must have the ability to mix two or more fluids thoroughly and in a reasonable amount of time. For effective mixing, the contact area between the fluids must be increased and the distance over which diffusion acts must be decreased. In order to achieve this, several mixing mechanism are employed, such as turbulence, three-dimensional flows, chaotic advection and diffusion (Evans et al 1997). Figure 2-5 below shows the micromixer component of a micromachined chemical reaction system. Feeding channels, placed parallel and having the same pressure drop, bring fluids from the inlets to the mixing area where the diffusive mixing occurs (Koch et al 1999).

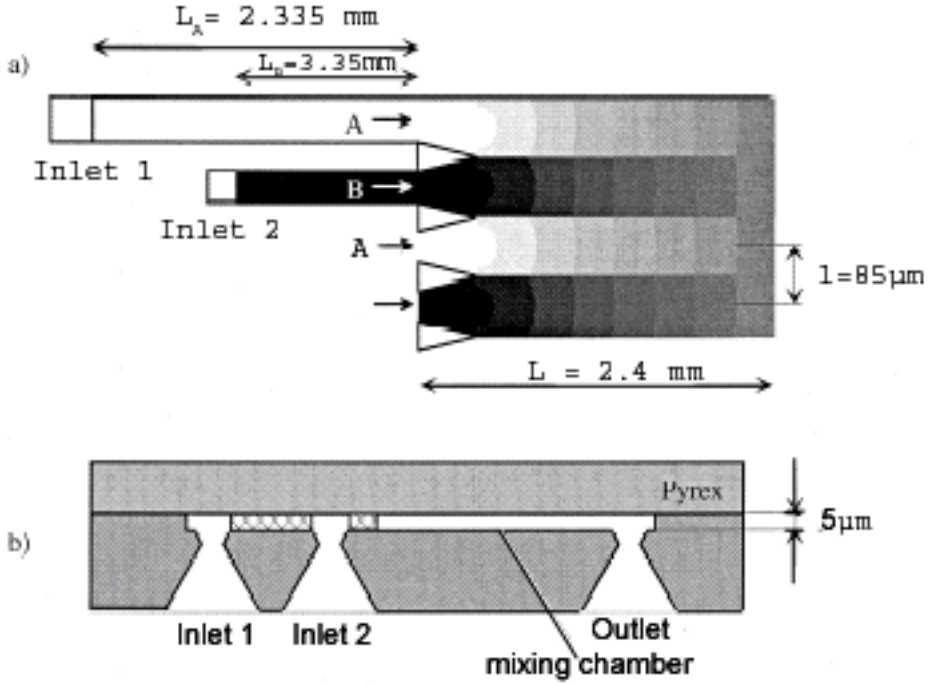

Figure 2-5 Schematic diagram of a micromixer, a component of a micromachined chemical reaction system by (Nguyen et al 1998)

In another system, a micro total analysis system (Guenat et al 2001), the micromixer has channels in a tree configuration, where the branches are successively subdivided in 2, 4, 8 and 16 branches. The two incoming fluids are split into 16 small laminae and are then

combined in a triangular mixing chamber. Refer to Figure 2-6.

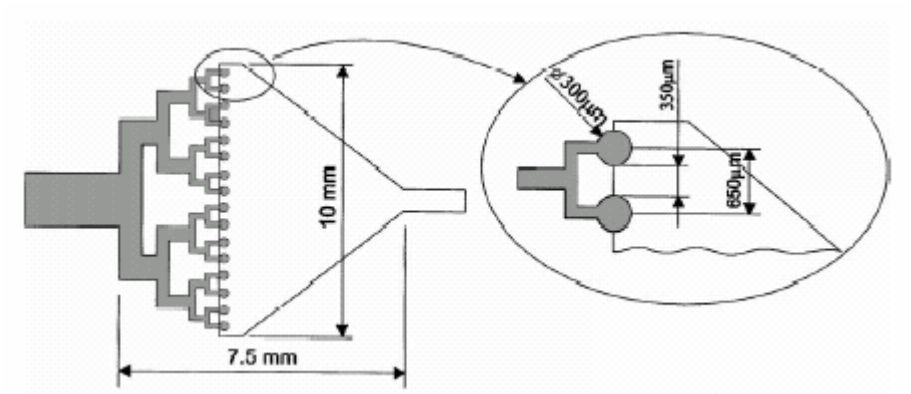

Figure 2-6 Topside view of the micromixer for a micro total analysis system by (Guenat et al 2001)

2.2.3 MICROPUMPS

Micropumps are used in numerous fields such as chemical process control, medical drug delivery systems, environmental control, and biotechnological applications to name a few. In all of these applications, the main requirement is that of low energy consumption needed so that systems can be portable and battery powered. The ability to turn off the flow or to deliver small and precise amount of liquid are needed for drug delivery system, such as microsyringes for diabetics or in a chemical analysis system. Micropump development began in 1980. Smits and Wallmark at the University of Stanford, created a peristaltic micropump using piezoelectric bimorphs as the actuation principle. This was followed by the work of Van de Pol and van Lintel et al with a reciprocating displacement pump with piezoelectric actuation (Van Lintel et al 1988) and a thermopneumatic driven micropump (Van de Pol 1990). Other micropumps with alternative actuation principles have, since then, been studied and manufactured.

An important characteristic of a micropump is its reliability which depends on several factors. The first is a self-filling feature, that is, the ability to create an underpressure in order to suck in liquid via the inlet valve and to fill the pump without trapping any gas pockets. This problem is known as priming, a major problem with almost all types of

micropumps. Another factor is the ability of the micropump to carry on pumping during a longer time period. Small gas bubbles in the pump chamber would expand and contract during the actuating of the chamber. This would eventually prevent the valves from opening since the maximum pressure reached during a stroke is too low, resulting in a reduced pump performance or even a complete failure. The third factor is the micropump's particle sensitivity, which is an inherent problem of check valve pumps. The moving valves get clogged up or suffer fatigue and failure. The reliability of a micropump due to the first and second factor can be improved by making sure that the device can pump both gas and liquid. This means that the pump needs to have a high compression ratio, which is the ratio of the stroke volume over chamber volume (Van der Wijngaart et al 2000).

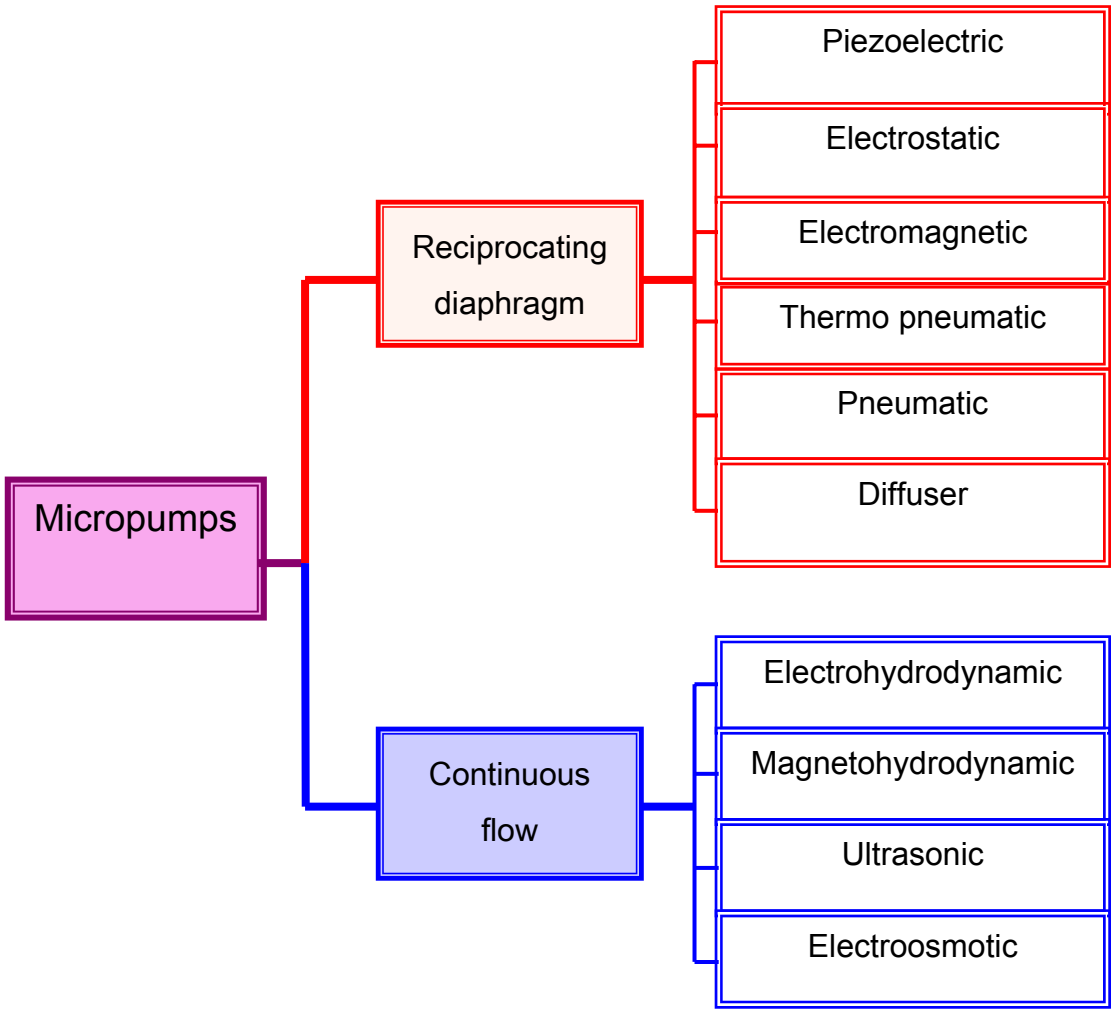

Figure 2-7 Classification of micropumps according to type of flow and actuation principle.

Fluid flow in MEMS is of low Reynolds number, which is the ratio that measures the relative importance of inertial forces to viscous forces. As such, conventional or axial turbomachinery will not work. At this miniscule dimension, viscous force dominates in relation to inertia while centrifugal forces are negligible. Therefore, a mechanical micropump can only work in three ways: positive displacement pump, continuous, parallel-axis, screw type rotary pump and continuous, transverse-axis, rotary pump. A microturbine can only work if the Re is higher than 1, which means that it must have an exceedingly high rpm (DeCourtye 1998).

Micropumps can be classified according to the type of flow: the reciprocating and the continuous flow micropumps (Fatikow and Rembold 1997). For each of these groups, they can be further divided according to their actuation principle. Among the reciprocating micropumps, several different actuating principles are used such as piezoelectric, electrostatic, magnetic, thermopneumatic, SMA or valveless diffuser. Among the continuous flow micropump, there are electrohydrodynamic (EHD), magnetohydrodynamic (MHD), ultrasonic and electroosmotic actuation. See Figure 2-7.

2.2.3.1 RECIPROCATING DIAPHRAGM MICROPUMP

In this section, the working principle of the reciprocating micropumps will be discussed, followed by their actuation principle. Then the continuous micropump and some examples of their actuation principle follow.

A reciprocating pump is one in which there is an excited oscillating membrane inducing periodic volume and pressure changes in the pump chamber. The membrane or diaphragm is driven by various actuation principles, as mentioned above.

A reciprocating diaphragm micropump usually consists of three parts: an inlet valve, an outlet valve and a pump chamber. These valves are usually static passive valves, ie they close completely in the backward direction making them able to withstand static back pressures. The micropump works by alternating between the supply and pumping phases.

During the supply phase, the diaphragm moves in a direction that enlarges the pump chamber volume, creating an underpressure in the chamber thus allowing fluid to flow through the inlet valve into the chamber. During the pumping phase, the diaphragm stroke reduces the chamber volume, creating an overpressure thus allowing fluid to flow through the outlet valve. The compression ratio is given by the ratio between the stroke volume and the chamber volume. Refer to Figure 2-8. In order to optimize the compression ratio, the chamber volume has to be minimized and the stroke volume of the actuator has to be maximized (Gerlach and Wurmus 1995).

The ratio of the stroke volume ΔVol and the chamber volume Vol_o of the pump is defined as the compression ratio ε:

$$\varepsilon = \frac{\Delta Vol}{Vol_o}$$

The compression ratio of micropumps is usually very small due to small stroke and large chamber volume.

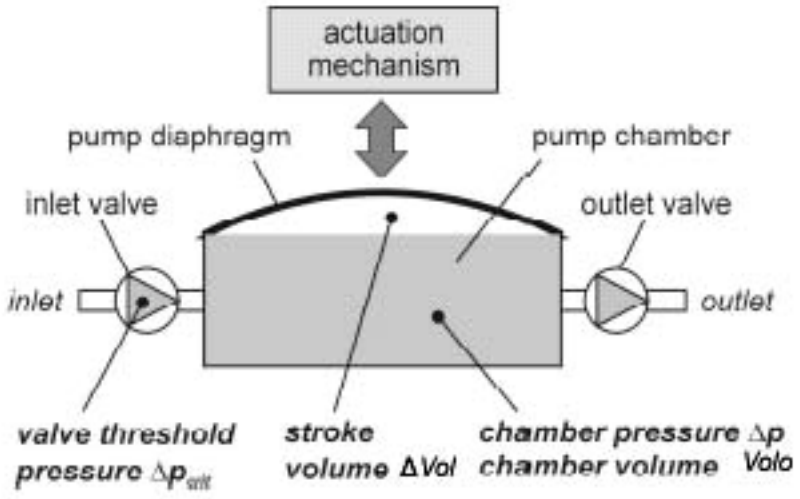

Figure 2-8 Compression ratio of micropumps (Woias 2001).

During its operation, the movement of the membrane causes a change in pressure |Δp| in the pump chamber. The valves open at a certain critical pressure difference Δp_{crit}. (Richter et al 1998):

$$|\Delta p| > |\Delta p_{crit}| \qquad (2\text{-}1)$$

Micropumps like any other microfluidic devices, need to be primed before use. Priming

involves 'rinsing' the system with the working liquid in order to remove any air bubbles. Air bubbles in the system or those that develop through outgassing of the liquid will prevent the micropump from functioning properly, reducing its efficiency. The accumulation of large amount of air bubbles may lead to complete failure. The presence of air increases flow resistance in the microchannels (Zengerle,R. et al 1995).

The compression ratio of a micropump is not critical if the pump is filled with incompressible fluid. However, real fluid has a finite compressibility and therefore works as a buffer in the pump chamber, exerting a damping effect on the pressure peak Δp. If this pressure peak Δp does not exceed a certain critical value, Δp_{crit}, the valves will not open and the pump will fail to function. The following set of criteria takes into account the damping behaviour of liquid and gas in micropumps (Richter et al 1998).

Table 2-1 Design rules for the compression ratio of micro diaphragm pumps.(Richter et al 1998)

Liquid micropumps	Gas micropumps	Liquid micropumps (self-priming and bubble-tolerant)
Only works if there are no gas bubbles in pump chamber		Pump rate depends on size of a gas bubble
$\varepsilon > k\lvert\Delta p_{crit}\rvert$	$\varepsilon > \frac{1}{\gamma}\frac{\lvert\Delta p_{crit}\rvert}{p_o}$	$\varepsilon > \frac{1}{\gamma}\frac{\lvert\Delta p_{crit}\rvert}{p_o}$
Δp_{crit} = 5 – 10 hPa	Δp_{crit} = 5 – 10 hPa	Δp_{crit} = 75 hPa
ε > 5 x 10^{-6}	ε > 0.01	ε > 0.075
Vol_o < 17 ml (for ΔVol = 85 nl)	Vol_o < 8.5 µl (for ΔVol = 85 nl)	Vol_o < 1.1 µl (for ΔVol = 85 nl)
where ε is the compression ratio, Δp_{cri} is the critical pressure difference, γ is the adiabatic coefficient and Vol_o is the chamber volume		

Assuming an ideal gas and adiabatic state changes with an adiabatic coefficient γ, the minimum compression ratio of a gas pump is given by the following equation:

$$\varepsilon > \frac{1}{\gamma} \frac{|\Delta p_{crit}|}{p_o} \tag{2-2}$$

where p_o is the atmospheric pressure and Δp_{crit} the critical pressure difference.

For liquid micropumps, the minimum compression ratio ε is given by:

$$\varepsilon > k|\Delta p_{crit}| \tag{2-3}$$

where k is the compressibility of the liquid. This is only valid under the condition that there are no gas bubbles in the micropump.

Liquid pumps usually contain gas bubbles. This may be due to the priming process, temperature changes during operation or gas bubbles transported into the pump chamber by the pump itself. Compressibility of gas is much larger than that of liquid and if the gas bubble is too big, the pressure peak Δp may become smaller than Δp_{crit}, in which case, the pump will fail. The criterion for the compression ratio of liquid pumps with gas bubbles is the same as that of gas pumps.

2.2.3.2 ACTUATION PRINCIPLE OF RECIPROCATING DIAPHRAGM MICROPUMPS

Most of the micropumps developed so far are of reciprocating diaphragm type and among the actuation principle, piezoelectricity is the most common. An advantage of piezoelectric actuation is its comparatively high stroke volume, a high actuation force and a fast mechanical response. It's disadvantages are a comparatively high actuation voltage and the complicated mounting procedure of the piezoceramic disk.

Piezoelectric micropumps consist of a piezoelectrically driven actuator usually a thin piezo disk glued onto the diaphragm as in the case of a silicon micropump for liquids and gases developed by (Linneman et al 1998). Apart from the diaphragm, the pump contains a valve unit consisting of an inlet and an outlet cantilever valve. When an electric field is applied

between the silicon diaphragm and the upper side of the piezoceramic material, a contraction of the material occurs and the diaphragm deflects towards the pump chamber. This creates the overpressure described above. When the voltage is removed, the diaphragm returns to its original position, thus creating the underpressure state.

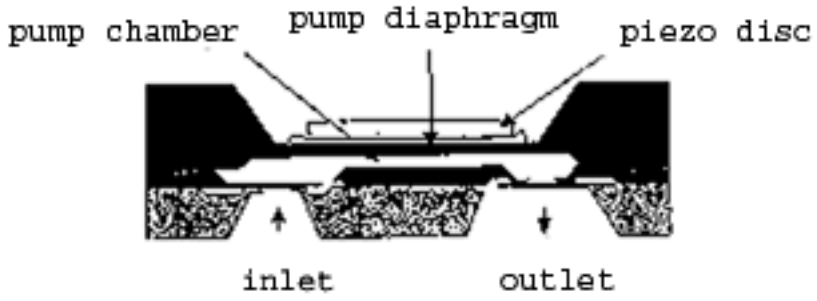

Figure 2-9 Piezoelectric micropump by (Linneman 1998)

Electrostatic actuation offers a very fast mechanical response, allowing operation frequencies of up to several kilohertz and has a low power consumption. Its main disadvantage is the small stroke volume. Over time, there is usually a degradation of the actuator performance due to a build-up of surface charges at the isolator inside the capacitor which eventually reduces the stroke volume (Woias 2001). Figure 2-10 shows an electrostatic micropump by (Zengerle,Z. et al 1995). It consists of a displacement unit and two passive check valves. If the voltage is switched on, the pump diaphragm bends towards the counterelectrode due to the electrostatic forces. The fluid is sucked in through the inlet valve. When the voltage is turned off, the diaphragm relaxes and the fluid is pushed out through the outlet valve. If the fluid moves from inlet to outlet valves only, the pump is known as a unidirectional pump. In this example, the valve is designed such that it has a mechanical resonance frequency between 1 kHz and 2 kHz. At low actuation frequencies (1 Hz – 800 Hz), the pump works in the forward mode. At higher frequencies (2 kHz – 6 kHz) it works in the other direction. This is a bidirectional pump.

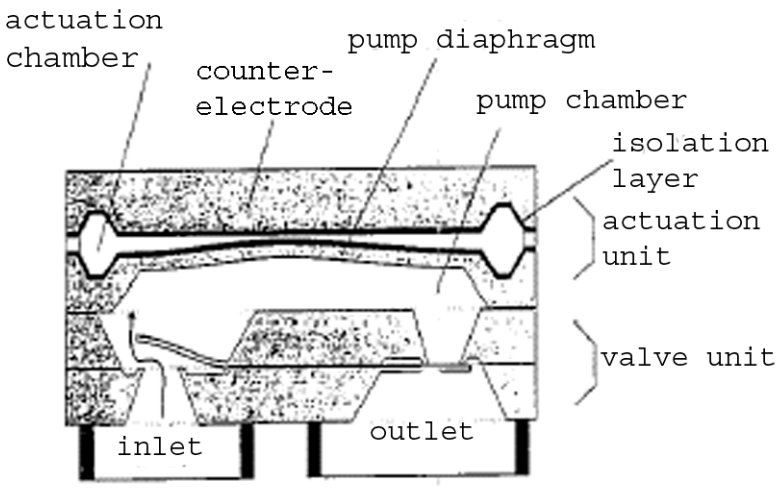

Figure 2-10 Schematic view of an electrostatically driven diaphragm pump by (Zengerle,Z. et al 1995).

The main advantage of the electromagnetic actuation is a slightly faster mechanical response than thermopneumatic. An electromagnetically driven micropump developed by (Gong et al 2000) is shown in Figure 2-11 below. It consists of an electromagnetic actuator, a pump chamber and passive microvalves. The actuator is located at the top and is a planar coil made of Fe-nickel alloy. When the electric current is turned on, a magnetic force is created thus deforming the membrane. This opens the in-valve, which then allows the liquid to enter the pump chamber. When the current is turned off, the membrane recovers its original state and the out-valve opens, allowing liquid to flow out of the chamber.

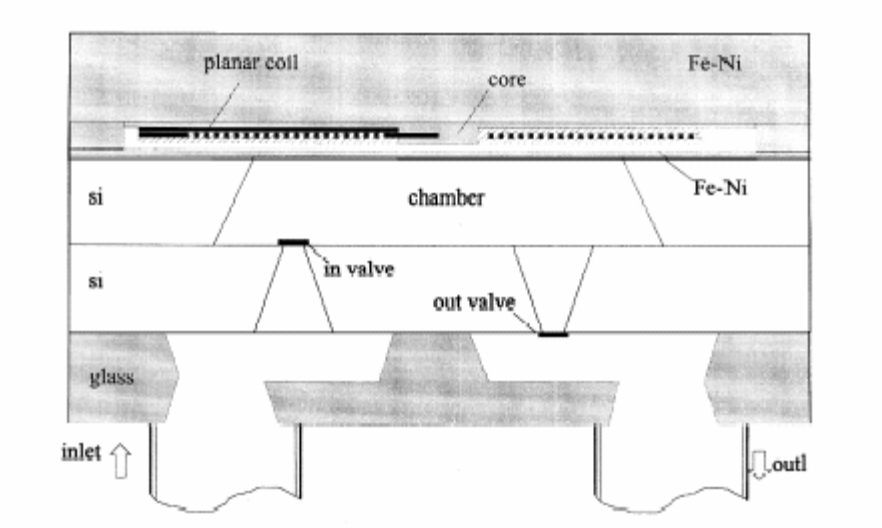

Figure 2-11 Structure diagram of four-layer microelectromagnetic micropump by (Gong et al 2000).

Micropumps using thermopneumatic actuation can be made very compact and volume strokes of up to several 100 μm to achieve high pump rates can be obtained. A disadvantage of this actuation is its relatively long thermal time constant of the air-filled actuation chamber which limits the actuation frequency to around 50 Hz. Its typical power consumption of about several Watts means that portability from using a battery is not possible (Woias 2001).

A thermopneumatic micropump by (Kim et al 2005) consists of a glass layer, an indium tin oxide (ITO) heater, a polydimethylsiloxane (PDMS) thermopneumatic chamber, a PDMS membrane and a PDMS cavity. When voltage is applied to the heater, the air in the chamber expands and the membrane deflects forcing the fluid out through the diffusers. When it is cooled, the air chamber decreases in volume and the membrane relaxes to its original position causing fluid to enter the chamber via the diffusers. Refer to Figures 2-12 and 2-13.

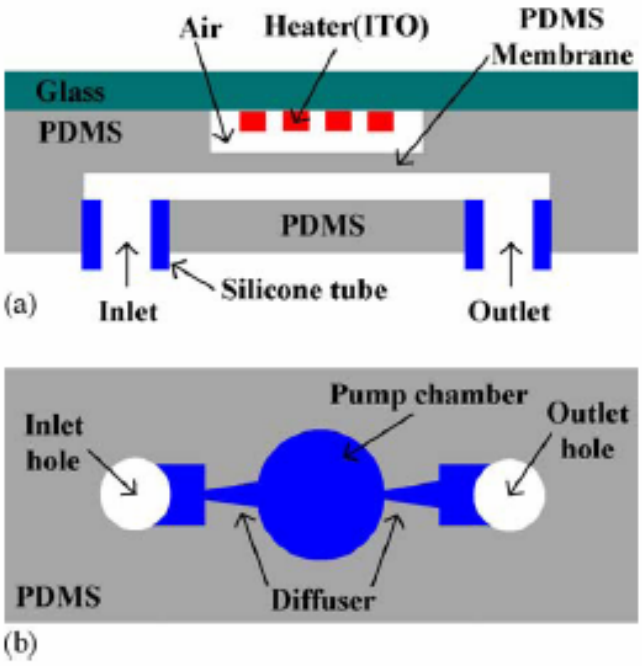

Figure 2-12 A thermopneumatic pump by (Kim et al 2005)

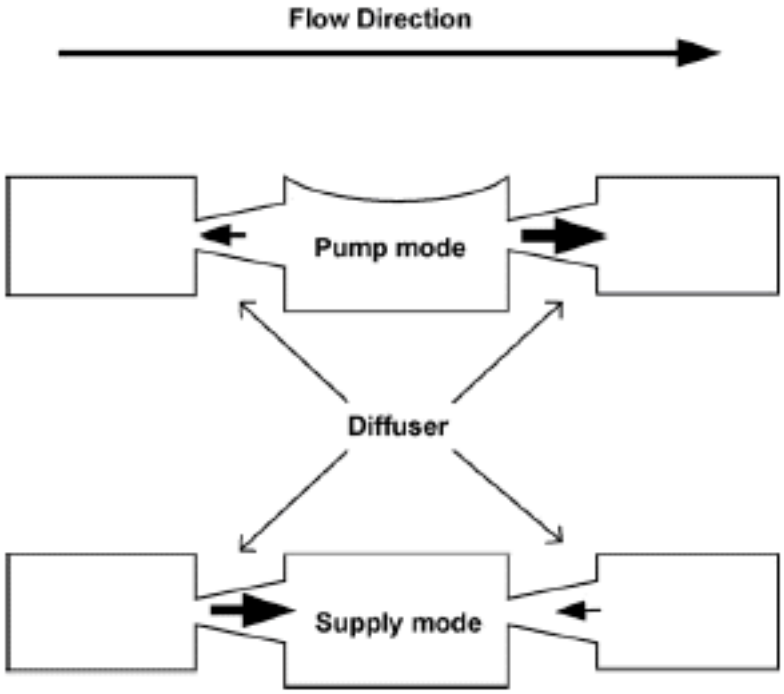

Figure 2-13 Conceptual operation of the thermopneumatic diffuser pump.

Micropumps based on SMA actuation are able to provide pumping pressures of several

hundred kilopascals. A micropump developed by Eiji Makino, Takashi Mitsuya and Takayuki Shibata (Makino et al 2001) uses an SMA actuator with a check-valve structure. The main element in the SMA actuator is a TiNi thin film diaphragm with a memorized flat shape. The actuator chamber is formed by putting a glass cap over the diaphragm. When a bias pressure is applied at room temperature the diaphragm deforms. When heated, the diaphragm returns to its original flat shape. The check valves open and close in response to the movement of the diaphragm. The diaphragm deforms outwards when the pressure is applied, pushing the liquid out via the outlet valve. When heated, the diaphragm returns to its original shape, sucking liquid in via the inlet. Refer to Figure 2-14.

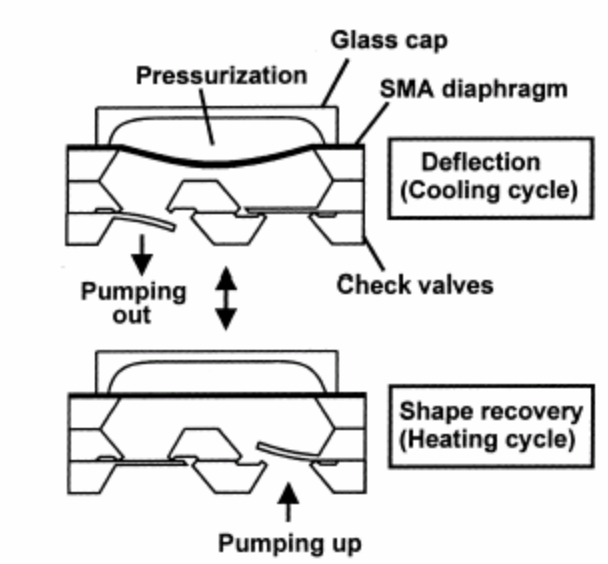

Figure 2-14 A schematic view of the working of an SMA micropump by Makino, Mitsuya and Shibata (Makino et al 2001).

The main advantage of the valveless diffuser micropump is due to the simplicity in the design of the valves. It has a relatively simple construction and is insensitive to particles in the fluid media. Diffuser micropump uses pyramid shaped diffusers as dynamic passive valves. The diffuser's general task is to decelerate or accelerate fluid flow by changing its cross-sectional area along the flow axis. The difference in the cross-sectional area of these diffusers means that they have different flow resistances in the forward and the reverse directions. An example is one by (Gerlach and Wurmus 1995), as shown in Figure 2-16. This pump uses nozzles with an opening angle of 70.5^0. It is fabricated in silicon by

anisotropic wet etching. The large opening angle is defined by the <111>-planes in the silicon. The converging walls offer a forward direction while the diverging walls, the reverse direction. This is shown in Figure 2-15.

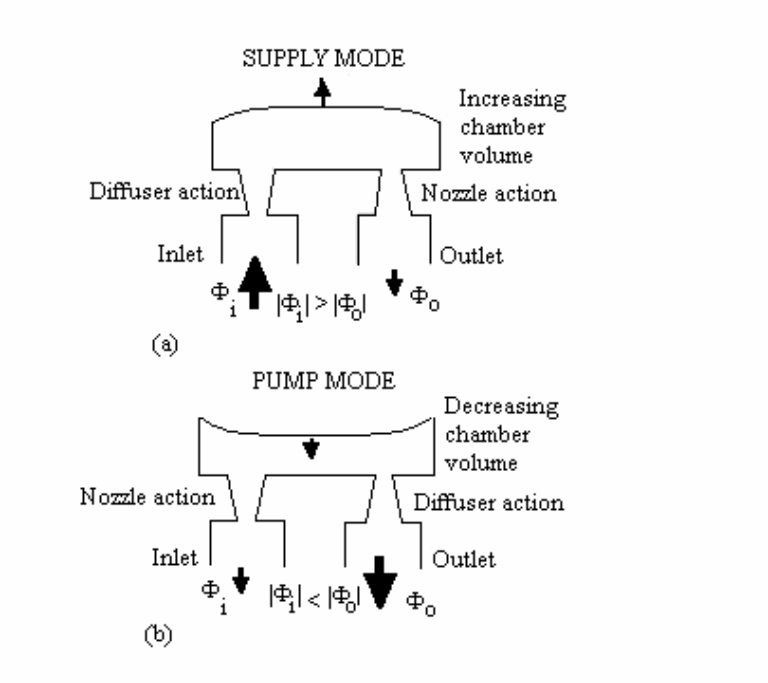

Figure 2-15 The working principle of the diffuser micropump

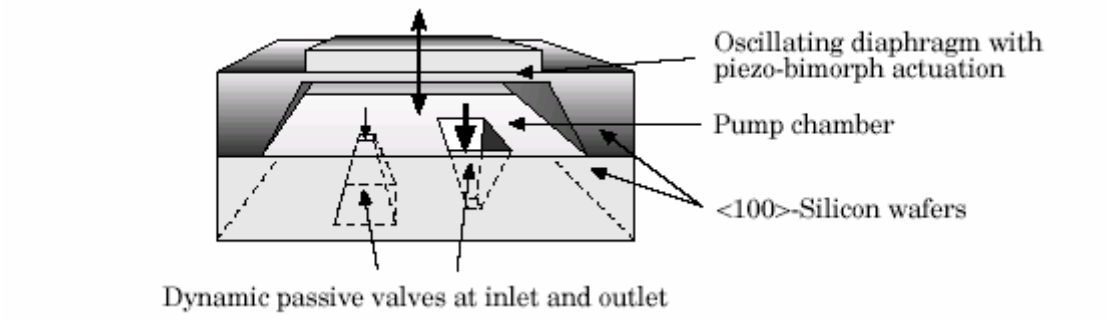

Figure 2-16 The dynamic diffuser micropump by (Gerlach and Wurmus 1995).

2.2.3.3 CONTINUOUS FLOW MICROPUMPS

These are based on a direct transfer of a nonmechanical or mechanical energy form into the movement of a fluid. These are sometimes known as “non-mechanical” micropumps i.e. with no moving parts. Micropumps with passive valves or diffuser valves have high fluidic

impedance. The use of "active" channels as in these continuous flow micropumps such as electrohydrodynamic and ultrasonic pumps, provides a solution to the impedance problem. The main advantage for these micropumps is the simplicity in their structure which is usually a microchannel with electrode arrangements. Their performance, however depend on the fluid properties, and usually require ionic liquids. Gas transport is excluded. The working principle of these micropumps differ widely depending upon how the energy is produced. A few types are mentioned below (Woias 2001).

Electrohydrodynamic (EHD) micropumps are mainly used in medical or biological applications since the liquids involved have high ionic conductivity. The pumping source in these micropumps can be the Coulomb force acting on ions injected from an emitter electrode into the fluid by electrochemical reactions. The pumping source can also be the result of the interaction between a conductivity gradient and a travelling wave of potential, as in the case of (Fuhr et al 1992).

Magnetohydrodynamic (MHD) micropumps, a variation of the above EHD micropumps, uses the Lorentz force as the pumping source. Electromagnetic energy is converted into mechanical work in the fluid media. MHD involves the study of flow of electrically conducting liquids in electric and magnetic fields. MHD can be used for pumping fluids as well as for the stirring and mixing (Jang and Lee 2000) (Lemoff and Lee 2000) (Zhong et al 2002).

Ultrasonic pumping is based on the phenomenon of acoustic streaming. A flexural plate wave (FPW) device, a thin membrane, is used to produce flexural wave which propagates in the membrane. When this occurs, a high intensity acoustic field appears in the fluid near the membrane, thus causing the fluid to flow in the direction of the wave propagation (Nguyen and White 1999).

The electroosmotic flow (EOF) micropump can typically generate pressure differences greater than 1 atm. Its operation is based on the flow of an electrolyte solution across a microchannel with an external electrical field applied on its walls. Charge is generated at the liquid-solid interface causing ions to form in the liquid. The ions move in response to

the applied field dragging the surrounding liquid with them, causing a net motion of liquid, which is known as electroosmotic flow (Zeng et al 2001). The pump shown in Figure 2-17 (Brask et al 2005) uses a thin layer of conducting pumping liquid driven by electro-osmosis to drag a nonconducting working liquid by viscous forces. It delivers fluid at the flow rate per volt of 0.03 nL/V/s, which is quite small and is therefore suitable for precise flow manipulation rather than for pumping bulk volume.

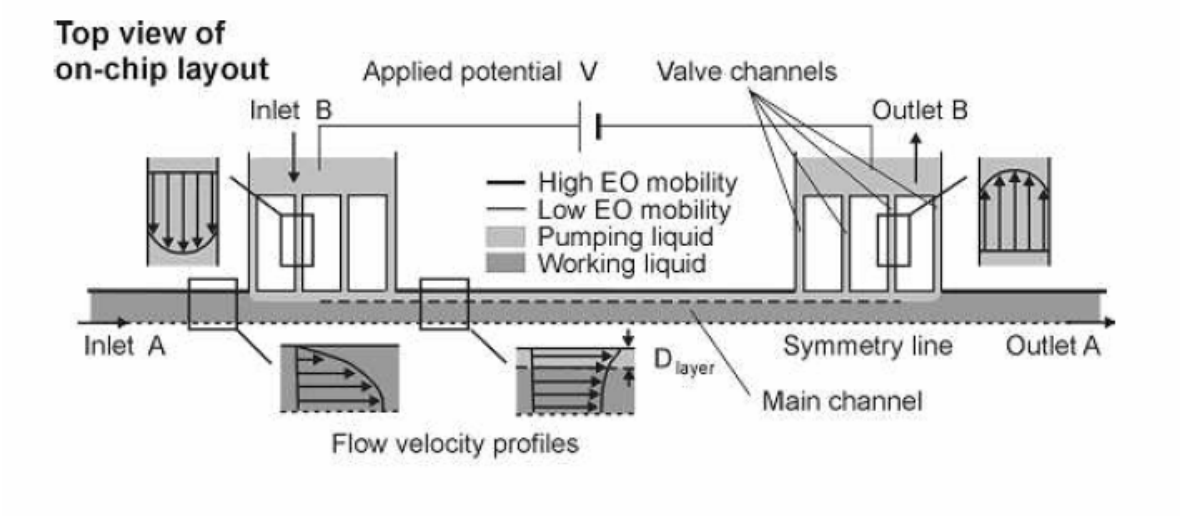

Figure 2-17 Top view of a two-liquid viscous micropump driven by electroosmotic pumping. (Brask et al 2005)

2.3 MICROFABRICATION TECHNOLOGY

MEMS manufacturing is based on well-developed techniques of integrated circuit manufacturing on silicon wafers. The principle is the same: alternating thin film deposition with selective etching until the desired geometric structure emerges. The crystalline structure of the silicon, and its orientation are decisive in the effect of etching, in particular for mobile mechanical parts. Three main technologies are mentioned here: bulk micromachining, surface micromachining and the LIGA process.

In bulk micromachining, the silicon substrate is dissolved away, producing mechanical elements such as beams, membranes and other structures. This is a more established process and many commercial products such as sensors and accelerometers are produced

via this method. Bulk processes generally make use of anisotropic silicon etchants to produce structures bounded by crystal planes in the silicon substrate. Figure 2-18 shows some of the types of bulk micromachining techniques from (Varadan et al 2001).

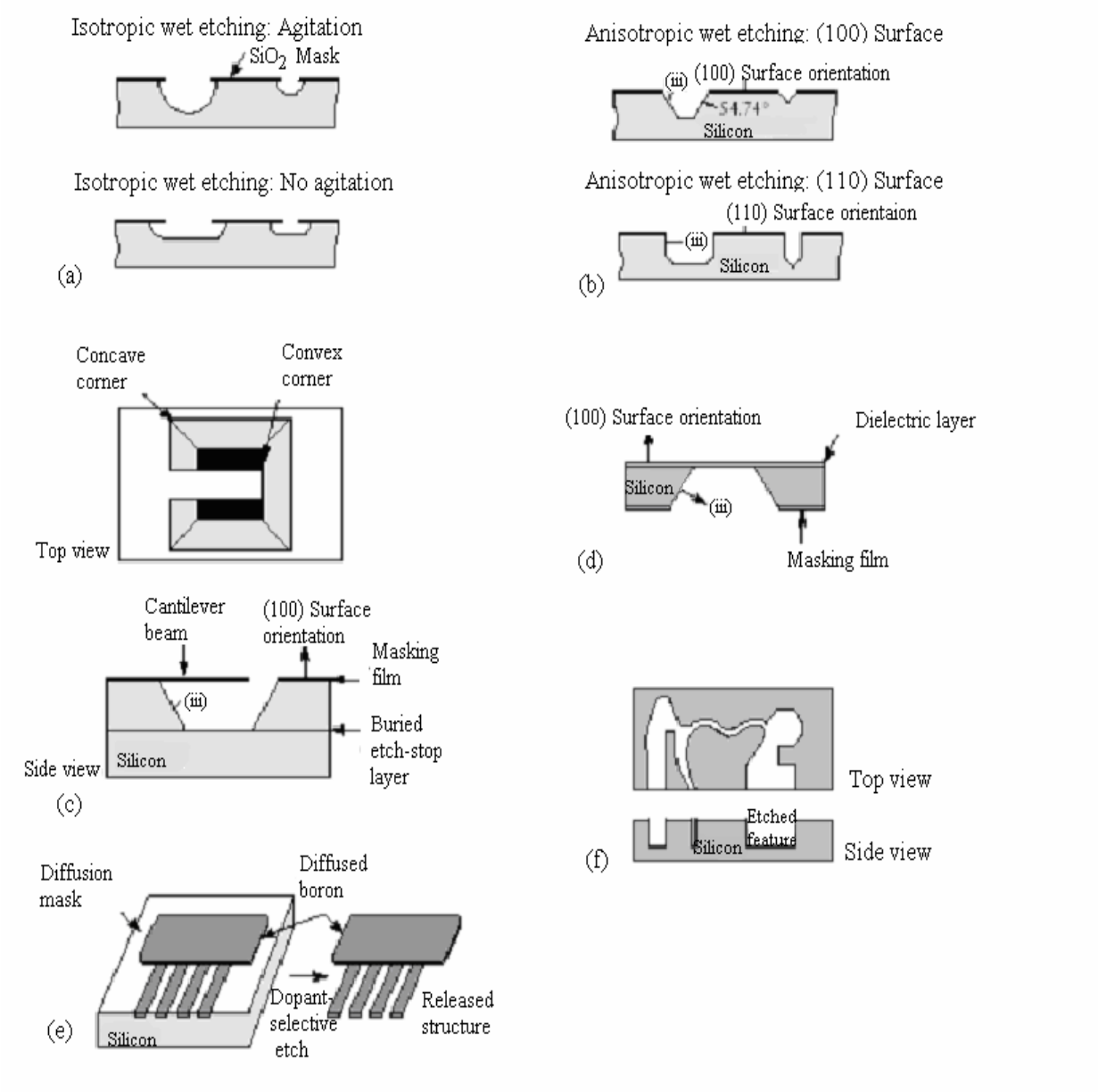

Figure 2-18 Bulk silicon micromachining. (a) Isotropical etching, (b) Anisotropic etching, (c) Anisotropic etching with buried etch-stop layer, (d) Dielectric membrane released by back-side bulk etching, (e) Dopant-dependant wet etching, (f) Anisotropic dry etching. (Varadan et al 2001)

In surface micromachining, alternating layers of silicon dioxide and polysilicon are deposited and patterned into various shapes. The final step is a release etch which removes the silicon dioxide layer but does not affect the polysilicon layer. This results in a mechanical element which is free from the substrate and is able to move. This process is a relatively recent development. It generally uses only lithographic patterning to define lateral geometries (Fukuda and Menz 1998). Figure 2-19 shows some typical surface micromachining processes (Varadan et al 2001).

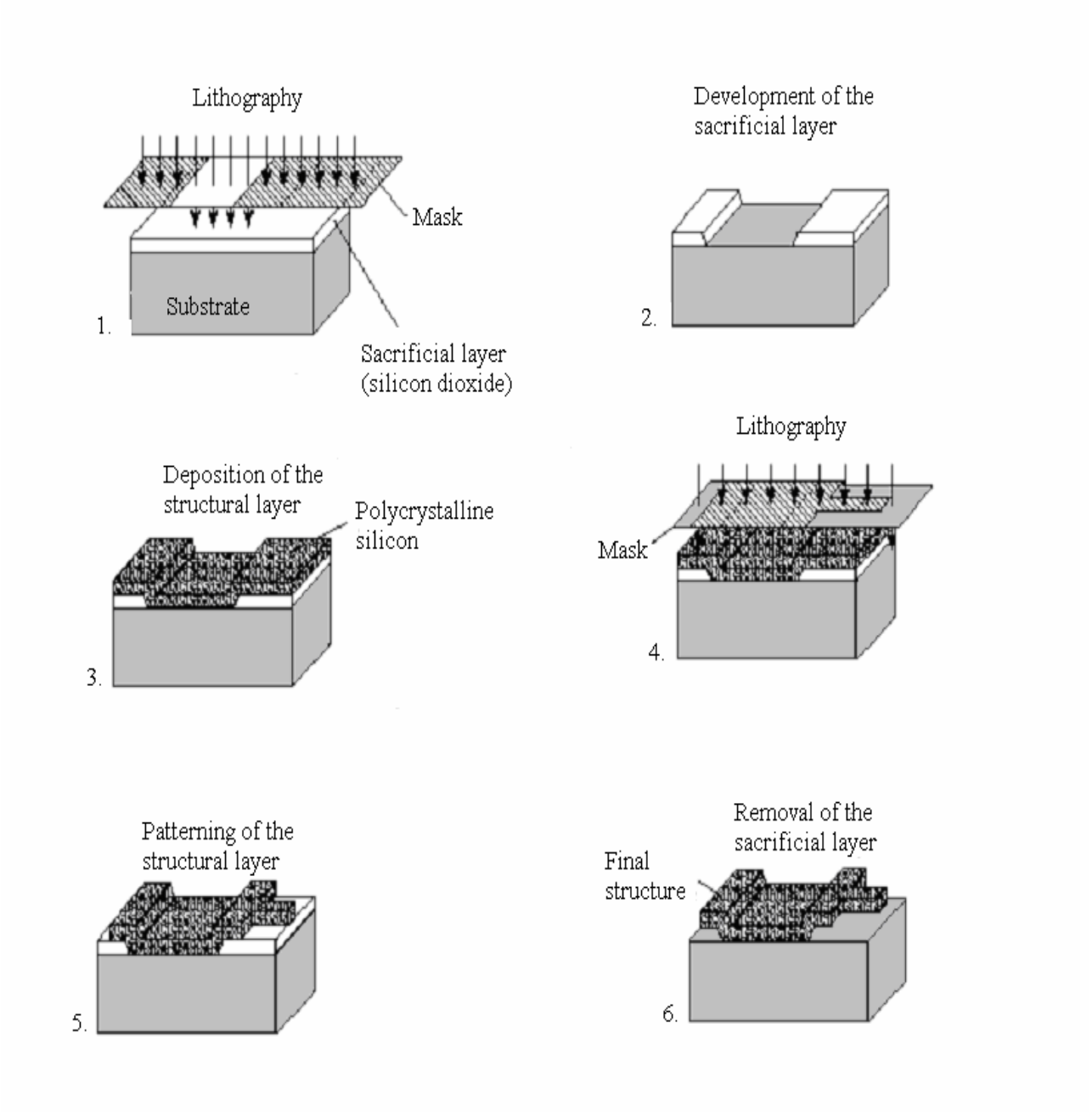

Figure 2-19 Processing steps of typical surface micromachining. (Varadan et al 2001)

The LIGA process was developed at the Research Center Karlsruhe (Forschungszentrum Karlsruhe, FZK) in the early 80's to make diffusion nozzles for uranium enrichment. A thick layer of up to several 100 μm of PMMA (polymethylmethacrylate, plexiglass) is deposited on a metal substrate. Structures are patterned by parallel and high-energy X-ray lithography. The gaps are galvanically filled with metal such as gold, copper or nickel. The rest of the unirradiated plastic is removed and a metallic microstructure remains. This can then be used as a mold for the mass production of plastic parts by micromolding techniques (Thielicke and Obermeier 2000) (Fatikow and Rembold 1997). Figure 2-20 shows some LIGA processes (Varadan et al 2001). The advantage of LIGA is that it allows a high aspect ratio. Alternative processes developed at the FZK include the use of ceramics and other materials.

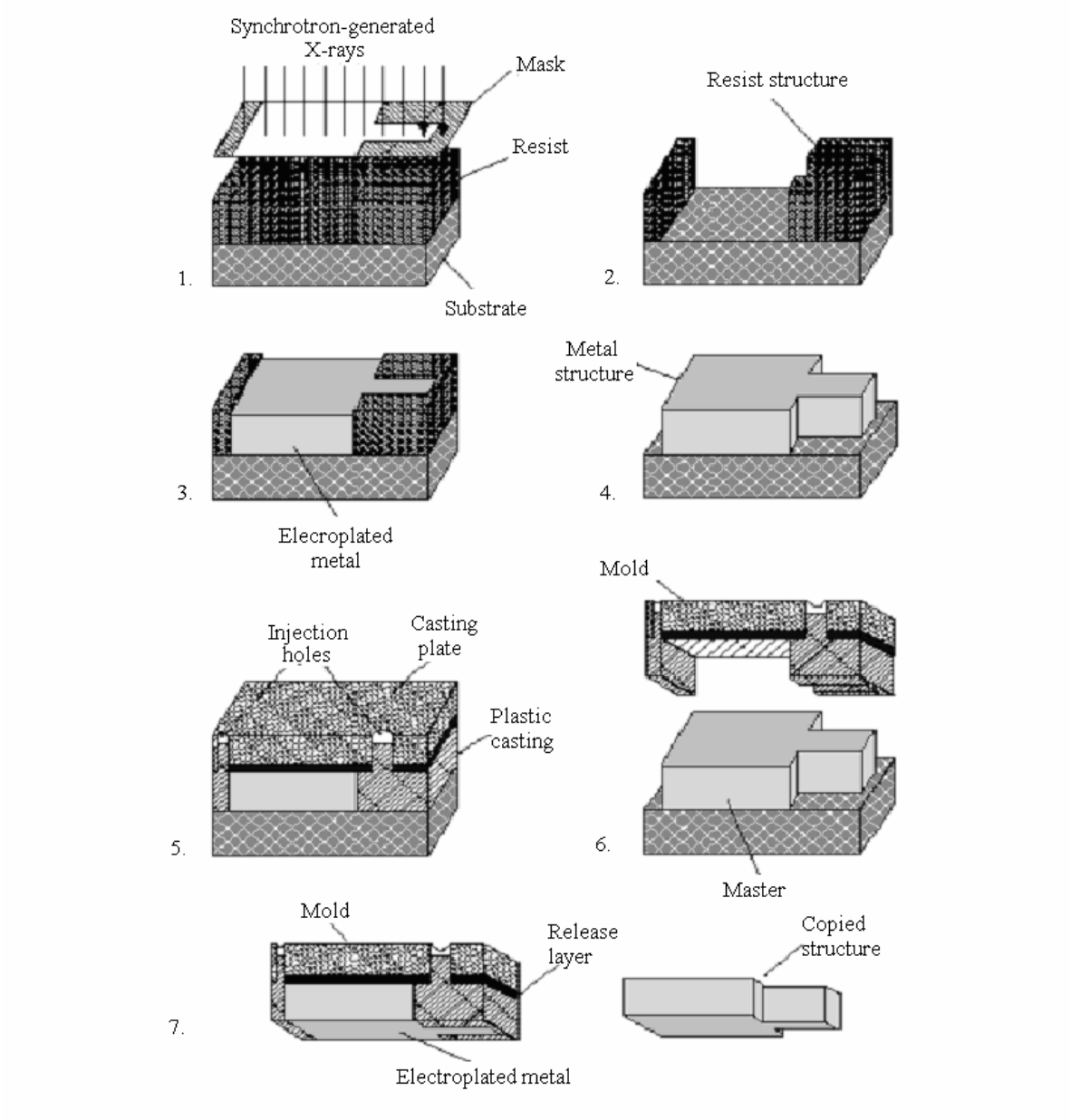

Figure 2-20 LIGA process. (Varadan et al 2001)

2.4 REVIEW OF MEMS MODELLING

Modelling is the process of developing a valid mathematical representation of the system under scrutiny. There are three steps in this process: acquisition, simplification and the validation of the model. Acquisition involves the development of differential equations and boundary conditions that describe the underlying physical principles and is based on theory and/or measurements. Simplification is the process in which assumptions are made in order to reduce the complexity of the full model equations. Validation involves the comparison of the values obtained by the model and those of experiments. If the two sets of data agree, then the model is validated. Once validated, the model can be used to predict the results of other similar experiments.

Simulation is the process in which the models are solved, usually producing numerical solutions. This process basically involve two steps, the first is to define the application domain for which the model is valid. The next step is to iteratively or recursively input a set of data to the model to produce a consistent solution. The device performance is predicted under various operating conditions (Nathan and Baltes 1999).

The design process can be examined from a top-down or bottom-up approach. In the top-down approach, one starts with the system level progressing to the subsystem and finally to the process level. A different type of modelling is used at each level. The bottom-up approach, sometimes known as the verification design path, starts with process level modelling proceeding to the system level. Figure 2-21 illustrates a simplified overview of these levels.

-

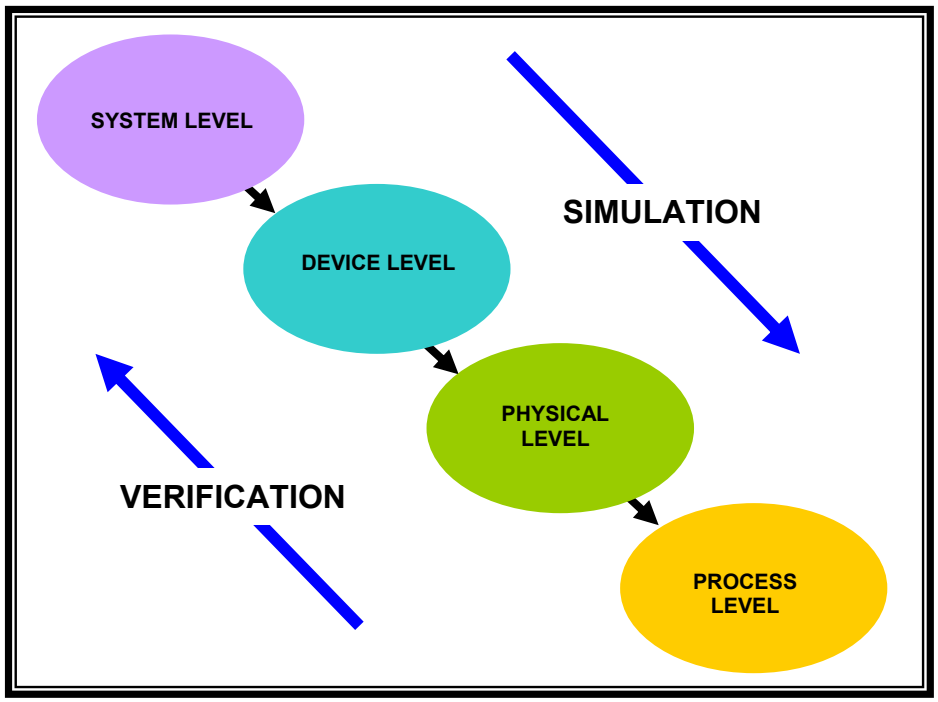

Figure 2-21 The modelling levels for MEMS. Adapted from S.D.Senturia.

System level modelling involves a higher level of abstraction. The emphasis is on functional simulation where the behaviour and performance of the system as a whole are characterized. One approach is to analyse the system's different physical domains, translating the variables into electrical values. Another approach is to analyse the system into different behavioural domains. To describe the dynamic behaviour of the system either block diagrams or lumped-element circuit models can be used, producing a set of ordinary differential equations (ODE). These are usually in the form of state equations, a coupled set of first-order ODE for the state variables of the system. Examples of tools for system level analysis are circuit simulators for example AccuSim from Mentor, AnalogArtist from Cadence or MATLAB/Simulink. Analog and Virtual Hardware Description Language (AHDL and VHDL) are sometimes used for system-level simulation.

Device level modelling involves creating a macro-model or reduced-order model of the component of the system. The model is a simplified set of equation representing the terminal characteristics of the subsystem. The essential physical description of the device, both static and dynamic behaviour, is obtained. Device modelling tools use the same techniques as in system-level modelling. CAD tools that have reduced-order modelling include Analogy and CoventorWare from Coventor Inc. These however are limited to linear and single domain systems.

Physical level modelling, also known as 3D modelling, provides greater structural detail of the device. A set of partial differential equations (PDE) is obtained. These can be solved using approximate analytical solution or highly meshed numerical solution. The numerical methods used can be finite element method (FEM), finite volume method (FVM), or boundary element method (BEM). A number of CAD tools currently available are basically for 3D modelling. These include the FEM tool from ANSYS Multiphysics, CFD, Coyote Systems, IntelliSuite by Intellisense and CoventorWare from Coventor Inc.

Process modelling involves the process sequence in the manufacture of the device. The model must incorporate the different fabrication sequence and the suitability of various materials for the process. For example, the modelling of anisotropic etching of silicon helps in the bulk-micromaching process, the modelling of thin film deposition of amorphous silicon may be needed for surface micromachined process and the modelling of polyimide's response to X-ray radiation may be required in a LIGA process. IntelliSuite provides process modelling (Schneider et al. 2000) (Tang 1997).

For this thesis, the modelling is carried out at the physical level. The flow of fluid is characterised by the partial differential equation called the Navier-Stokes equations. (Aumeerally and Sitte 2001)

2.5 LITERATURE REVIEW OF MEMS MODELLING

The lumped mass model is used in the modelling of a valveless diffuser micropump by Olsen, Stemme and Stemme (Olsen, Stemme and Stemme 1999). In this model, the

structure is divided into lumped mass elements, which can be described individually by simple analytic models and simple relations can also be formulated between these elements. For example, the diaphragm is formulated using Newton's second law, the conservation of mass law is used on the chamber volume and energy equation is used to analyze the flow rate. An electric circuit is used to illustrate the micropump and the equations are solved using MATLAB. Diaphragm properties were calculated using the FEM software ANSYS.

Gong et al (Gong et al 2000) used the Runga-Kutta method to solve the set of differential equations expressing the micropump's two pumping phases of liquid-in and liquid-out. ANSYS FEM software is used in analyzing the fluid flow through the microvalve and micropipe and the diaphragm deformation. The micropump's structure design and parameter optimization was done analytically.

Simulation by block diagram, using Simulink was carried out by Français and Dufour (Français and Dufour 1998). The dynamic model is obtained by studying the flow-in and flow-out phases of the micropump and representing these in blocks. Each block symbolizes the characteristics of a micropump element. The static characteristics of the micropump are analysed analytically.

In the paper by Day and Stone (Day and Stone 1999) the authors described the boundary integral method for solving the Stokes equation representing low-Reynold-number flow for thin gaps in a viscous micropump. The pump consists of Poiseuille flow of fluid between two plates and a cylinder placed along the gap perpendicular to the flow direction. In the boundary integral method, the behaviour of the inside of the volume is described by degrees of freedom located on the problem boundary using integral theorems. Once the solution is obtained in terms of the degrees of freedom, solutions inside the volume can then be calculated. This method does not handle complicated geometries well, especially for three-dimensional problems. It is usually used in conjunction with FEM, which is used to treat the complicated interior.

Electrical equivalent circuits have been used in the modeling and simulation of microchannels in micropumps as in (Morris and Forster 2000) and (Voigt et al 1998). In

(Morris and Forster 2000), the concept of the electrical equivalent circuit is applied to the whole microchannel. In (Voigt and Wachutka 1998) the channel is divided into small slices of equal length and each is described by an RLC circuit.

In (Qiao and Aluru 2002), the electrical modeling technique was used to determine the flowrate and pressure for a micromixer, where the flow is driven by a combined pressure and electrical gradient. Here only a network consisting of resistances was used. Capacitors were not incorporated.

Brask, Goranović and Bruus (Brask et al 2003) used electrical equivalent circuit to determine the flow rate of a low-voltage electro-osmotic micropump. Their calculations were compared with the numerical simulation of computational fluid dynamics (CFD) and found to have good qualitative agreement of within 3%.

In (Chatterjee and Aluru 2005), the electrical circuit modeling was applied to an integrated microfluidic system with models for fluidic transport, mixing, chemical reactions and separation. They achieved their objectives with "very little computational expense, while maintaining the desired level of accuracy". Here the electrical circuits consists of both resistors and capacitors. The capacitors were used to account for the electrical double layer in the fluidic transport.

In this thesis, the electrical circuit concept is applied to layers of fluid within the channel, so that the different flow rates can be visualized and the transient flow in the microchannel can be demonstrated.

2.6 CHALLENGES IN MEMS CAD TOOLS FOR MICROFLUIDIC APPLICATION

Due to the nature of MEMS devices, especially its size and manufacturing cost, it would be very difficult if not impossible to create without first designing and visualising them. With a simulation tool, it is easier, faster and much less expensive to build a MEMS device. It is absolutely necessary to use a simulation tool so that the time it takes from designing to

completion of the component is reduced significantly. It is less costly to modify, if there are mistakes in the design, before it is actually prototyped or manufactured. The acceleration of the development cycle leads to a reduction in cost (Jakovljevic et al 2000). A simulation tool can be used to predict and improve device characteristics. The accurate analysis of these characteristics leads to an optimisation of the device and hence improves system performance (Funk et al 1997).

A typical CAD should have three basic components: a geometry builder where the geometry of the device could be drawn, a simulation module where the problem is solved using the relevant governing equations, and a visualization module where the simulation results can be displayed (Korsmeyer et al 2004). In order to create useful MEMS fluidic devices, the CAD tool must have as its underlying principle the models that definitively characterise the operation of the device. For devices that handle gases, the effects of slip-boundary conditions, thermal creep, viscous dissipation and compressibility have been studied. Both conventional, continuum model and molecular-based models have been attempted (Gad-el-Hak 2002). Such CADs must be able to handle fluids within the length scales that involve both noncontinuum fluid effects molecular models as well as continuum models. (White, J. 2004).

CAD tools can be categorized as either field-solvers or network simulators. Field-solvers can solve complex partial differential equations, using FEM or boundary-element method (BEM). These equations are a detailed description of the physical design of the MEMS device. They are complex equations taking a lot of time to solve. Network simulators are required for system level modelling. These give a description of the system with a building-block orientation. Simpler ordinary differential equations are used to describe the system. For the design of MEMS, field-solvers are available and are widely used, such as ANSYS/Multiphysics. System-level tools are also available, such as CoventorWare and Saber.

ANSYS seems to be the popular choice for researchers doing FEM analysis of MEMS structures. Ulrich and Zengerle (Ulrich and Zengerle 1996) uses ANSYS/FLOTRAN for the mechanical and fluid-mechanical simulation of KOH-etched microvalve. Others such

as Gong et al (Gong et al 2000), Mehner et al (Mehner et al 1998), Arik et al (Arik et al 1999) and Nedelcu and Moagar-Poladian (Nedelcu and Moagar-Poladian 1999) also used ANSYS FEM software.

The application of computational fluid dynamics (CFD) CAD system is demonstrated by Giridharan et al (Giridharan et al 2001) for the modelling of devices such as microplume mixer, membrane pump, microvalve etc. N.T.Nguyen and J.M.White (Nguyen and White 1999) designed a micropump based on acoustic streaming in water and the numerical model which consists of the continuity equation, the momentum equation and the energy equation are solved using CFD software, such as CFD-ACE+ .

For microelectronics, highly sophisticated design tools with a well-defined "top-down" design path and "bottom-up" verification path are available. Tool suites include circuit representation, extraction from layout of devices and parasitics and verification of interconnect between layout and schematic (Fedder 1999). An equivalent of such a comprehensive suite of design tools for microfluidic MEMS is now commercially available, although it is still in its infancy stage and has not reached the maturity of the design capabilities of CAD for microelectronics. The CAD tool CoventorWare^{TM} (2004) has both the system-level modeling tool ARCHITECT^{TM} and the detailed-level capabilities from the CoSolve^{TM} component which is a coupled electromechanical solver using the finite element method for mechanical analysis and boundary element method for the electrostatic analysis.(Korsmeyer et al 2004).

Most researches (Wang et al 2004), (Korsmeyer et al 2004), (Chakrabarty and Su 2005), (McCorquodale 2003) are in favour of the top-down approach where device designers begin working at the system level at the start of the new design cycle. Once the behaviour of the entire device is understood and promising design identified, detailed numerical modeling can then be carried out in order to confirm the system-level results and to optimize the design parameters. An integrated microfluidic system is a complex system comprising of several, even hundreds, of components which can be of magnetic, mechanical, optical, chemical or biological in nature and along with the supporting analog and digital components. With such a system, a top-down approach is favoured to the

traditional bottom-up approach, so as to reduce costly and time-consuming redesign effort.

Microfluidic systems consist of a complex network of hundreds of thousands of fluidic channels, which are basically of the same structure. In such systems, device modeling which requires detailed numerical analysis "can be very expensive and tedious" (Chatterjee and Aluru 2005). Wang, Lin and Mukherjee (Wang et al 2004) stated that when applied to the design of 'lab-on-a-chip', "numerical computation methods and bottom-up design approaches can lead to unacceptably long design cycles". Qiao and Aluru (Qiao and Aluru 2002) stated that "the use of detailed numerical simulations can be very expensive and prohibitive for microfluidic system" Circuit modeling technique is usually employed for the analysis and design of complex microfluidic systems.

The purpose of this thesis is to determine models that can give quick calculations for an interactive CAD with dynamic animations. Current calculations are too time consuming and not suitable. Calculations based on Finite Element Analysis have slow and time consuming algorithms, which make interactive CAD unworkable. Efficient design tools are required to shorten this process. These interactive CAD tools need to be able to give quick yet accurate results. Equivalent electrical circuit modelling provide an efficient tool for the analysis and design of complex microfluidic systems, which can have thousands of microchannels. Although it is not as accurate as device modeling, it is however accurate enough for an understanding of the basic system behaviour. In cases where circuit modelling does not give a good picture or that a more accurate detailed analysis is needed then device modelling can be used. The results obtained from electrical circuit modelling can be compared with data from experiments as well as with those obtained using a finite element software such as ANSYS.

CHAPTER 3: PROBLEM STATEMENT AND PROPOSED SOLUTION

The design process of any device forms an important part of its creation, from the conception of the idea to the realisation of the device. At each step, careful considerations have to be made in order that the specification is met, in the most cost efficient way and in the shortest possible time. For macroscopic devices, engineers usually create smaller scale models after the design process is carried out, in order to test its functionality. For microdevices which are of the order of 1 to 500 μm scale, creation of a scale model is not so practical, although one can create a larger macroscopic models instead. However, in the case of microfluidics, the flow in microscale does not behave in the same way as that in macroscale, where turbulence predominate and effect of gravity is taken into consideration. At the microscale level, viscosity and friction plays a greater role and effect of gravity is negligible. The importance of CAD tools in the design of microsystem cannot be emphasized enough.

3.1 PROBLEM STATEMENT

Visualisation using FEM is too slow if it is used for the whole micropump structure. For this thesis, FEM will be used for a small section of the micropump, the flow in the microchannel, and this will be compared with the electrical model. FEM or boundary-element method (BEM) can solve complex partial differential equations. These equations are detailed description of the physical design of the MEMS. They are complex equations taking substantial time to solve. For example, FEM uses basis functions to approximate the solution to the differential equations. These local basis functions are generated by meshing the domain of interest and parameterising the desired solution locally on each mesh element. This parameterised solution converts a continuous PDE problem to a coupled system of ordinary differential equations that can be integrated in time. For multiple devices system, FEM explicit dynamical simulations are computationally intensive, making them difficult to use when a large number of simulations are needed (Hung et al 1997)

(Hung and Senturia 1999).

The flow inside these channels can be represented mathematically by a partial differential equation involving the spatial variables, x y and z, as well as time. There is no closed-form analytical solution.

Another problem is in the modelling of fluid flow in expanding or contracting microchannels. The flow in these configurations is complicated, with variations in pressure and velocity in all the spatial directions as well as time. If the aperture angle of the diffuser is greater than a certain limit, than the flow changes dramatically, from steady laminar to turbulence.

3.2 HYPOTHESIS

Finite element method can solve complex partial differential equations, providing detailed solution but it involves meshing the system into small elements and is therefore time-consuming and labour intensive which can inflate the overall cost of design and manufacture. If faster approximations of the flow of fluid in microdevices can be found, then this research will contribute towards the development of a MEMS interactive, animated VR prototyping software package, which in turn contributes to faster, easier design of MEMS. One proposition is that one should be able to obtain an approximate solution without the need for complicated meshing and iterating the steps innumerably.

It is believed that one is able to apply the concept of system analysis to model the flow of the fluid in a micropump by decomposing the device into simpler components. The behaviour of each of these components will be represented by equations encapsulated in block diagrams. Block diagram modelling can be used to model the dynamic behaviour of the system under consideration.

Another hypothesis is that fluid flow is similar to electric current flow, so circuit models and the laws that govern the relationships between the voltages and currents in a circuit can be applied to systems involving fluid flow.

3.3 PROPOSED SOLUTION

In order to visualise the flow in a micropump for example, the user of our CAD, MAGDA first needs to design the device using the drawing board (Kellermann 2003). Our VR structures make use of the concept of "transparency" to show the fluid flow inside the micropump. The user is able to zoom in the image and see the fluid in detail. Once the design is done, the user has to incorporate its functionality using the Simulink interface where there are blocks representing the components of the device, in this case, valves, channels, diffusers, nozzles etc. The underlying models for these blocks are the flow equations that will be derived in this thesis. However, this thesis is not about software development. Not all the Simulink interface is implemented because it is not the purpose of this thesis to write code, but to derive the models. A programmer does the Simulink implementation.

For this thesis a systematic analysis of the modelling of fluid flow in microdevices such as the micropump is carried out. The different components of the micropump are analysed individually and one of these is the microchannel, which is an important constituent of many microdevices. These channels can have constant cross-sectional area or they can have expanding area as in diffusers or contracting area as in nozzles. In finite element modelling, the structure is divided up into elements, often in geometrical shapes such as squares, hexagon or triangle. For each element a local approximate solution is obtained and from the many local solutions, the global solution can be approximated. For this project, taking advantage of the fact that the fluid flow occurs in streamlines, the flow region is divided up into layers instead of tiny elements. There is no solution iteration to be done. The flow rate and hence velocity of each of these layers is then calculated directly.

Using the similarity between electric current flow in circuits and fluid flow in pipe systems, the concept of circuit modelling is used to calculate the flow of the layers of fluid in the channels, diffusers and nozzles. Further, the behaviour of the fluid as it enters the channel is studied using the analogy of transient response of RL circuits.

CHAPTER 4: BASIC THEORY

4.1 THE CONTINUUM MODEL

Although fluids are composed of tiny indivisible particles or molecules, constantly in motion, we are usually interested in the average or macroscopic effects of the molecules. The fluid is treated as an infinitely divisible substance, a continuum. Each fluid property is assumed to have a definite value at every point in space. Properties such as pressure, velocity and density are considered to be continuous functions of position and time.

4.1.1 GOVERNING EQUATIONS

The governing equations in the continuum model are derived from the fundamental physical laws of conservation of mass, momentum and energy. From the basic principle that matter can neither be created nor destroyed, we obtain the continuity equation, and from the conservation of momentum, the Navier-Stokes equation and the conservation of energy, the energy equation is derived. The parameter of concern in this thesis is the calculation of volume flow rates of the devices and this is carried out by using the continuity equation and the Navier-Stokes equation. Since temperature is not taken into consideration, the energy equation is not used.

4.1.1.1 CONTINUITY EQUATION

We consider a closed, fixed and finite volume $\forall$ within a finite flow region, with the control surface S defined as the surface surrounding the volume. Refer to Figure 4-1. Since mass is conserved, the increase in mass within the control volume is due to the net flow of fluid moving through the control surface. The mass conservation equation in differential form, also known as the continuity equation, is given by:

$$\frac{\partial \rho}{\partial t} + \nabla \cdot (\rho \vec{V}) = 0 \qquad (4\text{-}1)$$

where the vector differential operator del is defined as

$$\nabla \equiv i_x \frac{\partial}{\partial x} + i_y \frac{\partial}{\partial y} + i_z \frac{\partial}{\partial z},$$

ρ is the density of the fluid, t is time and $\vec{V}$ is the flow velocity

The integral form of the conservation of mass equation is given by:

$$\frac{\partial}{\partial t} \iiint_{\upsilon} \rho d\forall + \iint_{s} \rho \vec{V} \cdot \vec{n} dS = 0 \qquad (4\text{-}2)$$

where $d\forall$ is the elemental volume inside the finite control volume, $\vec{n}$ the unit vector normal to the surface and dS is the elemental surface area..

For both the above equations, the first term represents the rate of change of mass within the control volume and the second term represents the net rate of mass flux out through the control surface. For incompressible flow, the rate of density change of the fluid particle remains constant along a particle path. In this case, the first term is negligible compared with the components of the second terms. (Fay 1994). The equation of mass conservation becomes:

$$\nabla \cdot \vec{V} = 0 \qquad (4\text{-}3)$$

Once the volume through the control surface is determined, we can obtain the volume flow rate which is defined as the volume of fluid flowing per unit time across the control surface. The volume flow rate Q is given by the equation:

$$Q = \iint \vec{V} \cdot \vec{n} dS \qquad (4\text{-}4)$$

where $\vec{V}$ is the velocity vector, $\vec{n}$ is the unit vector normal to the surface and dS is the elemental surface area.

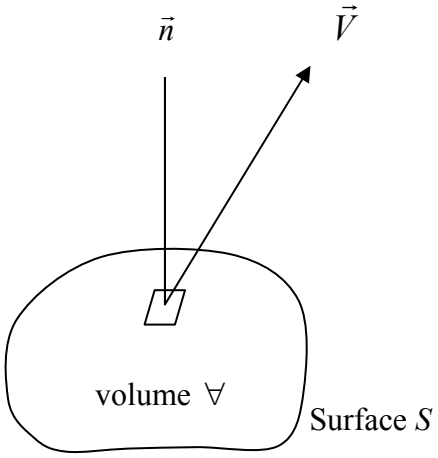

Figure 4-1 Finite control volume fixed in space

4.1.1.2 NAVIER-STOKES EQUATION

The Conservation of Momentum equations, also known as the Navier-Stokes equations, are derived from the Newton's second law: F = ma. The vector form of the Navier-Stokes equation of motion for an incompressible fluid is given by:

$$\frac{\partial \vec{V}}{\partial t} + \left(\vec{V} \cdot \nabla\right)\vec{V} = -\frac{1}{\rho}\nabla p + \vec{g} + \nu\nabla^2\vec{V} \qquad (4\text{-}5)$$

where $\vec{V}$ is the velocity vector, t is time, p is pressure, ρ is the density of the fluid, $\vec{g}$ is the gravitational acceleration and ν is the kinematic viscosity of the fluid, which is the ratio of absolute viscosity to density (i.e. $\nu = \mu/\rho$).

For convenience, a new variable $p^* \equiv p - \rho\vec{g} \cdot \vec{R}_i$, where $\vec{R}_i$ is the position vector, is used and the Navier-Stokes equation for an incompressible, inviscid flow becomes: (Fay 1994)

$$\frac{\partial \vec{V}}{\partial t} + \left(\vec{V} \cdot \nabla\right)\vec{V} = -\frac{1}{\rho}\nabla p^* + \nu\nabla^2\vec{V} \quad \text{if } \rho, \mu = \text{const} \qquad (4\text{-}6)$$

The terms on the left-hand side represents the acceleration of the fluid and can be

represented by the shorthand notation $D\vec{V}/Dt$. So equation (4-6) becomes:

$$\frac{D\vec{V}}{Dt} = -\frac{1}{\rho}\nabla p^* + \nu\nabla^2\vec{V} \tag{4-7}$$

The operator D/Dt is known as the substantial derivative operator. Physically, it is the time rate of change following a moving fluid element. It is composed of the local derivative, $\partial/\partial t$, which is physically the time rate of change at a fixed point, and the convective derivative, $\vec{V}\cdot\nabla$, which is physically the time rate of change due to the movement of the fluid element from one location to another in the flow field where the flow properties are spatially different. The substantial derivative applies to any flow-field variable. If, as in this case, the variable is velocity, the left hand term of equation (4-7) means that the velocity of the fluid element is changing as the element moves past a point in the flow field because at that point the flow field velocity itself may be fluctuating with time (the local derivative) and also the fluid element is on its way to another point in the flow where the velocity is different (the convective derivative). (Anderson 1996)

In cartesian coordinates, the x, y and z components of the Navier-Stokes equation are given by (Fay 1994):

$$\frac{\partial u}{\partial t} + u\frac{\partial u}{\partial x} + \upsilon\frac{\partial u}{\partial y} + w\frac{\partial u}{\partial z} = -\frac{1}{\rho}\frac{\partial p^*}{\partial x} + \nu\left(\frac{\partial^2 u}{\partial x^2} + \frac{\partial^2 u}{\partial y^2} + \frac{\partial^2 u}{\partial z^2}\right) \tag{4-8}$$

$$\frac{\partial \upsilon}{\partial t} + u\frac{\partial \upsilon}{\partial x} + \upsilon\frac{\partial \upsilon}{\partial y} + w\frac{\partial \upsilon}{\partial z} = -\frac{1}{\rho}\frac{\partial p^*}{\partial y} + \nu\left(\frac{\partial^2 \upsilon}{\partial x^2} + \frac{\partial^2 \upsilon}{\partial y^2} + \frac{\partial^2 \upsilon}{\partial z^2}\right) \tag{4-9}$$

$$\frac{\partial w}{\partial t} + u\frac{\partial w}{\partial x} + \upsilon\frac{\partial w}{\partial y} + w\frac{\partial w}{\partial z} = -\frac{1}{\rho}\frac{\partial p^*}{\partial z} + \nu\left(\frac{\partial^2 w}{\partial x^2} + \frac{\partial^2 w}{\partial y^2} + \frac{\partial^2 w}{\partial z^2}\right) \tag{4-10}$$

In cylindrical coordinates, the components in the radial (i_r), tangential (i_θ) and axial directions (i_z) are given by (Fay 1994):

$$\left(\frac{\partial V_r}{\partial t}+V_r\frac{\partial V_r}{\partial r}+\frac{V_\theta}{r}\frac{\partial V_r}{\partial \theta}+V_z\frac{\partial V_r}{\partial z}-\frac{V_\theta^2}{r}\right)$$
$$=-\frac{1}{\rho}\frac{\partial p^*}{\partial r}+\nu\left[\frac{\partial^2 V_r}{\partial r^2}+\frac{1}{r}\left(\frac{\partial V_r}{\partial r}\right)+\frac{1}{r^2}\left(\frac{\partial^2 V_r}{\partial \theta^2}\right)+\frac{\partial^2 V_r}{\partial z^2}-\frac{V_r}{r^2}-\frac{2}{r^2}\left(\frac{\partial V_\theta}{\partial \theta}\right)\right] \tag{4-11}$$

$$\left(\frac{\partial V_\theta}{\partial t}+V_r\frac{\partial V_\theta}{\partial r}+\frac{V_\theta}{r}\frac{\partial V_\theta}{\partial \theta}+V_z\frac{\partial V_\theta}{\partial z}-\frac{V_\theta V_r}{r}\right)$$
$$=-\frac{1}{\rho r}\frac{\partial p^*}{\partial \theta}+\nu\left[\frac{\partial^2 V_\theta}{\partial r^2}+\frac{1}{r}\left(\frac{\partial V_\theta}{\partial r}\right)+\frac{1}{r^2}\left(\frac{\partial^2 V_r}{\partial \theta^2}\right)+\frac{\partial^2 V_\theta}{\partial z^2}-\frac{V_\theta}{r^2}+\frac{2}{r^2}\left(\frac{\partial V_r}{\partial \theta}\right)\right] \tag{4-12}$$

$$\left(\frac{\partial V_z}{\partial t}+V_r\frac{\partial V_z}{\partial r}+\frac{V_\theta}{r}\frac{\partial V_z}{\partial \theta}+V_z\frac{\partial V_z}{\partial z}\right)$$
$$=-\frac{1}{\rho}\frac{\partial p^*}{\partial z}+\nu\left[\frac{\partial^2 V_z}{\partial r^2}+\frac{1}{r}\left(\frac{\partial V_z}{\partial r}\right)+\frac{1}{r^2}\left(\frac{\partial^2 V_z}{\partial \theta^2}\right)+\frac{\partial^2 V_z}{\partial z^2}\right] \tag{4-13}$$

4.1.1.3 HEAD LOSS

As a fluid flows through a channel, energy is irreversibly converted to unwanted thermal energy and loss of energy via heat transfer. For viscous fluid flow, heat loss is mainly due to friction. As the fluid passes from one section, A, to another section B, the difference in the mechanical energy of the fluid at these two positions gives the total head loss. Energy losses can be classified into two groups: major losses and minor losses. Major losses are due to frictional effects and minor losses due to entrances, fittings, area changes, valves etc. For laminar flow through a microchannel, the energy loss is given by (White, F. 1994):

$$h_f=\frac{64\mu}{2\rho g}V\sum_i\frac{\ell_i}{d_i^2} \tag{4-14}$$

where μ is the fluid viscosity, ρ is the density of the fluid, ℓ is the length of the channel, d is the diameter of the channel and V is the average velocity. Head loss has the dimensions of

energy per unit mass [$f\ell / m$], which is equivalent to dimensions of [ℓ^2 / t^2], where f is force, m is mass, ℓ is length and t is time.

Minor losses are due to changes in the shape or size of the microchannel, resulting in flow separation. Energy is dissipated by violent mixing in the separated zones. The minor head loss is given by:

$$h_m = \frac{V^2}{2} \sum_i K_i \qquad (4\text{-}15)$$

where *K,* a dimensionless constant determined experimentally, is the loss coefficient in the singularities.

The values of *K* are given in table below: (Bendib and Français 2001)

Table 4-1 Loss Coefficients (K) for the changes in microchannel shape and size. (Bendib and Français 2001)

SINGULARITIES	K	
expansion	$(\beta - 1)^2$ where β = a/A, a is small cross-section, A is large cross-section	
contraction	$\left(\frac{1}{0.59 + 0.41\beta^2} - 1\right)^2$	
bends	circular 90^0	0.4 to 0.9
	square 90^0	1.3 to 1.9

Figure 4-2 Changes in shape of a microchannel flow: (a) expansion (b) contraction (c) 90° square bend and (d) 90° circular bend

4.1.1.4 STARTING FLOW IN A CIRCULAR CHANNEL

For fluid flowing in unsteady manner, i.e. dependent on time, in a circular channel the Navier-Stokes equation (4.6) in cylindrical coordinates becomes:

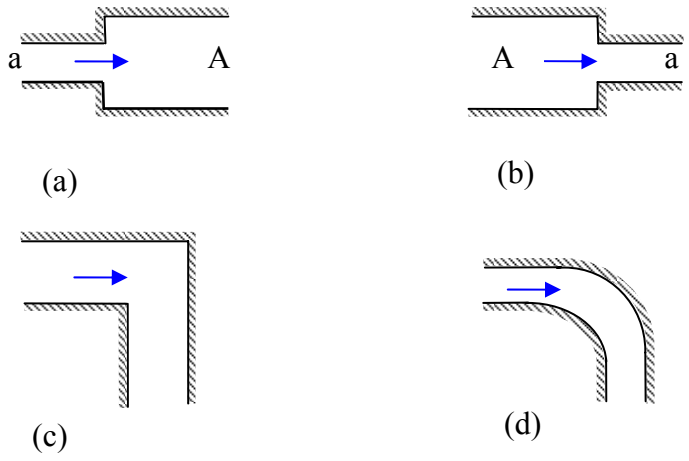

$$\frac{\partial u}{\partial t} = -\frac{1}{\rho}\frac{dp}{dx} + \nu\left(\frac{\partial^2 u}{\partial r^2} + \frac{1}{r}\frac{\partial u}{\partial r}\right) \tag{4-16}$$

The fluid is initially at rest at $t = 0$. A sudden, uniform and constant pressure gradient dp/dx is applied. The problem for this starting-flow equation was solved by Szymanski

(1932), as mentioned in (White, F 1991), and is given by :

$$\frac{u}{u_{\max}} = \left(1 - r^{*2}\right) - \sum_{n=1}^{\infty} \frac{8J_o\left(\lambda_n r^*\right)}{\lambda_n^3 J_1\left(\lambda_n\right)} \exp\left(-\lambda_n^2 \frac{\nu t}{r_o^2}\right) \qquad (4\text{-}17)$$

where $u_{\max} = \left(-\frac{dp}{dx}\right)\frac{r_o^2}{4\mu}$, $r^* = \frac{r}{r_o}$ and

where J_0 denotes the Bessel function of the first kind, λn the roots of the Bessel function, r_o the channel's radius, r* the dimensionless radius.(White, F. 1991). The velocity profiles for the starting flow in a channel is shown in Figure 4-3.

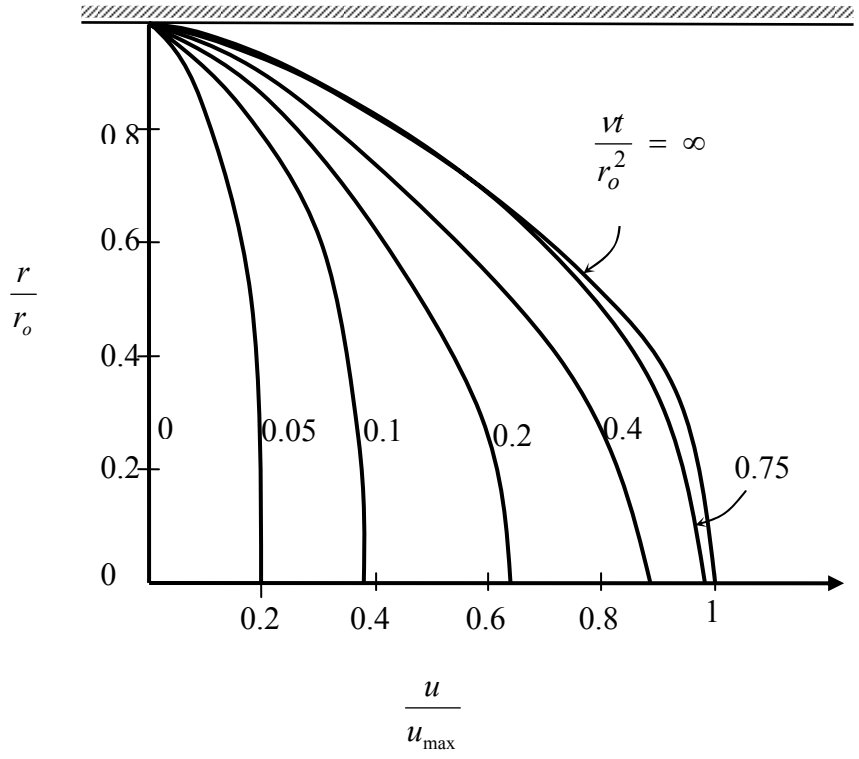

Figure 4-3 Instantaneous velocity profiles for starting flow in a channel (White, F. 1991).

4.2 FLUID FLOW IN MICRODEVICES

In macroscopic scale, liquid flow in a pipe can be laminar, transitional or turbulent, depending on the Reynolds number Re. This number is the ratio of inertial forces to viscous forces and is given by:

$$\mathrm{Re} = \frac{\rho V D}{\mu} \qquad (4\text{-}18)$$

where D is the characteristic dimension of the pipe or device. When the Re is small (less than 2100), the flow is laminar and when it increases the flow reaches a transitional phase where the flow is partly laminar with intermittent bursts of irregular behaviour. When the Re is further increased (above 4000), the flow becomes turbulent, having random fluctuations with particle mixing. The velocity has unsteady components normal to the channel axis as well as the predominant component along the channel (Munson et al 1998). For microdevices, which has dimensions in the order of microns, the Re is very small (less than 1), even if the velocity is not. The flow is laminar, moving in smooth streamlines. It is rarely turbulent.

In this analysis, only liquid flow is considered, so compressibility effect is neglected. The flow is treated as incompressible flow. In incompressible flow, density is constant with respect to pressure as well as temperature. Although density is sensitive to temperature changes, in this analysis the temperature is considered as a constant. The flow is further restricted to Newtonian fluid, specifically water, in which case the viscosity is constant.

4.2.1 MICROCHANNELS

As a fluid enters a microchannel, it undergoes two distinct regions of flow. In the beginning, it goes through the entrance region where the flow profile undergoes changes from flat shape to a more rounded and eventually to the characteristic parabolic shape. Once it reaches this position where the profile is parabolic, it is in the fully developed region of the flow. Refer to Figure 4-4.

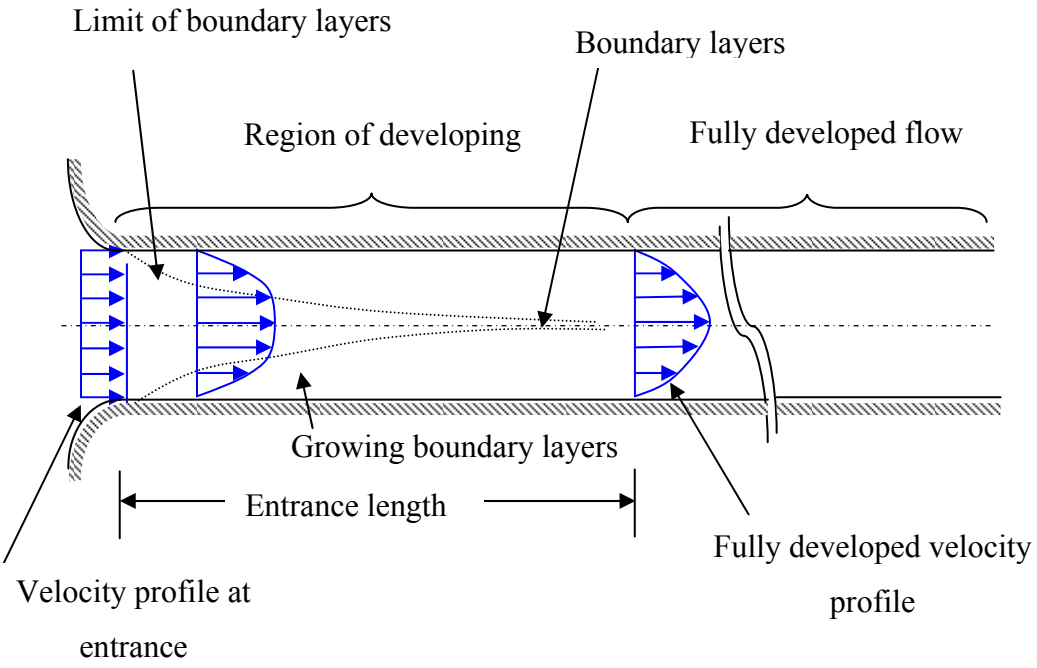

Figure 4-4 Developing velocity profiles from the entrance region to the fully developed region in a microchannel.

4.2.1.1 ENTRANCE REGION

The entrance region of a microchannel is one in which the flow is not fully developed. It is also know as the inlet flow region. The length from the inlet to the fully developed flow region is known as the entrance length. For a circular duct, the entrance length L_{FD} is given by (Shah and London 1978) in (Schetz 1993):

$$\frac{L_{FD}}{D} = \frac{0.6}{1 + 0.035\ \mathrm{Re}} + 0.056\ \mathrm{Re} \qquad (4\text{-}19)$$

If the entrance is well-rounded, the velocity profile is nearly uniform. As the fluid enters the channel, boundary layers form at the entrance. Fluid at the walls of the channel slows down while the fluid in the centre accelerates, according to the continuity law. Due to viscous effects, the boundary layers thicken downstream, join together until the channel is filled with these boundary layers. At a certain position in the channel, x_L , the flow profile develops into a parabolic shape. There is an excess pressure drop across the entrance

length due to the increased shear forces in the entrance boundary layers as well as the acceleration of the core.

4.2.1.2 FULLY DEVELOPED LAMINAR FLOW

Once the fluid enters this fully developed region, the velocity flow profile remains the same parabolic shape. The pressure gradient is constant throughout this region. The velocity profile and pressure gradient is independent of the inlet conditions.

The flow rate for laminar flow in a circular pipe is given by the Hagen-Poiseuille equation (Zengerle and Richter 1994):

$$Q = \frac{\pi r^4}{8\mu\ell} \Delta p \qquad (4\text{-}20)$$

where r is the radius of the pipe, ℓ is its length, Δp is the applied pressure difference and μ is the viscosity of the fluid. Although equation (4-21) is for circular pipe, it can be applied to channels with square as well as rectangular cross-sectional areas of aspect ratios close to 1 if the radius is replaced by hydraulic diameter D_h given by:

$$D_h = \frac{4bh}{2(b + h)} \qquad (4\text{-}21)$$

where b is the width of the cross-section and h is the height.

4.2.2 DIFFUSERS AND NOZZLES

Nozzles and diffusers form part of the non-moving part micropump, acting as passive valves. Passive valves aim to have the fluid flow in one direction only. It should ideally have zero resistance in one direction and infinite resistance in the other direction. Nozzles are channels that have slowly converging walls while diffusers have gradually expanding walls.

Diffusers were designed to increase pressure and reduce kinetic energy. As a fluid enters the diffuser, its flow velocity decreases and the static pressure increases. Diffusers can be conical, pyramidal or planar. The flow in a diffuser is complex and is dependent on several factors such as the diffuser's geometric parameters, inlet Reynolds number, inlet boundary-

layer blockage factor, inlet turbulence, and pulsations.

The three most important parameters of diffusers and nozzles are area ratio, angle and inlet boundary-layer blockage factor $B_t=A_{BL}/A_1$, where A_{BL} is the wall area blocked or displaced by the retarded boundary-layer flow in inlet. Its performance decreases with blockage. (White, F. 1994)

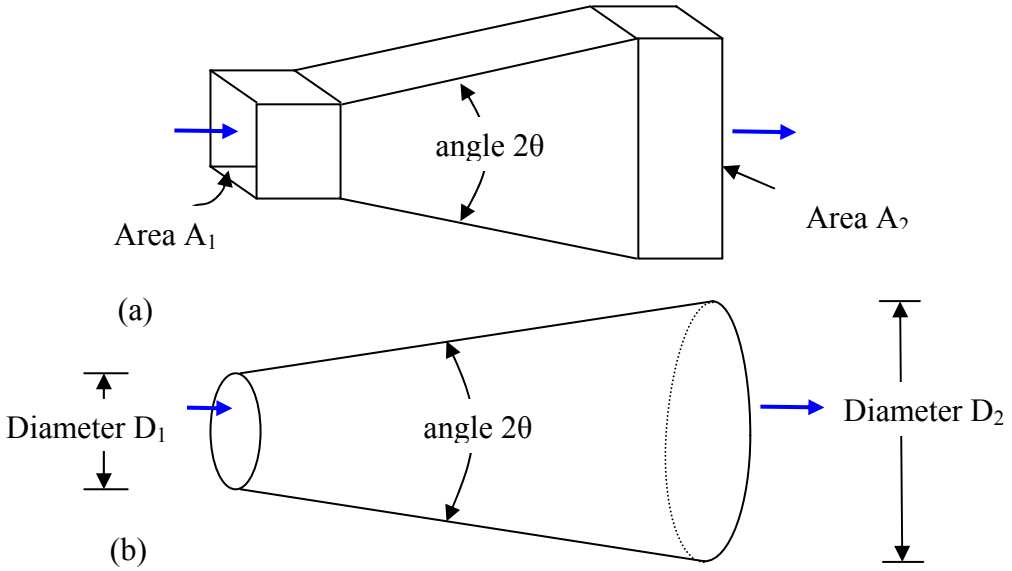

Figure 4-5 Geometry of: (a) a flat-walled diffuser and (b) a conical diffuser

4.2.2.1 NOZZLES

Nozzles transform pressure energy into kinetic energy. As a fluid goes through a nozzle, its flow velocity increases while its static pressure along the axis decreases. The fluid accelerates through the nozzle and the inlet velocity profile distortions become smoothed. Since the pressure decreases and the length is too short, fully developed flow cannot form in the nozzle. The effect of friction and turbulence are also reduced.(Schetz and Fuhs 1999)

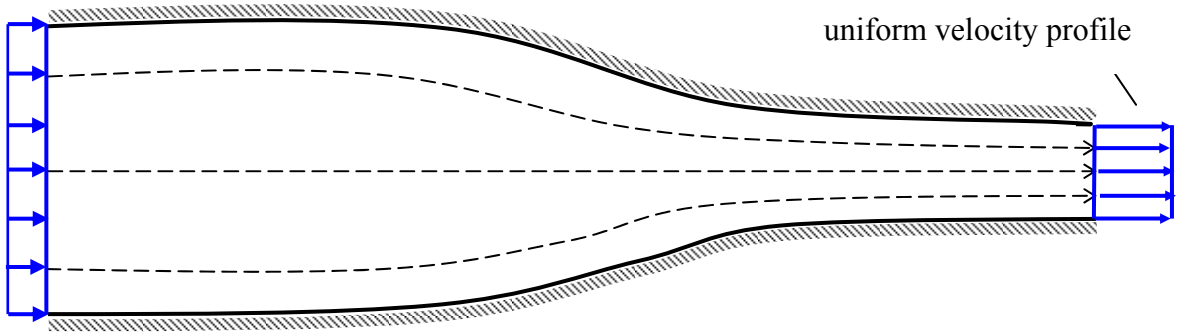

Figure 4-6 Nozzle flow

4.2.2.2 DIFFUSERS

Diffusers transform kinetic energy into pressure energy. Since the velocity decreases and the pressure increases in the flow direction, boundary layer separation can occur at the wall, especially when the area ratio between inlet and outlet A_2/A_1 is large. The fluid particles are moving through higher pressure area. If the Reynolds number is large, a boundary layer forms close to the wall where the particles velocity is smaller than the average velocity, due to dissipation. As they move further in, the pressure increases until they reach a point at which they can no longer advance and will eventually flow backwards. This form a boundary layer separation where vortices form and are kept in motion by friction stresses and by turbulent stresses exerted by the unseparated flow. This separated flow is usually unsteady. As for the particles in the unaffected core, they are in effect flowing in a smaller cross-section of the channel, experiencing a smaller pressure increase than expected. The friction stresses experienced by the separated flow leads to additional pressure loss. The ratio of the actual pressure increase to that of the theoretical pressure increase is the diffuser efficiency and is given by (Spurk 1997):

$$\eta_D = \frac{(p_2 - p_1)_{real}}{(p_2 - p_1)_{ideal}} \tag{4-22}$$

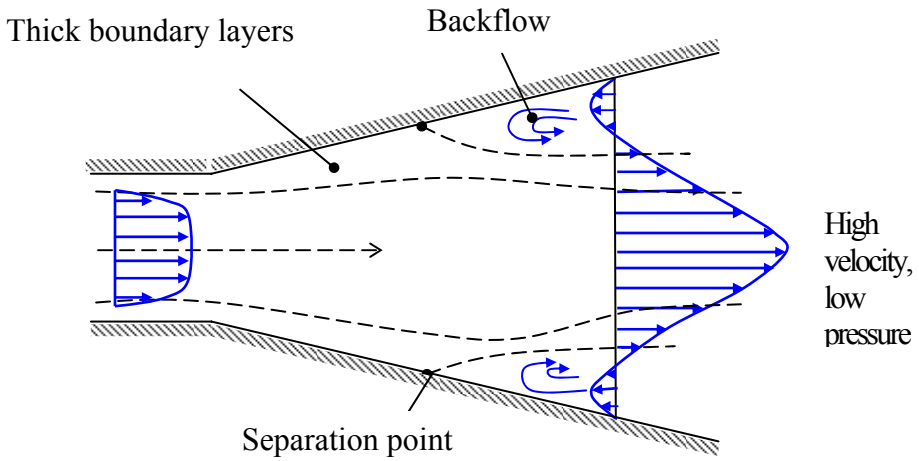

Figure 4-7 Boundary layer separation in a diffuser

4.2.3 EQUIVALENT ELECTRIC CIRCUIT MODELLING

An electrical circuit network is used in the modelling of the layered fluid flow for the purpose of the MAGDA implementation. This arises out of the concept of systems similarity, where physically different systems such as mechanical, fluidic, thermal or electrical, result in similar differential equation and similar response behaviour. Systems similarity is based on the concept of effort and flow variables. (Woods and Lawrence 1997)

The effort variable is the across variable of the system which represents potential or the ability to do work. In mechanical systems, the effort variable is force. In electrical systems, the effort variable is the voltage. In thermal systems the effort is temperature and in fluidic systems it is pressure.

The flow variable is the through variable of the system which represents the rate at which work can be done. It is the variable that changes with time. In mechanical system, the flow variable is velocity, in electrical system it is current, in thermal system the variable is heat

flow and in fluidic system it is volume flow rate.

From the effort and flow variable, one can obtain the impedance which is the ratio of the effort to flow. Impedance can be static, as in the case of resistance, or dynamic, as in capacitance and inductance. Effort = impedance x flow.
Capacitance, inductance and resistance are the passive components in an electric circuit.

For an electric system, the effort variable of the system represents the across variable (voltage) and the flow variable represents the through variable (current). This is known as the e→V convention (Senturia 2001). In this convention, the potential energy is associated with energy storage in capacitors. For fluidic system, the e→V convention assigns pressure (effort) as the across variable, analogous to voltage, and the volume flow rate (flow) as the through variable, analogous to current. For mechanical system, the e→V convention assigns force to voltage, velocity to current and displacement to electric charge. Refer to Table 4-2.

Table 4-2 Generalized variables for electrical, fluidic and mechanical systems using the e→V convention. (Senturia 2001)

Energy Domain	**Effort**	**Flow**	**Momentum**	**Displacement**
Electric Circuits	Voltage	Current	…	Charge
Incompressible fluid flow	Pressure	Volumetric flow	Pressure momentum	Volume
Mechanical translation	Force, F	Velocity, υ	Momentum,	Position

In f→V convention, the velocity (flow) is the across variable, and force (effort) is the through variable. In HDL convention, the across variable of a mechanical system is displacement while the through variable is force. (Romanowicz 1998)

CHAPTER 5: DERIVATION OF LAYERED FLOW MODEL

Fluid flow in MEMS devices is usually laminar, that is, following smooth streamlines and is seldom turbulent. The Reynolds number of the flow is less than 1, and inertial forces are negligible compared to viscous forces, which are more dominant. Since the speed of sound is quite high in liquid, the flow velocities seldom approach this speed.

5.1 MICROCHANNELS

This section discusses how the resistances of the layers of fluid in the circular and rectangular microchannels are derived. The flow region is divided into several layers. In order to determine the equivalent resistances of each layer, the velocity distribution need to be determined first. This is carried out by solving the Navier-Stokes equation in the appropriate coordinate system. For the case of the circular microchannel, the resistance is derived analytically using the Navier-Stokes equation in cylindrical coordinates. For the rectangular one, a numerical technique is employed using the Navier-Stokes equation in cartesian coordinates. The flow rates for each of the layers can be obtained from the velocity distribution. From these, the resistances can then be determined.

In this analysis, it is assumed that the flow is laminar, i.e. in smooth streamlines with no turbulence, that the fluid is incompressible, i.e. its density does not change along the streamline under consideration, and that the velocity of the fluid at the walls of the microchannel is zero (non-slip boundary condition). The flow of the fluid is driven by a pressure difference between the entrance and the exit. Assuming that the fluid flows from a region of higher pressure at the entrance, to a region of lower pressure at the exit, then the pressure gradient, $\partial p/\partial z$, is negative. The flow is steady, that is, the velocity does not change with respect to time. This type of flow is known as Poiseuille flow.

5.1.1 CIRCULAR

The Navier-Stokes equation in cylindrical coordinates is given by equations (4-11 – 4-13). Assuming that the steady is flow means that there is no acceleration. So the left-hand terms equal to zero.

Since the flow is laminar, the streamlines of the flow are all parallel to the channel axis. So the fluid velocity components in the radial and tangential directions are zero i.e. $V_r, V_\theta = 0$. The axial velocity component, V_z, depends only on the radial coordinate r. The equation simplify to:

$$\frac{\partial^2 V_z}{\partial r^2} + \frac{1}{r}\left(\frac{\partial V_z}{\partial r}\right) - \frac{1}{\mu}\frac{\partial p^*}{\partial z} = 0 \qquad (5\text{-}1)$$

where $p^* \equiv p - \rho\vec{g} \cdot \vec{R}_i$, $\vec{R}_i$ is the position vector and $\vec{g}$ is the gravitational acceleration.

Since V_z is a function of the radial distance *r* alone and p^* is a function of axial distance *z* alone, we can use total derivatives instead of partial derivatives. In horizontal microchannel flow, the effect of gravity is negligible, so *p** becomes *p*. The above equation then simplifies to:

$$\frac{d^2 V_z}{dr^2} + \frac{1}{r}\frac{dV_z}{dr} = \frac{1}{\mu}\frac{dp}{dz} \qquad (5\text{-}2)$$

Integrating the above equation once:

$$r\frac{dV_z}{dr} = \frac{r^2}{2\mu}\frac{dp}{dz} + k_1 \qquad (5\text{-}3)$$

where k_1 is the constant of integration.

At the centreline, $r = 0, \frac{dV_z}{dr} = 0$ so $k_1 = 0$

Dividing equation (5-3) by r, it becomes,

$$\frac{dV_z}{dr} = \frac{r}{2\mu}\frac{dp}{dz} \qquad (5\text{-}4)$$

Integrating equation (5-4),

$$V_z = \frac{r^2}{4\mu}\frac{dp}{dz} + k_2 \tag{5-5}$$

where k_2 is the constant of integration.

It is assumed that at the walls, where $r = a$, the velocity of the fluid is zero, i.e. $V_z = 0$. This is known as the non-slip boundary condition. Applying this condition to equation (5-5), then

$$k_2 = \frac{a^2}{4\mu}\frac{dp}{dz} \tag{5-6}$$

By substituting equation (5-6) into equation (5-5), the solution to the differential equation is obtained:

$$V_z = \frac{a^2 - r^2}{4\mu}\left(-\frac{dp}{dz}\right) \tag{5-7}$$

where a is the radius of the channel, μ is the viscosity of the fluid and p is the hydrostatic pressure.

The volumetric flow rate Q is found by integrating the velocity distribution, equation (5-7), across the cross-sectional area of the microchannel:

$$Q = \int_{\text{sec } tion} V_z dA \tag{5-8}$$

For the total flow rate, the integration is from 0 to a, the radius of the channel:

$$Q_{total} = \int_0^a V_r (2\pi r) dr \tag{5-9}$$

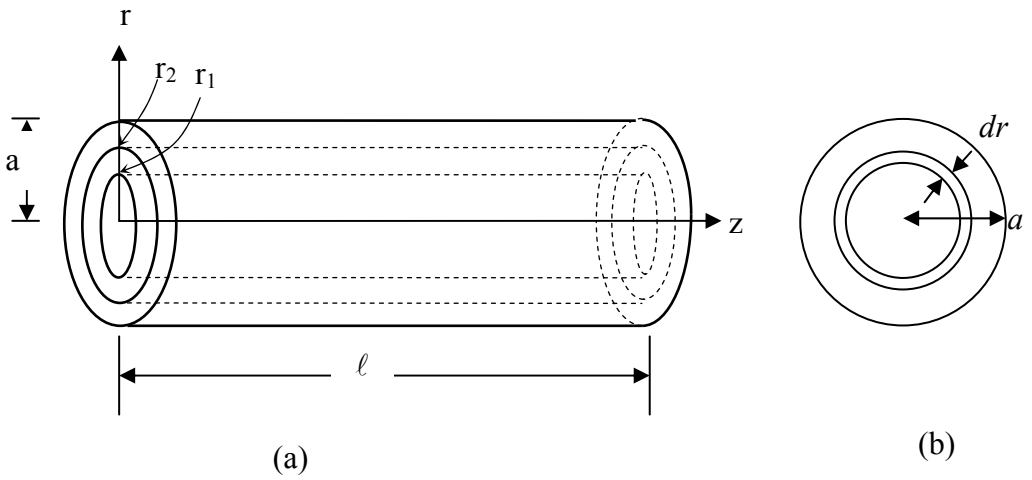

Figure 5-1 Layers in the circular microchannel flow in: (a) longitudinal and (b) cross-sectional views.

If the microchannel of length ℓ and radius a is divided into annular layers of width dr, the flow rate Q_{layer} of each layer (refer to Figure 5-1) is obtained by substituting equation (5-7) into (5-9) and integrating from r_1 to r_2:

$$Q_{layer} = \frac{\pi}{2\mu}\left(-\frac{dp}{dz}\right)\int_{r_1}^{r_2} r\left(a^2 - r^2\right)dr \tag{5-10}$$

$$= \frac{\pi}{2\mu}\left(-\frac{dp}{dz}\right)\left|\frac{r^2a^2}{2} - \frac{r^4}{4}\right|_{r_1}^{r_2} \tag{5-11}$$

$$= \frac{\pi}{2\mu}\left(-\frac{dp}{dz}\right)\left[\left(a^2\,\frac{r_2^2}{2} - \frac{r_2^4}{4}\right) - \left(a^2\,\frac{r_1^2}{2} - \frac{r_1^4}{4}\right)\right] \tag{5-12}$$

$$= \frac{\pi}{8\mu}\left(-\frac{dp}{dz}\right)\left[2a^2\left(r_2^2 - r_1^2\right) - \left(r_2^4 - r_1^4\right)\right] \tag{5-13}$$

where r_1 and r_2 are the inner and outer radii of the layers.

For the lumped-element model of the mechanical effect of Poiseuille flow, using e→V (effort→voltage) convention as explained in Section 4.2.3, the resistance is given by (Senturia 2001):

$$R = \frac{\Delta p}{Q} \tag{5-14}$$

where the resistance is the ratio between the effort (or across) variable, pressure difference, to the flow (or through) variable, volume flow rate. Refer to Section 4.2.3.

The resistance for each layer can be determined by using equation (5-14). Since p depends only on z and does not depend on r or θ, so dp/dz is a constant. By rearranging the terms, equation (5-13) becomes:

$$\frac{\Delta p}{Q_{layer}} = \frac{8\mu\ell}{\pi\left[2a^2\left(r_2^2 - r_1^2\right) - \left(r_2^4 - r_1^4\right)\right]} \tag{5-15}$$

where Δp is the pressure difference between the entrance and exit of the microchannel and ℓ is its length. Substituting equation (5-14) into equation (5-15), the resistance for each layer is given by (Aumeerally and Sitte 2003, 2006):

$$R_{layer} = \frac{8\mu\ell}{\pi\left[2a^2\left(r_2^2 - r_1^2\right) - \left(r_2^4 - r_1^4\right)\right]} \tag{5-16}$$

where the absolute viscosity has the units $\frac{kg}{(m \cdot s)}$ or $Pa \cdot s$; the length is in m, radius in m and the resistance in $km/\left(m^4 \cdot s\right)$ or $Pa/\left(m^3/s\right)$

5.1.2 RECTANGULAR

To determine the equivalent resistance for flow in a rectangular microchannel (see Figure 5-2), a numerical approach is used. The Navier-Stokes equation in cartesian coordinates is given by equations (4.8) to (4.10). Assuming laminar flow, the velocity is a function of z only. There are no components of the velocity in the x- and y-directions. If w is the component of the velocity in z-direction, equation (4-10) is:

$$\frac{\partial w}{\partial t} + u\frac{\partial w}{\partial x} + \upsilon\frac{\partial w}{\partial y} + w\frac{\partial w}{\partial z} = -\frac{1}{\rho}\frac{\partial p^*}{\partial z} + \nu\left(\frac{\partial^2 w}{\partial x^2} + \frac{\partial^2 w}{\partial y^2} + \frac{\partial^2 w}{\partial z^2}\right),$$

Since the flow is steady, the left-hand terms which represent the acceleration are zero. For horizontal flow in microchannels, the gravitational effect is negligible, so p^* is substituted by p. Using $\nu = \mu/\rho$, therefore the equation simplifies to:

$$\frac{\partial^2 w}{\partial x^2} + \frac{\partial^2 w}{\partial y^2} = -\frac{1}{\mu}\frac{\partial p}{\partial z} \tag{5-17}$$

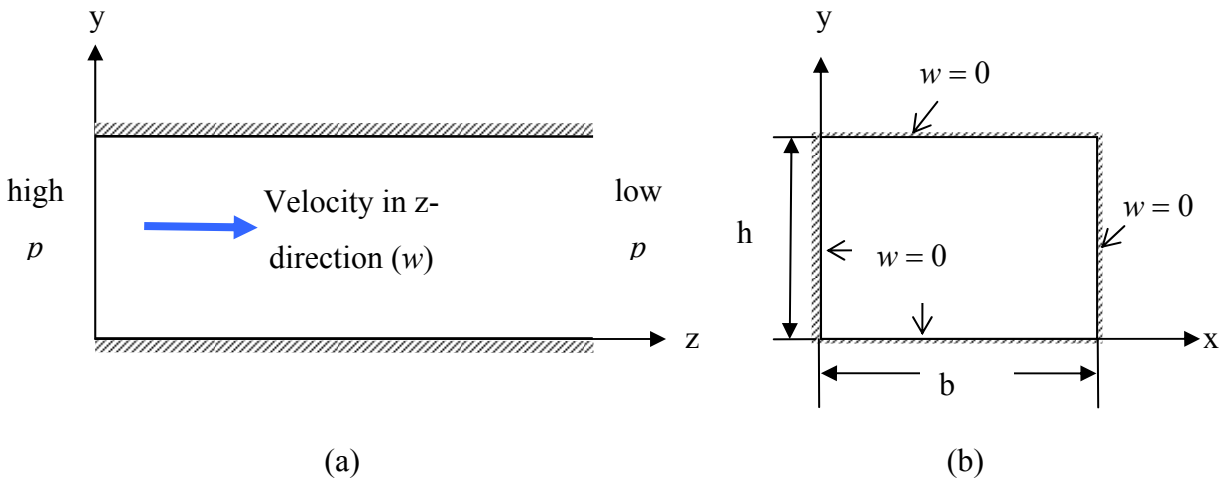

Figure 5-2 Rectangular microchannel in: (a) longitudinal and (b) cross-sectional view

The above equation can be simplified by nondimensionalising the velocity. This is done by substituting the following variable into the equation:

$$w^* = \left[\frac{\mu}{-\frac{dp}{dz}}\right] w, \tag{5-18}$$

We then obtain the Poisson's equation:

$$\frac{\partial^2 w^*}{\partial x^2} + \frac{\partial^2 w^*}{\partial y^2} = -1 \tag{5-19}$$

for $0 \le x \le b$ and $0 \le y \le h$, where b is the width and h is the height of the cross-section of the microchannel.

Equation (5-19) is an elliptic partial differential equation and to solve it computationally, a discrete form has to be used. Using a 5-point finite difference formula (Mathews and Fink 1992):

$$w_{ij} = \frac{1}{4}\left(w_{i+1,j} + w_{i-1,j} + w_{i,j+1} + w_{i,j-1} - 4w_{i,j} + h^2\right) \quad (5\text{-}20)$$

$\Delta x = \Delta y = h$, where h is the step-size.

The Dirichlet boundary condition where $w = 0$ is used along the walls of the channel. It is assumed that the no-slip boundary condition applies at the walls, where the velocity of the fluid is equal to zero. The program for this velocity calculation is written in MATLAB 6.5 and iterated 250 times with step-size 0.7 and error tolerance 0.001. The velocity profile is shown in Figure 5-3.

Once the values of w^* are obtained, the average velocity $\overline{w}$ is calculated by using:

$\overline{w} = \frac{Q}{area}$, where Q is the volumetric flow rate. Then:

$$Q = -\left(\frac{dp}{dz}\right)\left(\frac{1}{\mu}\right)\iint w^* dxdy \quad (5\text{-}21)$$

Since dp/dz is a function of z alone and w is a function of x and y, the only way that equation (5-17) can be satisfied is if dp/dz is a constant.

Resistance is given by equation (5-14). By rearranging equation (5-21) and substituting equation (5-14) in, the resistance for each layer of the fluid can be determined by:

$$R = \frac{\mu\ell}{\iint w^* dxdy} \quad (5\text{-}22)$$

where μ is the viscosity of the fluid (unit: $Pa \cdot s$), ℓ is the length (unit: m) of the microchannel and w^* is given by equation (5-18). The velocity is in m/s and resistance in $Pa \cdot s/m$

To determine the resistances of each layer, the cross-sectional area is divided into 3 equal parts. The denominator in equation (5-22) is calculated using trapezoidal rule. The limits of integration depend on the cross-sectional area of each layer. The code is implemented in MATLAB 6.5. (Aumeerally and Sitte Jan 2004, 2006)

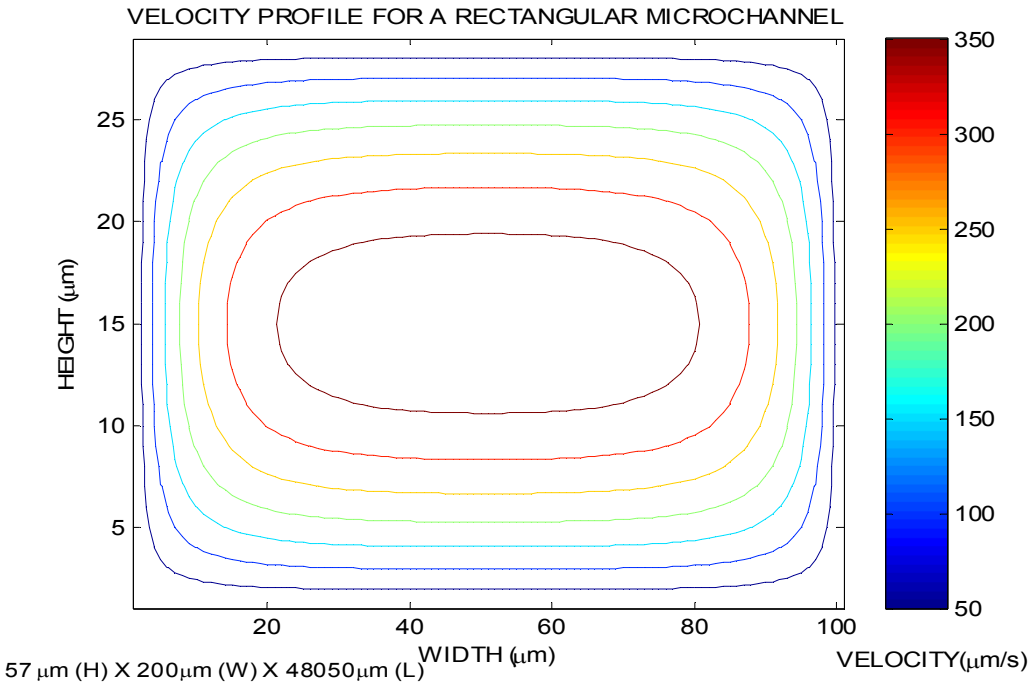

(a)

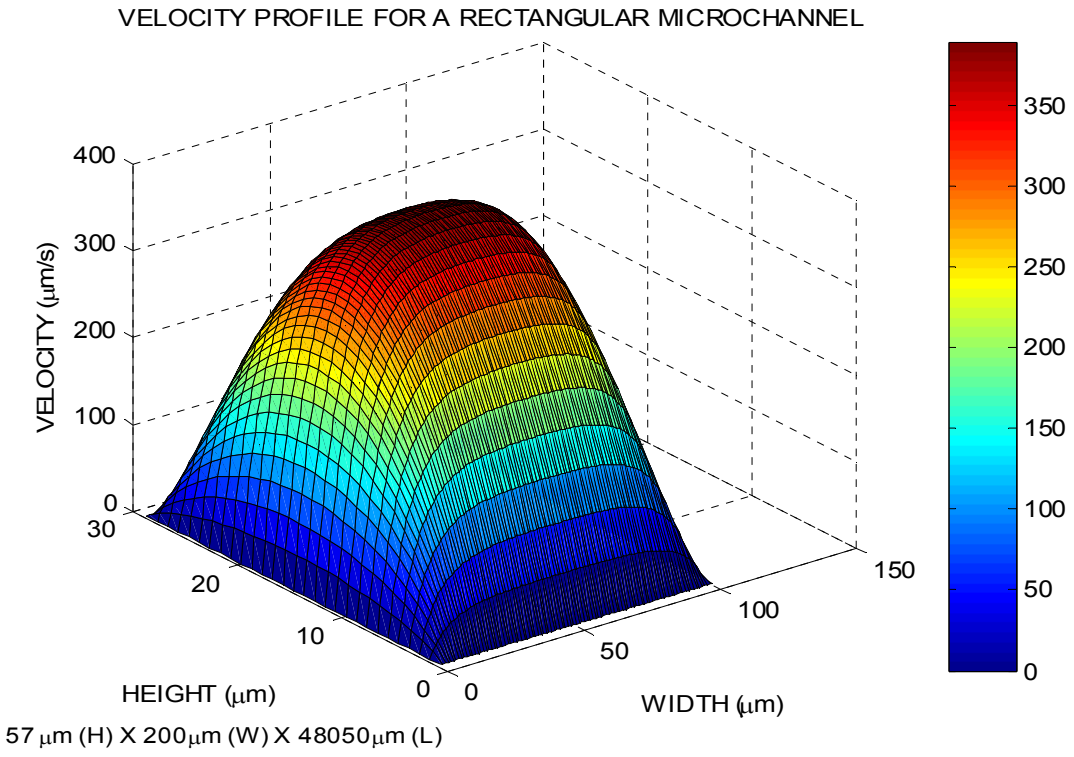

(b)

Figure 5-3 Velocity profile for a rectangular microchannel (a) cross-sectional view (b) side

view

5.2 DIFFUSERS AND NOZZLES

The flow in a diffuser is complex and is dependent on several factors such as the diffuser's geometric parameters, inlet Reynolds number, inlet boundary-layer blockage factor, inlet turbulence, and pulsations (White, F 1994). In this analysis (Aumeerally and Sitte Oct 2004) a simplification of the flow is carried out with the assumption that each layer of fluid in the diffuser flows steadily as in a channel with constant cross-sectional area.

Consider Poiseuille flow in a circular channel where the velocity distribution is given by equation (5-7):

$$V_z = \frac{a^2 - r^2}{4\mu}\left(-\frac{dp}{dz}\right)$$

where a is the radius of the channel, μ is the viscosity of the fluid and p is the hydrostatic pressure. Using the above equation, the pressure difference between the ends of the channel is given by:

$$p_1 - p_2 = \frac{8\mu}{\pi} Q \int_{z_1}^{z_2} r^{-4} dz \qquad (5\text{-}23)$$

Equation (5-23) can be applied to flow in a converging-diverging channel assuming that the inertial forces are negligible and neglecting entry and exit effects (Batchelor 1967), where r is the variable radius of the channel and is a function of z. Refer to Figure 5-4.

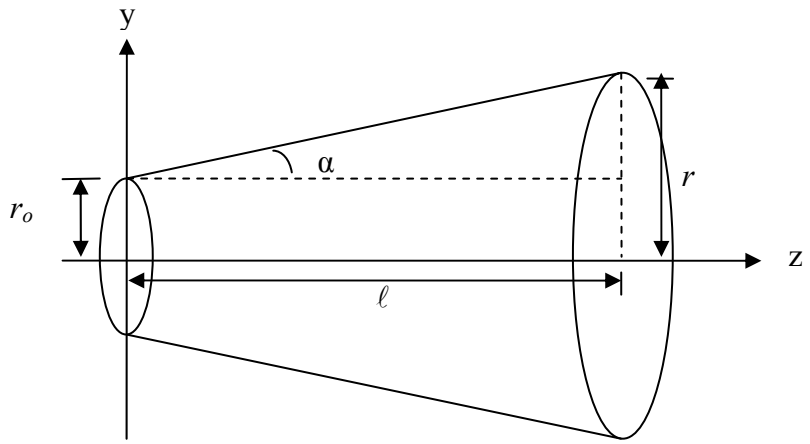

Figure 5-4 Expansion section of the diffuser.

If α is the aperture angle for the diverging section of a diffuser (Figure 5-4 and region 2 of Figure 5-5), and is small (<10°) so that $\tan\alpha \approx \alpha$, then by substituting the following equation:

$$r = r_o + \alpha\ell \tag{5-24}$$

where r_o is the radius at the diffuser's throat, ℓ is the length of the expansion section and r is the radius at the larger end of the diffuser, into equation (5-24):

$$\Delta P_2 = \frac{8\mu Q}{\pi}\int_0^{\ell}\frac{1}{(r_0 + \alpha\ell)^4}\,dz \tag{5-25}$$

where $\Delta P_2 = p_1 - p_2$, is obtained.

Using the substitution variable $\xi = r_0 + \alpha\ell$ and $dz = d\xi/\alpha$ into equation (5-25), the following is obtained:

$$\Delta P_2 = \frac{8\mu Q}{\pi}\int_0^{\ell}\frac{1}{\alpha\xi^4}\,d\xi \tag{5-26}$$

After integrating with respect to the variable ξ and substituting the value of z back into the resulting equation, the following equation is obtained:

$$\Delta P_2 = \frac{8\mu Q}{3\pi\alpha}\left[\frac{-1}{(r_o + \alpha\ell)^3}\right]_0^{\ell} \tag{5-27}$$

To simplify the results the variable, $\lambda = \alpha L_d / r_o$ is introduced into equation (5-27), obtaining:

$$\Delta P_2 = \frac{8\mu Q}{3\pi\alpha}\left(\frac{-1 + (1 + \lambda)^3}{r_o^3(1 + \lambda)^3}\right) \tag{5-28}$$

Finally, after some algebraic manipulations, the following equation relating the applied pressure difference between the two ends of the diffuser and the dimensions of the diffuser is obtained:

$$\Delta P_2 = \frac{8\mu Q L_d}{3\pi r_o^4}\left(\frac{3 + 3\lambda + \lambda^2}{(1 + \lambda)^3}\right) \tag{5-29}$$

where ΔP_2 is the pressure difference between the two ends of the diffuser, L_d is the total length of the diffuser and r_0 is the throat radius.

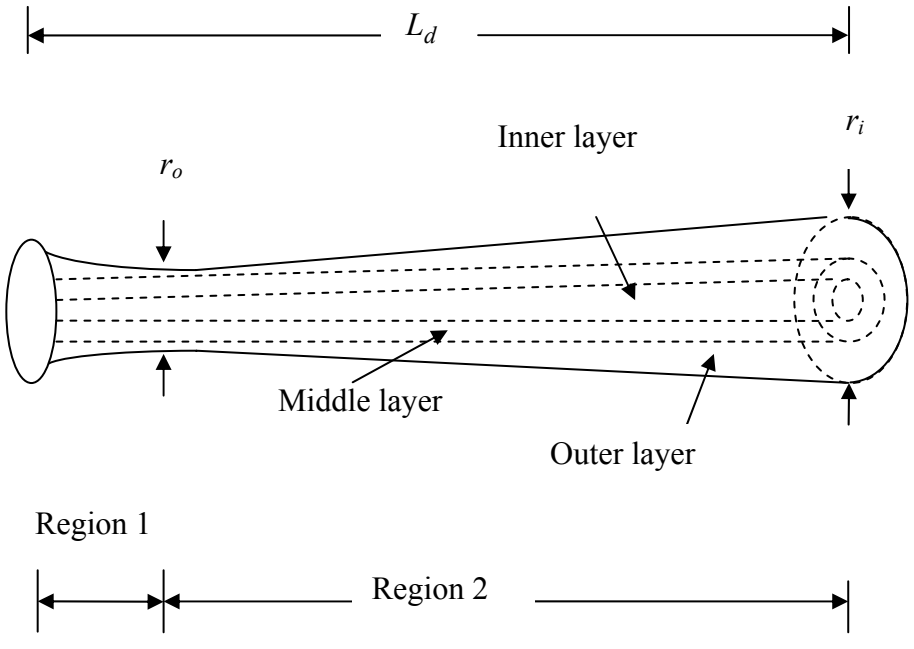

Figure 5-5 The two regions and the three layers of fluid in a conical diffuser

For region 1, the pressure difference ΔP_1 is given by (Heschel et al 1997):

$$\Delta P_1 = \frac{8\mu Q}{\pi}\left(-\frac{1}{r_i^3}\right)\left(\frac{6\beta^4 + 10\beta^2 - 1}{6\beta^2\left(\beta^2 - 1\right)^3} + \frac{\left(4\beta^4 + 1\right)\tanh^{-1}\left(\frac{1+\beta}{\sqrt{1-\beta^2}}\right)}{\left(1-\beta^2\right)^{3\cdot 5}}\right) \tag{5-30}$$

where r_i is the radius at the inlet and

$$\beta = \frac{r_o}{r_i} + 1 \tag{5-31}$$

The total pressure difference across the diffuser with the curved inlet is the sum of the pressure difference in region 1 and region 2 i.e. $\Delta P = \Delta P_1 + \Delta P_2$. The resistance is given by equation (5-14). Then the total resistance for the diffuser is given by (Aumeerally and Sitte. Oct 2004):

$$R_{total} = \frac{8\mu L_d}{\pi}\left(\frac{3 + 3\lambda + 3\lambda^2}{3r_o^4(1+\lambda)^3} - \frac{1}{r_i^3}\left(\frac{6\beta^4 + 10\beta^2 - 1}{6\beta^2\left(\beta^2 - 1\right)^3} + \frac{\left(4\beta^4 + 1\right)\tanh^{-1}\left(\frac{1+\beta}{\sqrt{1-\beta^2}}\right)}{\left(1-\beta^2\right)^{3\cdot 5}}\right)\right) \tag{5-32}$$

For the inner and middle fluid layers in the diffuser, we assume that the flow is almost that of a circular channel and the resistance for each section can be determined by using equation (5-16) above (Aumeerally & Sitte 2003, 2006):

$$R_{inner} = \frac{8\mu\ell}{\pi\left[2a^2\left(r_2^2 - r_1^2\right) - \left(r_2^4 - r_1^4\right)\right]} \tag{5-33}$$

where a is the radius of the channel (unit: m), r_1 is the radius of the first layer (unit: m), r_2 is the radius of the second layer (unit: m), μ is the viscosity of the fluid (unit: $Pa \cdot s$) and ℓ is the length (unit: m) of the microchannel. The resistance is in $Pa/\left(m^3/s\right)$.

The resistance of the outer layer is the difference between the total resistance using equation (5-32) and the sum of the resistances of the inner and middle layers using equation (5-33).

CHAPTER 6: DERIVATION OF ELECTRICAL CIRCUIT MODELS

Equivalent electrical network is used in the modelling of the layered fluid flow where small electric circuit elements represent the flow in each device. The flow (through) variable representing the rate at which work can be done, is the volume flow rate. The effort (across) variable representing the potential or the ability to do work is the pressure difference between the channels or device. Refer to Section 4.2.3.

6.1 MICROCHANNELS

The concept of complex impedance have been used to model oscillating fluid flow in (Bardell and Forster 1998) and (Morris and Forster 2000), where the element impedances are:

$$Z_R = R, \quad Z_L = \sigma L, \quad Z_c = \frac{1}{\sigma C} \tag{6-1}$$

where σ is the complex-frequency variable, R is the resistance, L the inductance and C the capacitance.

To represent the flow of the different layers in the channels, parallel circuit components are used. The idea is to incorporate the whole as a Simulink model into our MEMS CAD prototyping tool, where Simulink provides a convenient design interface to model functional components.

In this model, the current represents the volume flow, the voltage is the pressure difference, the resistance are due to the viscous forces, and the inductance depends on the mass of the fluid.

6.1.1 STEADY FLOW IN A CIRCULAR MICROCHANNEL

The resistance, R of the fluid flow in the microchannel is given by equation (5-14):

$$R = \frac{\Delta P}{Q}$$

where ΔP represents the pressure difference applied across the microchannel and Q represents the volumetric flow rate. The inductance, L is given by:

$$L = \frac{\rho \ell}{A} \tag{6-2}$$

where ρ is the density of the fluid, ℓ is the length of the channel and A is the cross-sectional area of the channel.

Since we are considering steady, laminar flow, i.e. time independent, so the voltage is a DC source and $\sigma = 0$, the complex-frequency variable, for the resistors and inductors. Therefore equation (6-1) becomes:

$$Z_L = 0 \text{ and } Z_C = \infty \tag{6-3}$$

The layered flow for a liquid in a steady, laminar flow can be represented by resistances in parallel as shown in Figure 6-1.

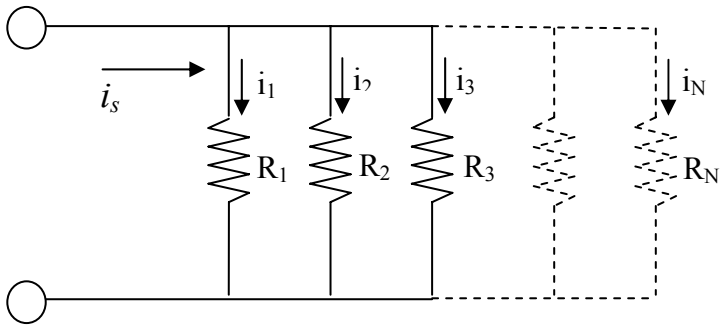

Figure 6-1 Electric circuit representation for the fluid sections in the circular microchannel

Each branch of the electric circuit in Figure 6-1 above represents the flow for each section in the microchannel. The current flow for each section is calculated by using the current division rule:

$$i_n = \frac{1/R_n}{\sum_{n=1}^{N} 1/R_n} i_s \qquad (6\text{-}4)$$

where n is the number of layers, i_s is the total current and R_n the sum of the resistances for each branch.

This can be extended to the case of oscillating pressure flow in which case, AC analysis is used and the resistance R is replaced by impedance Z. The electric circuit will then include inductors in series with the resistors for each branch, as shown in Figure 6-2. (Aumeerally and Sitte 2003, 2006)

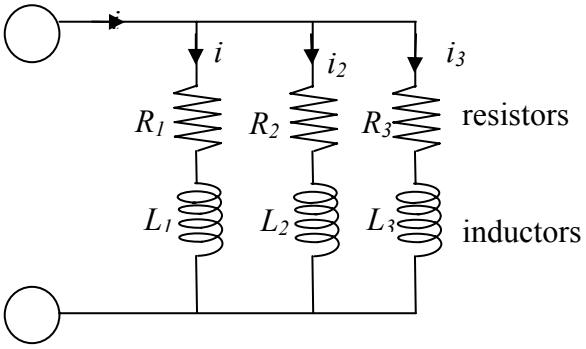

Figure 6-2 Resistors and inductors in series

6.1.2 STARTING FLOW IN A RECTANGULAR MICROCHANNEL

The main objective of this analysis is to show dynamic visualization in time-scaled virtual reality. The steady velocity profiles derived in Chapter 5 are considered as the limiting solutions for large times after a steady pressure gradient is applied. In this section, how the steady-state velocity profiles evolve with time is considered. The fluid is initially motionless at the instant the pressure gradient is applied, i.e. at time $t = 0$. When the pressure, which is constant and uniform, is applied, the fluid begins to flow. This flow gradually approaches the steady Poiseuille flow as described in Chapter 5. It is assumed that the microchannel is very long and entrance and exit effects are not considered. Thus at times $t \geq 0$, the velocity is dependant only on the radius or the height of the microchannel and time. See Figure 6-3.

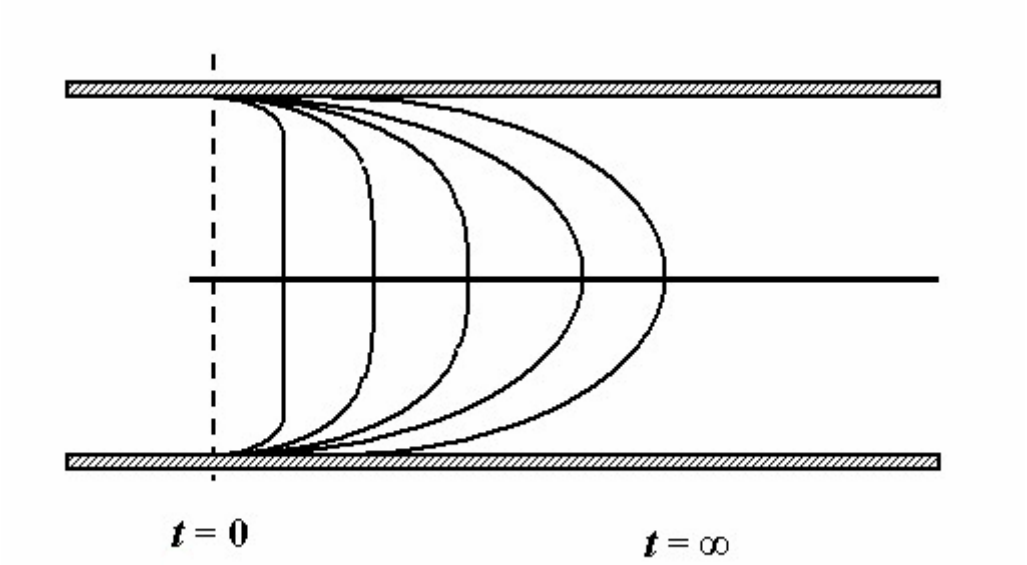

Figure 6-3 Velocity profiles at different values of *t* for the start-up flow in pressure-driven flow (Leal 1992).

To simulate the behaviour of the start-up velocity profile, the three layer flow concept is applied and the flow is represented by three parallel branches of inductor and resistor in series, as in Figure 6-2, with each branch representing each layer of the fluid. Similarly, as in the case of the circular microchannel, the resistance *R* here is given by equation (5-14) and the inductance, L by equation (6-2).

Since the pressure gradient is applied suddenly at time $t = 0$, achieving a constant and uniform value instantaneously, a step-function input is used to represent this pressure gradient. For each branch of the RL circuit in Figure 6-2 the current (i.e. volumetric flow rate) is given by the equation (Ong 1998):

$$i(t) = \frac{1}{L}\int_0^t (V_t - iR)dt \qquad (6\text{-}5)$$

where V_t is the voltage increase, i is the current, L the inductance and R the resistance. The integral equation (6.5) is implemented in Simulink (©Matlab) and the results are discussed

in Chapter 7. (Aumeerally and Sitte Jan 2004)

6.2 STEADY FLOW IN MICRODIFFUSERS AND MICRONOZZLES

As in the layered flow model for a circular microchannel presented in section 6.1.1, the volumetric flow rate of the diffuser is also represented by current, the pressure difference by voltage, the viscous forces by resistance, and the mass of the fluid by inductance. Assuming that the fluid flow is laminar, steady and that no flow separation occurs, the flow rate in the diffuser will be the same as for the nozzle, which is just the diffuser with fluid flowing in the other direction. The flow of the layers for the nozzle (or diffuser) can be represented by resistances in series and in parallel as shown in Figure 6-4. Each branch of the electric circuit represents the flow for each fluid layer and is the sum of the resistances in region 1 and region 2 of the diffuser. Refer to Figure 5-5 above. The current flow for each layer is calculated by using the current division rule in equation (6.4):

$$i_n = \frac{1/R_n}{\sum_{n=1}^{3} 1/R_n} i_s \qquad (6\text{-}6)$$

where n is the number of layers and is equal to 3, i_s is the total current and R_n the sum of the resistances for each branch ie $R_n = R_i^1 + R_i^2$ for the internal layer, $R_n = R_m^1 + R_m^2$ for the middle layer and $R_n = R_o^1 + R_o^2$ for the outer layer.

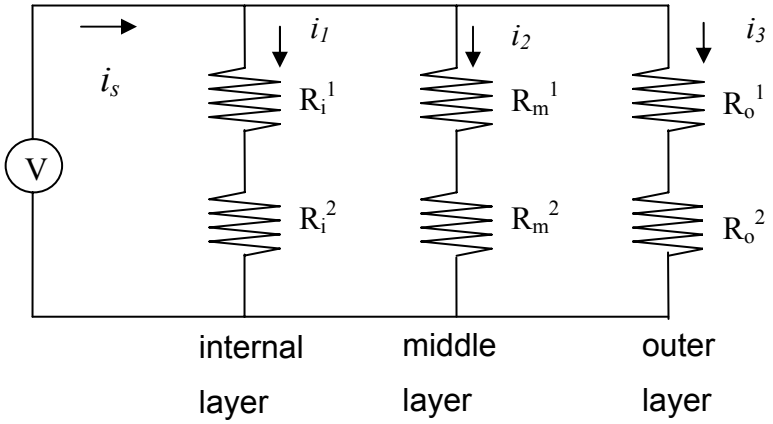

Figure 6-4 Electric circuit representation for the fluid layers in sections of the diffuser

The electrical model of Figure 6-4 is implemented in Simulink in the same way as for the layered flow in a circular channel (Aumeerally and Sitte 2003, 2006).

CHAPTER 7: SIMULATION AND RESULTS

In this chapter, the simulation analyses are discussed. For circular microchannels, both steady and transient starting flows are analysed. This is followed by starting transient flow for square microchannels and steady flow in conical diffuser and nozzles.

7.1 CIRCULAR MICROCHANNEL

For the steady laminar flow analysis, the circular microchannel of length 2.6 cm and diameter 203 μm as described in (Mala and Li 1999) is used. For the transient starting flow analysis, microchannels with diameters ranging from 50 to 101.6 μm from the same authors are used.

7.1.1 STEADY LAMINAR FLOW

The flow region is divided into three annular layers of equal cross-sectional area. The resistance of each layer is calculated using equation (5-16). The electrical circuit model as shown in Figure 6-1 is implemented in Simulink (©Matlab) and the values of the current (i.e. flow rate) for each section will be used by the VR module. The system representation for steady flow in circular microchannel is shown in Figure 7-1. The length and radius of the microchannel and the pressure difference are inputs to the system. The volumetric flow rates for each layer are the output of the system. The user sees only this blackbox representation and needs to specify only the dimensions and the number of layers as the input variables. The outputs of the system are the flow rates for the layers. The underlying model, hidden below this blackbox, is the implementation of the current division rule of equation (6-4). This is shown in Figure 7-1 below.

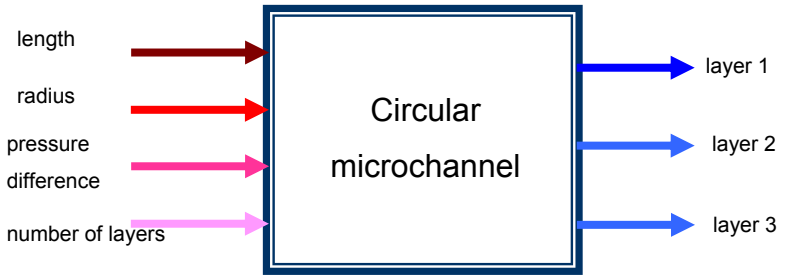

Figure 7-1 System representation for steady flow in circular microchannel.

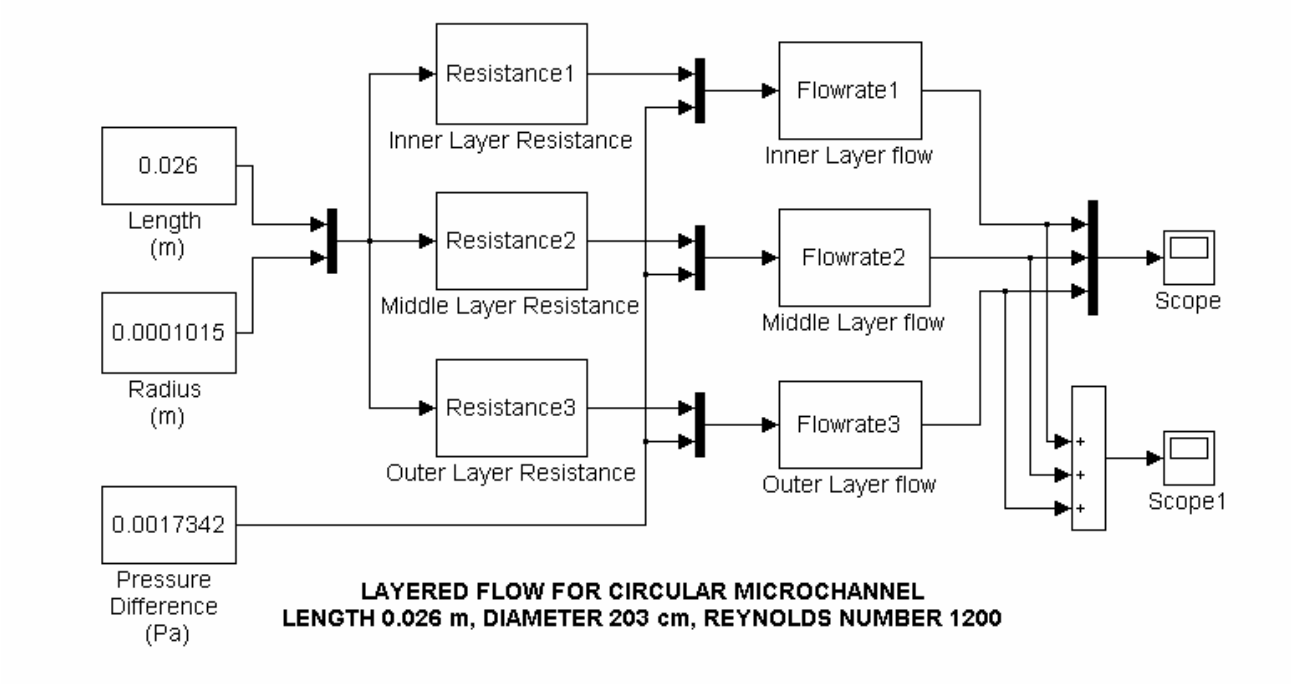

Figure 7-2 Simulink model for the current division for three sections in a circular microchannel with experimental data from (Mala & Li 1999).

7.1.2 UNSTEADY STARTING FLOW

The fluid is initially motionless at the instant of application of the pressure gradient. This nonzero pressure gradient is held at the same constant value after $t \geq 0$. At the beginning of the start-up flow, the velocity profile is flat in the middle, as shown in Figure 6-3. As time progresses, the middle section moves further and further away until the characteristic

parabolic shape of the steady velocity profile is attained. To simulate this unsteady behaviour of the flow, the electric circuit of Figure 6-2, in which each layer is represented by a series combination of a resistor and an inductor, is used. The current for each branch (i.e. the flow rate for each layer) is given by Equation 6.5. The solution to this equation can be obtained by implementing it in Simulink as in Figure 7-3. The transient time of a series RL circuit is given by (Boylestad 2000):

$$\tau = \frac{L}{R} \tag{7-1}$$

The experimental data from (Mala and Li 1999) provide for eight different values of circular microchannel dimensions. These values are used as inputs in the Simulink model of Figure 7-3

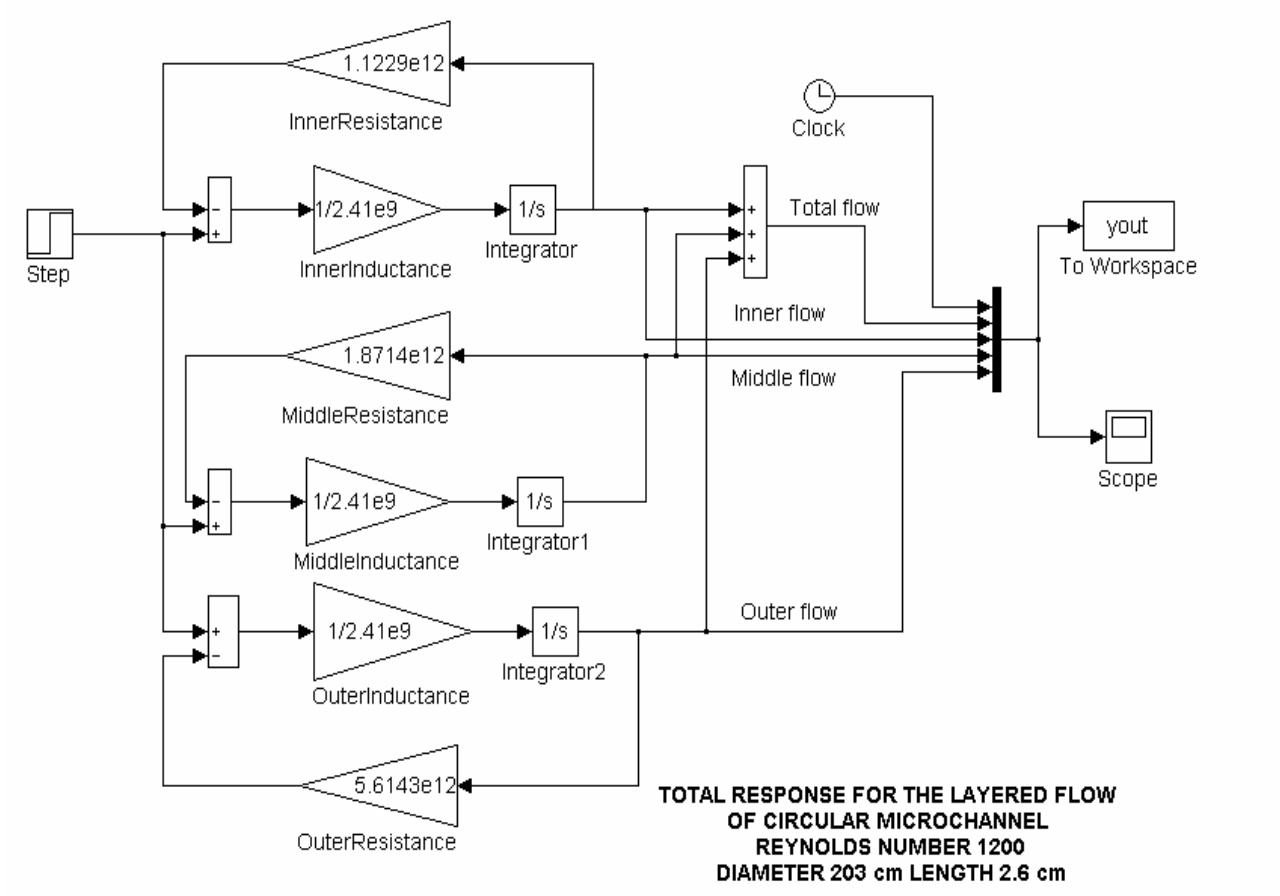

Figure 7-3 Simulink implementation of unsteady starting flow in a circular microchannel, data from (Mala & Li1999).

The output obtained from the Simulink model is shown in Figure 7-4. The topmost curve is the response for the microchannel as a whole, the second curve from the top is the response for the innermost fluid layer, the third curve shows the response of the middle fluid layer and the lowest curve shows the response of the outermost fluid layer. The innermost fluid layer has the fastest flow rate while the outermost layer, which is closest to the walls of the channel, has the slowest flow rate.

The transient part of the response is a very small portion of the total time. The outermost layer, nearest to the walls, achieves its steady state much faster than the innermost layer. The innermost layer reaches its steady state at a longer time than the outermost layer. Initially the viscous shear stress affects mainly the particles of the fluid near the wall, retarding their flow, while those in the central core region are able to accelerate uniformly. As time progresses, more particles are affected by viscous forces, causing the velocity profile to evolve into the parabolic steady-state shape. The response shown in Figure 7-4 reflects the transient behaviour of the flow of water when a sudden, uniform and constant pressure-gradient is applied to an initially motionless fluid in a microchannel, away from the entrance or exit. (Aumeerally and Sitte Jan 2006)

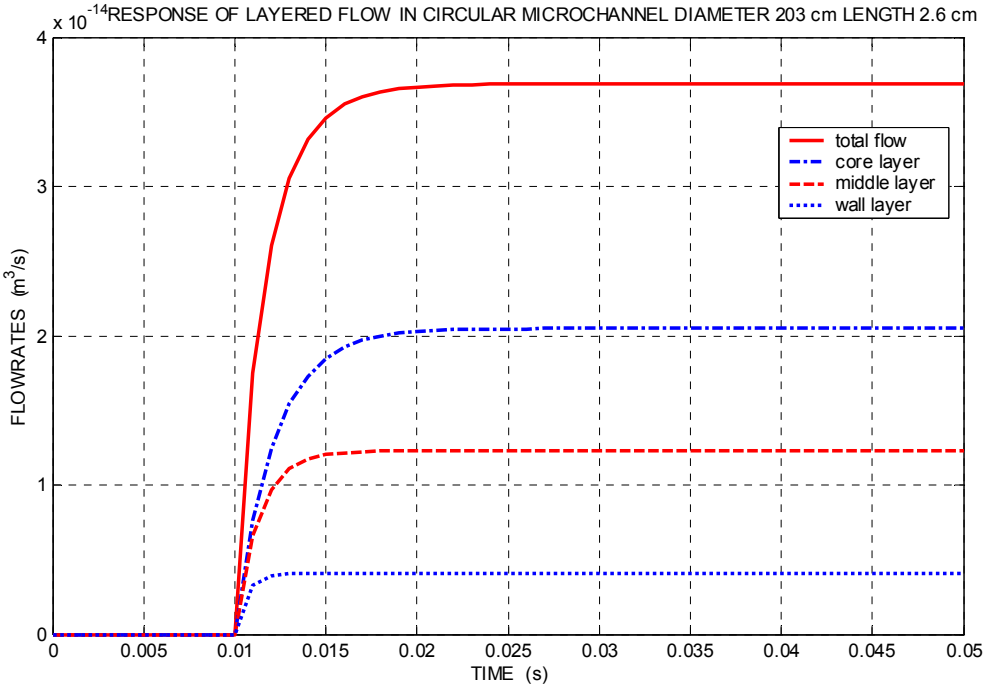

Figure 7-4 Total response of fluid flow in circular microchannels as obtained from

Simulink output.

7.2 SQUARE MICROCHANNEL

For square microchannels, the dimensions for three square microchannels given by (Judy et al 2002) are used. Here, the liquid used is methanol.

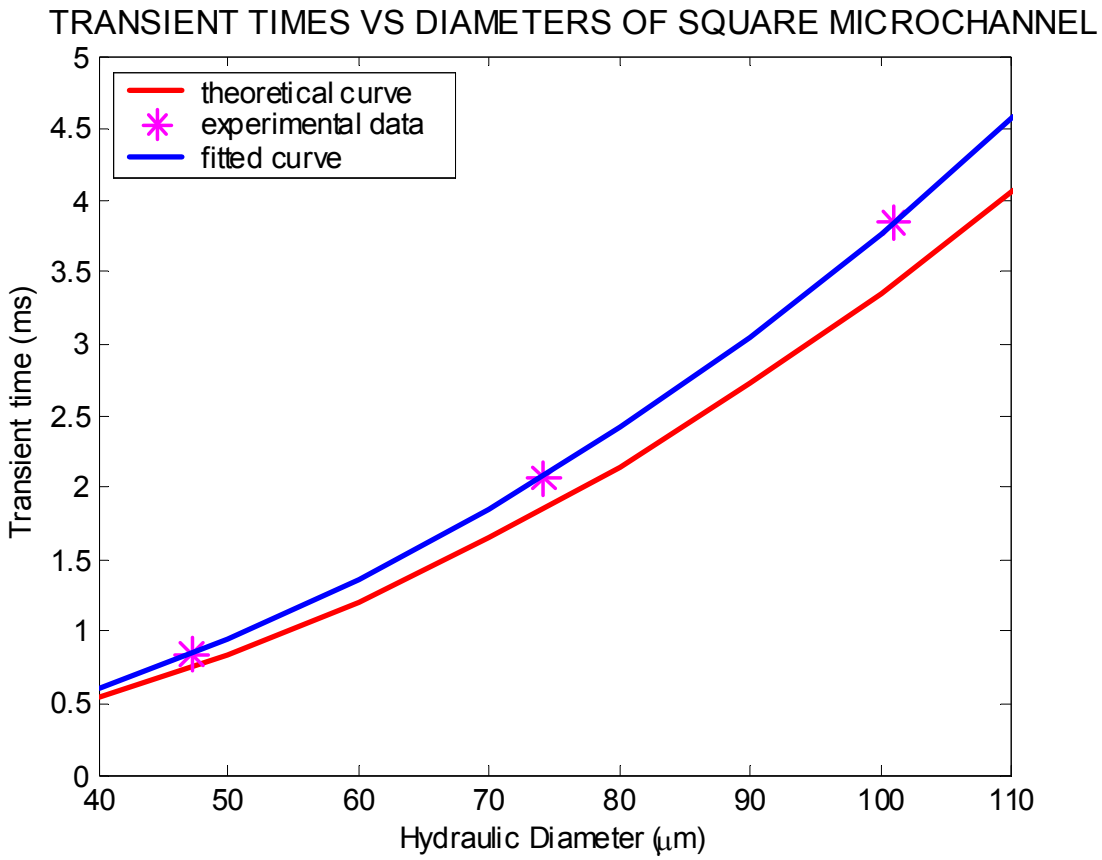

Figure 7-5 Comparison of experimental and theoretical data for square microchannels.

In this case, the concept of hydraulic diameter is used as an approximation for the dimensions of the square cross-section. The hydraulic diameter is defined as in equation (4-22):

$$D_h = \frac{4 * A}{P} \qquad (7\text{-}2)$$

where A is the cross-sectional area of the channel and P is the perimeter of the cross-

section.

The hydraulic radius of the square microchannel can be determined from the values of the hydraulic diameters as given in equation (7-2). This is then substituted into equation (5-16) to determine the resistances and then into equation (7-1) to obtain the theoretical curve of Figure 7-5. As in the case of the circular microchannel, the experimental curve is obtained from the Simulink output. A comparison of the values (see Table 8-3 below) shows a difference of about 11.1%.

7.3 SIMULATION OF DIFFUSER AND NOZZLE MICROVALVES

The values of the flow rates obtained for the microchannel, nozzle and diffuser are used as inputs into our VR module for an animated display. The resistances of the diffuser can be obtained from the model implemented in Simulink as in Figure 7-6. The values obtained from this are used as inputs for the next Simulink model of Figure 7-7, together with the resistances of flow in the nozzle direction. From the model of Figure 7-7, the efficiency of the nozzle/diffuser pair used as valves can be determined from the ratio of the conductance for the flow in the nozzle direction to that in the diffuser direction. The efficiency should be between 0 and 1. (Olsson et al. 1996) (Gerlach 1998) (Singhal et al. 2004)

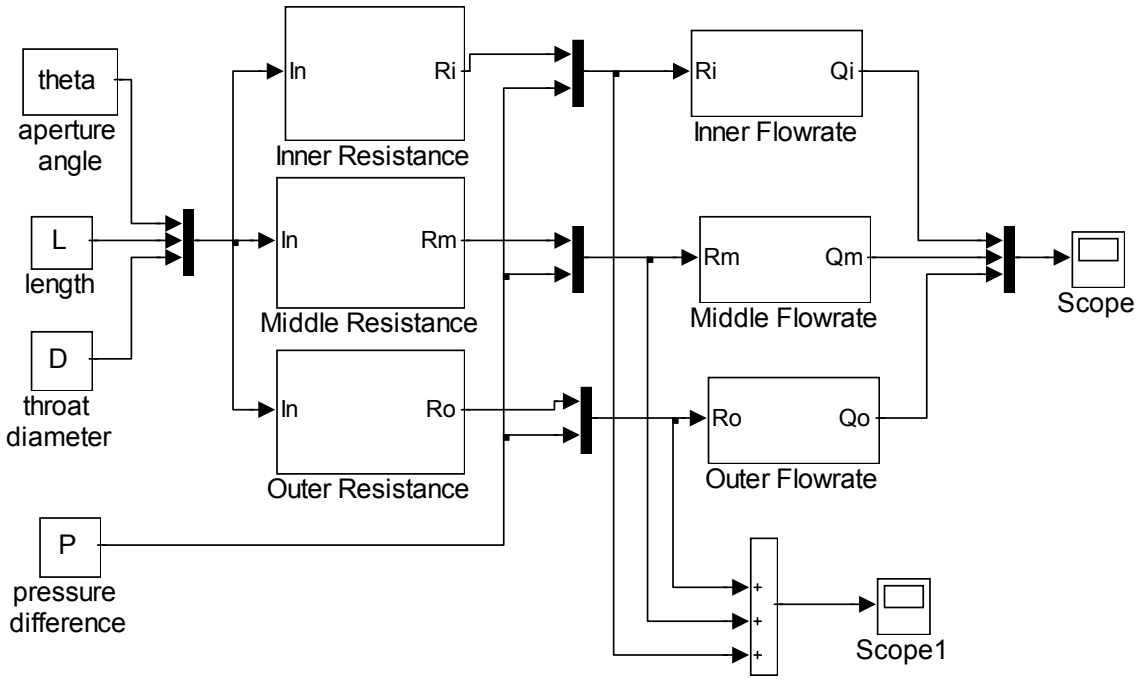

Figure 7-6 Simulink model for the flow rates and resistances for the three fluid layers in a diffuser.

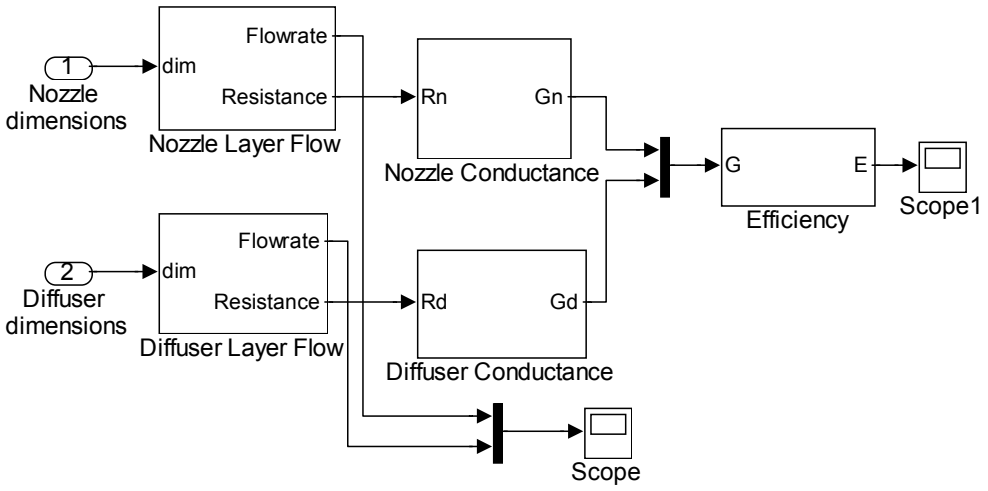

Figure 7-7 Simulink model for the efficiency of nozzle/diffuser valves

CHAPTER 8: VALIDATION AND DISCUSSION

The results of the simulations are compared with experimental data from the literature, with theory from the literature where available and also with the finite element software ANSYS, if applicable.

8.1 VALIDATION

In this section, validation is carried out for circular microchannels which, includes both steady and unsteady flow, steady flow in a rectangular microchannel, unsteady flow in square microchannels and finally steady flow in a microdiffuser. In terms of accuracy for the values of the total flow rate, comparison is made with experimental data obtained from the literature. As for the flow rates of the layers within the device, comparison is made with the finite element software Ansys. With regard to the speed of computation, the cpu times for the electrical model calculations implemented in Matlab are compared with Ansys.

8.1.1 CIRCULAR MICROCHANNELS

The results for the analysis of steady flow in circular microchannels are compared with experimental data from (Mala and Li 1999) for the total flow rates of the microchannels and with ANSYS for the layered flow rates. The fluid used is water at room temperature.

8.1.1.1 STEADY LAMINAR FLOW

The experimental total flow rates from (Mala and Li 1999) are compared with the results obtained from the electric model in Simulink as shown in Figure 7-2 and Figure 7-3. These are tabulated in Table 8-1. The percentage differences range from 1.3% to 6.1%.

Table 8-1 Comparison of total flow rates between experimental data of (Mala & Li 1999) and electric model for circular microchannels.

Total Flow Rate Compared with Experimental Data (Mala & Li 1999)			
Diameter of Microchannels (cm)	**Expt Flow Rate (m^3/s)**	**Electric model Flow Rate (m^3/s)**	**Percentage Difference (%)**
50.0	3.00E-09	3.07E-09	2.27
63.5	8.50E-09	7.98E-09	6.12
80.0	1.95E-08	2.01E-08	3.08
101.6	5.30E-08	5.23E-08	1.32
Average percentage difference			3.20

The flow rates for each layer obtained from the Simulink model of Figure 7-2 and Figure 7-3 are compared with the values obtained by direct substitution of the microchannels dimensions into the Hagen-Poiseuille equation (4.20):

$$Q = \frac{\pi r^4}{8\mu\ell}\Delta p$$

where r is the radius of the channel, ℓ is its length, μ is the viscosity of the fluid used, in this case water, and Δp is the applied pressure across the ends of the channel.

A finite element model of a stainless steel microchannel, length 3.2 cm and diameter 152 μm, is created using ANSYS. Meshing is done using Fluid element 141 and the graph of axial velocities for the laminar flow of water in the channel is obtained. This is shown in Figure 8-1. The values of these velocities are used to calculate the flow rate of the layers of fluid in the microchannel. The results are compared with those obtained by using the electrical model. This comparison is shown in Table 8-2 below.

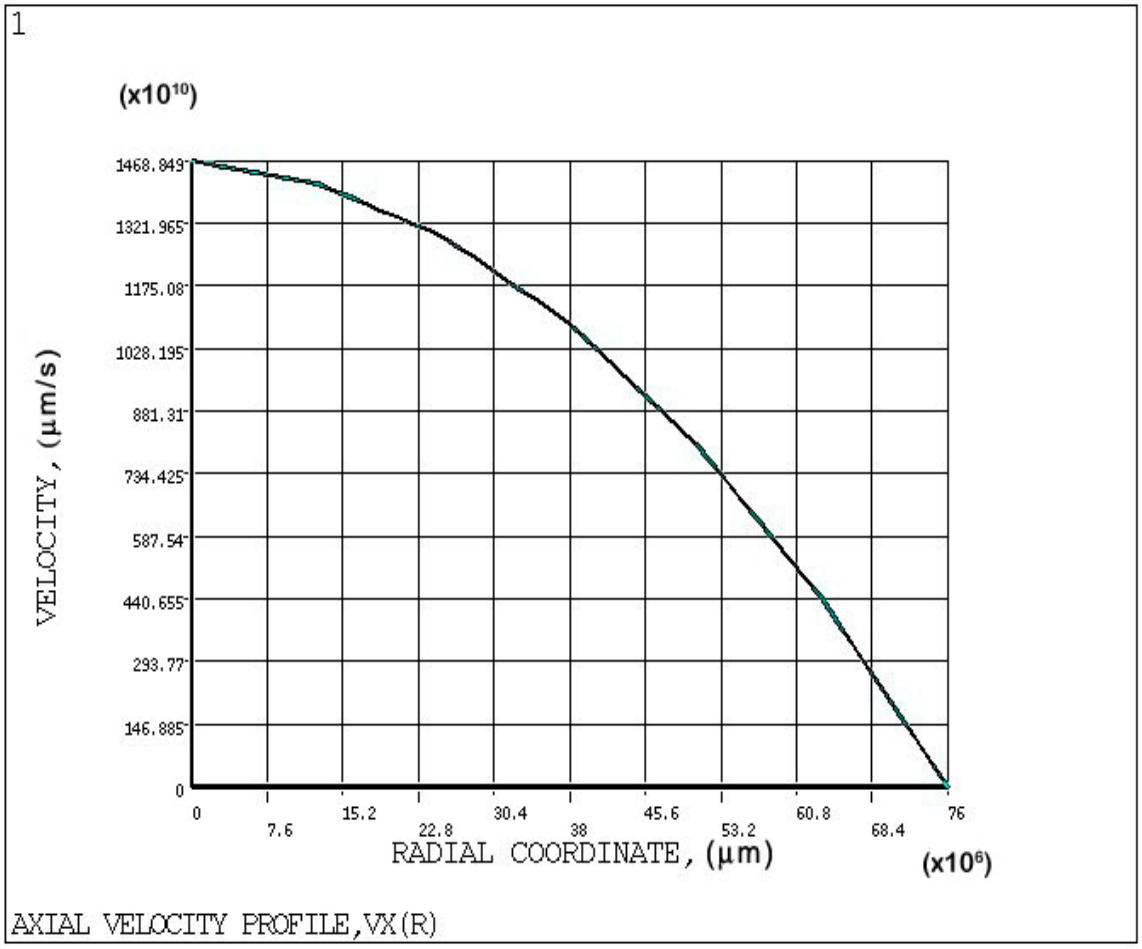

Figure 8-1 Contour plot for the axial velocity in a circular microchannel using ANSYS

The chart in Figure 8-2 shows a comparison of the values of the layered flow rates for the circular microchannel obtained by using the three techniques, i.e. electrical model, Hagen-Poiseuille equation and ANSYS.

The flow rate is dependent on the cross-sectional area and the average velocity of the fluid, as is evidenced from equation (5.8):

$$Q = \int_{\text{sec } tion} V_z dA$$

In this analysis the areas of the layers are made equal so the flow rates are dependent on the velocity only.

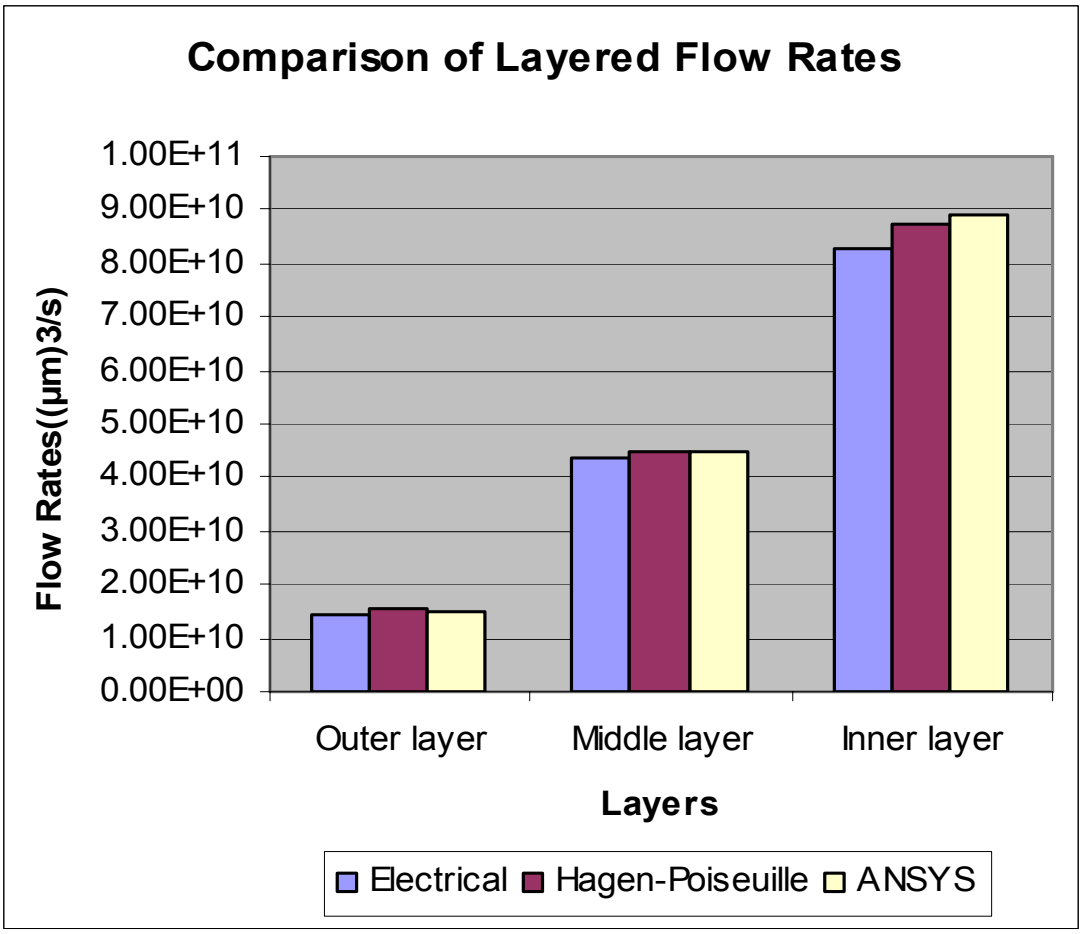

Figure 8-2 Comparison of layered flow rates using the electrical model, Hagen-Poiseuille equation and ANSYS for circular microchannel.

When compared with direct calculation using Hagen-Poiseuille equation, the electrical model gives an error ranging from 3.2% to 5.22%. Refer to Table 8-2 below. When compared with finite element model (ANSYS), an error range of 3.05% to 6.58 % is obtained. It should be noted that ANSYS simulations may have an error of up to 20%. The errors obtained by using the electric model are below this level.

Table 8-2 Comparison of layered flow rates between electric model and Ansys for circular microchannel.

Flow rates $(\mu m)^3/s$	Circular microchannel				
	Electrical Model	FEA Model (Ansys)	Hagen-Poiseuille	% difference with Ansys	% difference with Hagen-Poiseuille
Outermost layer	1.45e10	1.51e10	1.53e10	4.00	5.22
Middle layer	4.35e10	4.49e10	4.49e10	3.05	3.20
Innermost layer	8.30e10	8.88e10	8.73e10	6.58	4.97

8.1.1.2 UNSTEADY STARTING FLOW

The theoretical data is obtained by using the graph of Figure 4-3 from (White, F. 1991). Refer to section 4.1.1.4. From this graph, the following equation for time is given by:

$$t \approx r_o^2 / \nu \tag{8-1}$$

where v is the kinematic viscosity of the fluid, t the time taken to reach steady state and r_0 the radius of the channel. The transient time is given by t and the diameter of the microchannel is twice the radius, r_o. The radii of the eight circular microchannels from (Mala and Li 1999) are substituted in, the graph is plotted using Matlab and is represented by the red curve in Figure 8-3 below. The results obtained from the Simulink model, represented by the blue curve in Figure 8-3, are compared with the theoretical curve.

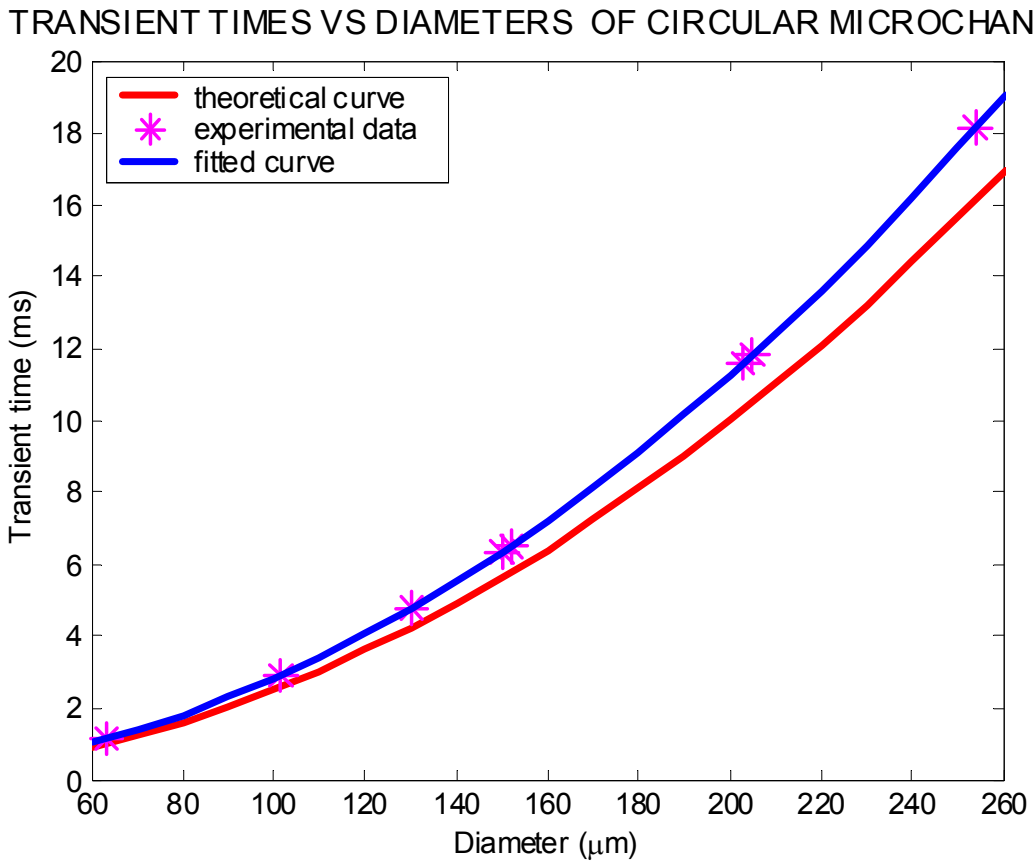

Figure 8-3 Comparison of experimental data with theoretical calculations of transient times for circular microchannels.

A numerical comparison is made between the experimental data and theoretical data, shown in Table 8-3 below. The percentage difference is about 11.1%.

Table 8-3 Comparison of theoretical with experimental transient time for circular microchannels.

CIRCULAR MICROCHANNELS			
diameter (μm)	theoretical time (ms)	experimental time (ms)	% difference
63.5	1.008	1.134	11.11
101.6	2.581	2.903	11.11
130.0	4.225	4.753	11.11
150.0	5.625	6.328	11.11
152.0	5.776	6.498	11.11
203.0	10.300	11.59	11.11
205.0	10.510	11.82	11.11
254.0	16.130	18.15	11.13

8.1.2 RECTANGULAR MICROCHANNEL

To validate the total volumetric flow rate of the rectangular microchannel obtained from the electrical model implemented in Simulink, experimental data from (Park et al 2003) is used. The rectangular microchannel has a length of 48050 μm, height 57 μm and width 200 μm. A pressure difference of 6250 Pa is applied across the channel. The working fluid is deionized water at 25.5°C at which the density is 996 kg/m^3 and viscosity is 0.0009 Pa.s. The mass flow rate is 0.5 mg/s.

Table 8-4 below shows the comparison between the experimental volumetric flow rate with the total flow rate obtained from the electrical model. An error of 2.19% is obtained. The total flow rate is also calculated by using the hydraulic diameter concept as given in equation (4-20) above. This gives an error of 19.32%. It should be noted that the aspect ratio of this rectangular microchannel is 0.285, much less than 1. As stated before, a rectangle of aspect ratio greater than 1 will not give an accurate answer when the hydraulic

diameter concept is used. The total flow rate obtained using the electrical model gives a much lower error than using the hydraulic diameter concept.

To validate the flow rates of the layers of fluid in the microchannel, a 2D finite element model of the microchannel is created using ANSYS. Meshing is done using fluid element 141 and the graph of axial velocities for the laminar flow of water in the channel is obtained. This is shown in Figure 8-4 below.

Table 8-4 Comparison of Total Flow rates between Electrical Model, Hagen-Poiseuille Approximation and Experimental Data for Rectangular Microchannel (Park et al 2003)

	Rectangular microchannel		
	Electrical Model	Experimental	% difference
Total flow rate $(\mu m)^3/s$	5.13e8	5.02e8	2.19
	Hagen-Poiseuille D_H approximation	Experimental	
Total flow rate $(\mu m)^3/s$	4.05e8	5.02e8	19.32

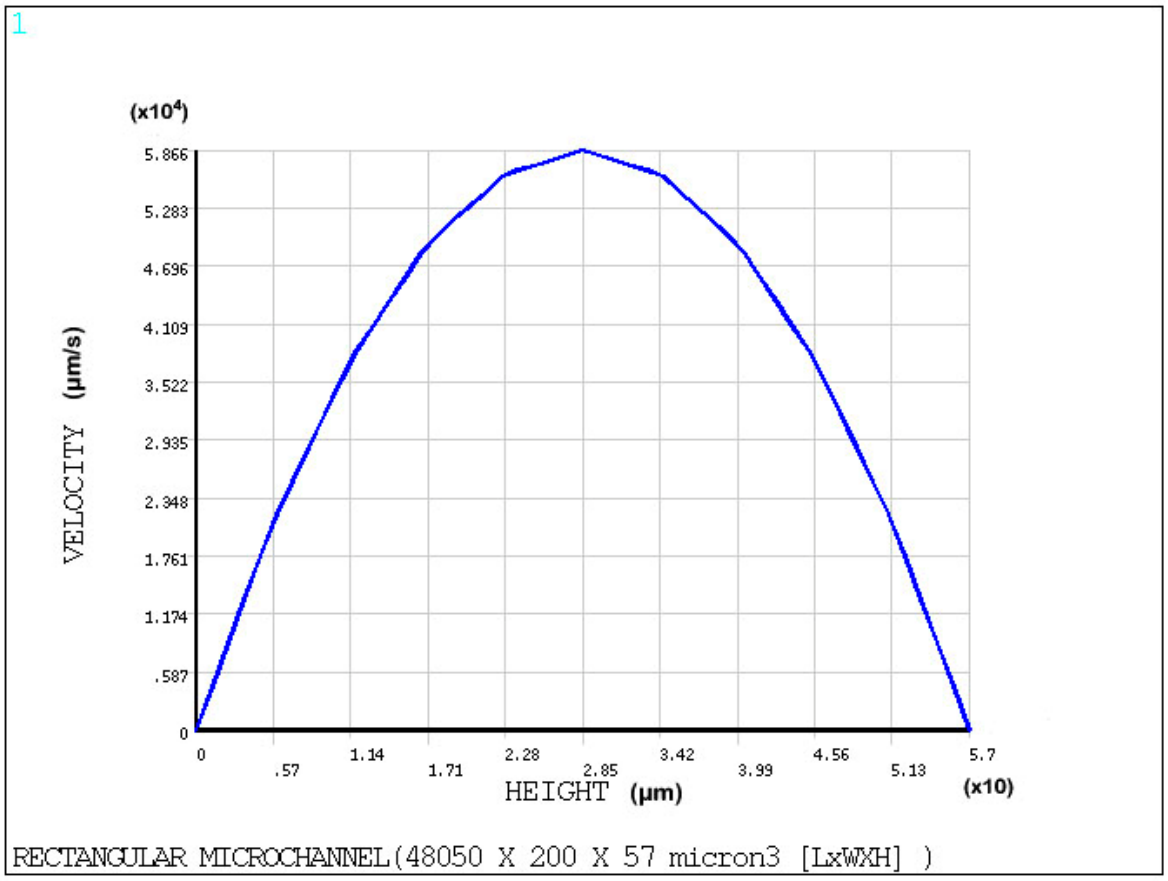

Figure 8-4 Velocity Across the Outlet for a Rectangular Microchannel using 2D Analysis in ANSYS

Figure 8-4 above shows the graph of the velocity of the microchannel across the width of the cross-section obtained from a 2D analysis in ANSYS. This demonstrates the characteristic parabolic velocity profile for steady laminar flow in a microchannel. The fluid in the centre of the channel has the highest velocity, while those at the walls reach zero velocity. The velocities for the layers of fluids are obtained from this graph and the results tabulated in Table 8-5 below.

Table 8-5 Comparison between Electrical Model and Numerical Calculation in Matlab

Flow rates $(\mu m)^3/s$	Rectangular microchannel		
	Numerical Model	Electrical Model	% difference
Outermost layer	0.634e8	0.639e8	0.79
Middle layer	1.782e8	1.795e8	0.73
Innermost layer	2.718e8	2.723e8	0.18

Table 8-5 above shows the comparison of the layered flow rates obtained via the electrical model implemented in Simulink block diagrams to that obtained via finite-difference numerical model implemented in Matlab as described in Section 5.1.2 above. The percentage difference ranges from 0.18% to 0.79%. Since the flow rate is dependent on the cross-sectional area and the average velocity of the fluid, in this analysis the areas of the layers are made equal so the flow rates are dependent on the velocity only.

Table 8-6 below shows a comparison of the layered flow rates obtained from the electrical model implemented in Simulink with that of ANSYS. The percentage difference obtained ranges from 24.7% to 44.7%. It should be noted that ANSYS recognizes that their simulations may have an error of up to 20%. A chart comparing the values obtained using the 3 techniques is shown in Figure 8-5 below.

Table 8-6 Comparison between Electrical Model and ANSYS for the Flow Rates of Rectangular Microchannel

Flow rates $(\mu m)^3/s$	Rectangular Microchannel		
	Electrical Model	ANSYS	% difference
Outermost layer	0.64e8	0.85e8	24.7
Middle layer	1.79e8	1.22e8	46.7
Innermost layer	2.72e8	1.88e8	44.7

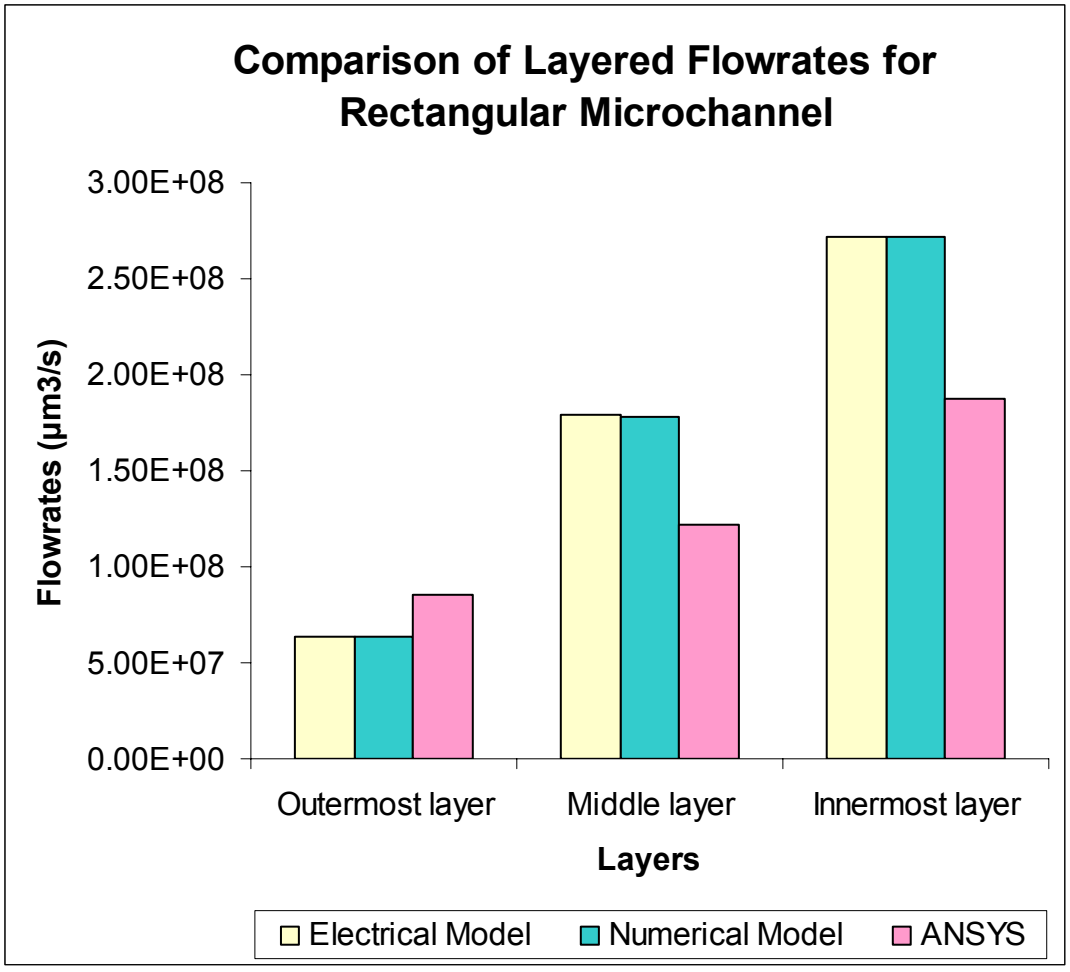

Figure 8-5 Comparison of Layered Flow Rates using the Electrical Model, Matlab and ANSYS Calculations

8.1.3 UNSTEADY STARTING FLOW IN SQUARE MICROCHANNELS

For square microchannels, the dimensions for three square microchannels given by (Judy et al 2002) are used. Here, the liquid used is methanol. A comparison of the transient times obtained by using the series RL electrical circuit model implemented in Simulink is made with data from the numerical analysis of viscous fluid flow in circular channel carried out by Szymanski (1932). This numerical result is reproduced in (White, F. 1991) and is shown in Figure 4-3.

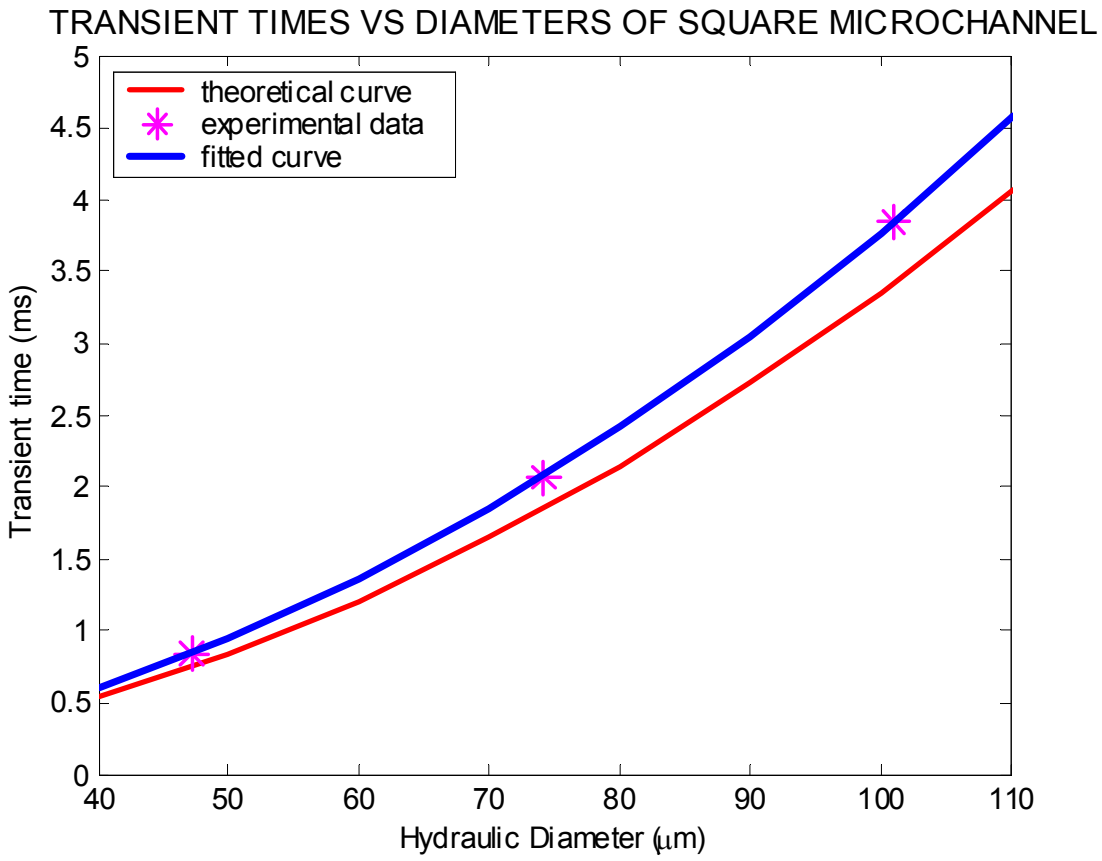

Figure 8-6 Comparison of experimental (Judy et al 2002) and theoretical data for square microchannels.

Figure 8-6 above shows the comparison of experimental data from (Judy et al 2002) to theoretical data. The diameter of the channels are converted to hydraulic diameters and applied to equation (8-1) above to obtain the theoretical curve. The experimental curve is obtained by substituting the experimental data to the electrical model implemented in

Simulink using equation (7-1). As in the case of the unsteady flow analysis for circular microchannel, the experimental curve is obtained from the Simulink output. A comparison of the values (see Table 8-7 below) shows a difference of about 11.1%.

Table 8-7 Comparison of theoretical to experimental transient time for square microchannels.

Hydraulic diameter (μm)	Theoretical time (ms)	Experimental time (ms)	% difference
47.1	0.744	0.8365	11.11
74.1	1.84	2.07	11.09
101	3.419	3.846	11.10

8.1.4 LAMINAR FLOW IN A MICRODIFFUSER

As an example, a conical diffuser of length 1200 μm, aperture angle 6.3° and throat radius 10 μm is used (Heschel et al 1997). The flow rates for a range of pressure difference are calculated using equations (5-29) and (5-30) and these are shown in Figure 8-7 below. The flow rates calculated using the electrical model of equations (5-32) and (5-33) are also shown in the same figure. As can be seen, the electrical model gives exactly the same values as the analytical ones. However when compared with experimental data, both the analytical model traditionally used, as well as the electrical model give values that deviate increasingly more as the pressure difference goes above 100 mbar.

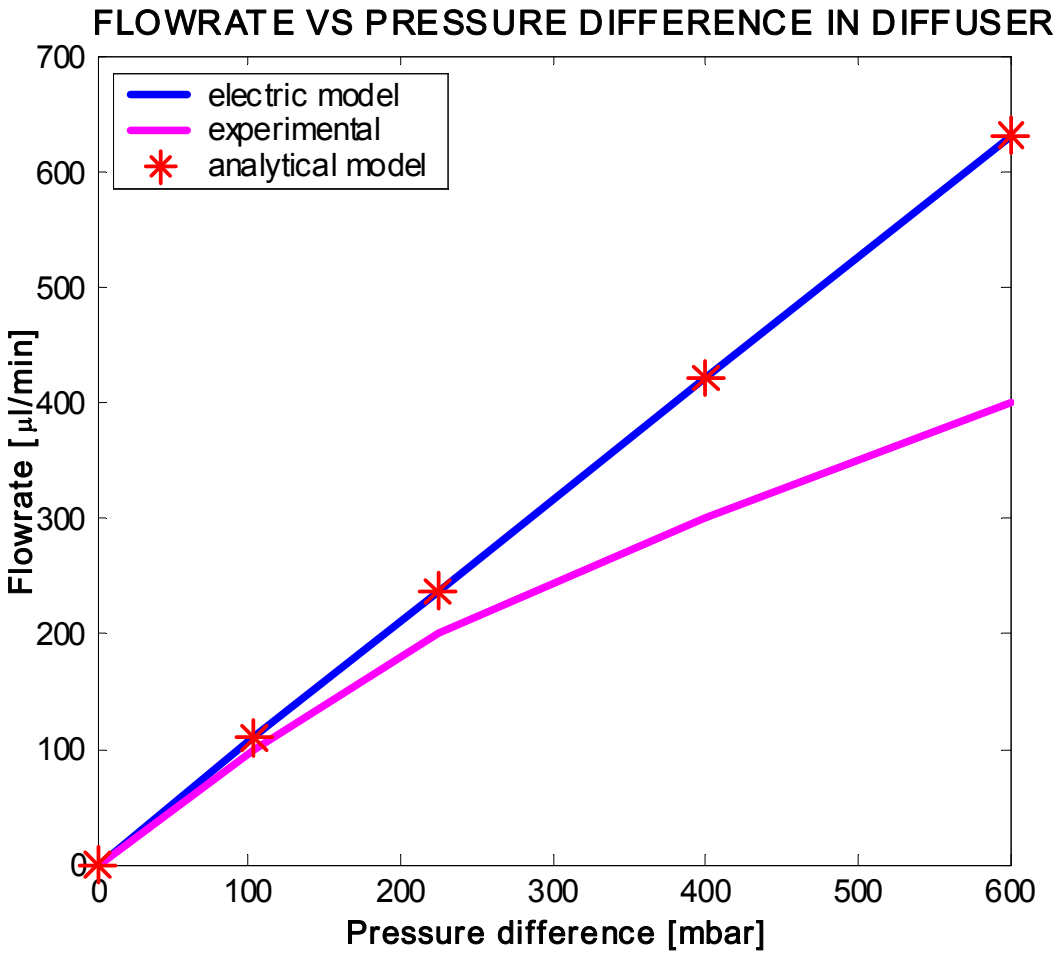

Figure 8-7 Relationship between flow rates and pressure difference using experimental data (Heschel et al 1997), electric and analytic model for a diffuser.

A comparison is made between values of the layered flow rates obtained from experiments and analytical data and are shown in a chart in Figure 8-8 below. The percentage differences between the experimental data and the values of the electrical and analytical model are shown in Table 8-8 below. As before, there is no difference between the electrical model values and the analytical values.

Future research is aimed at refining the method, including the effect of turbulences.

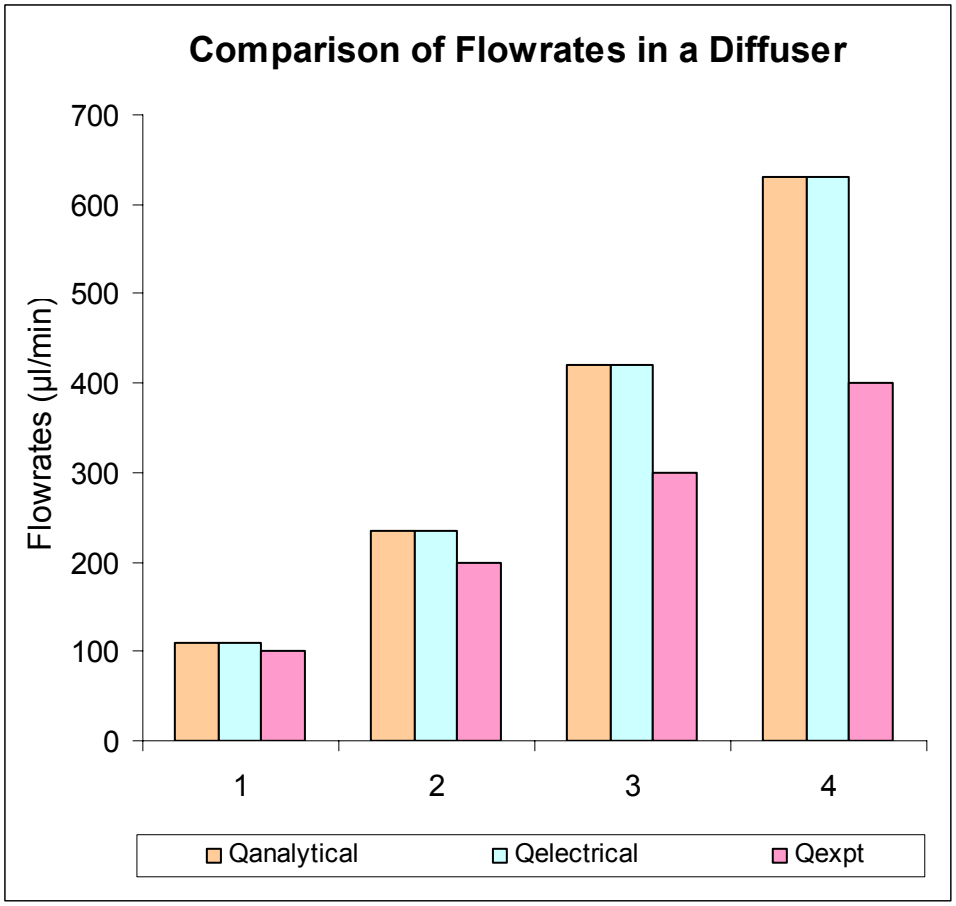

Figure 8-8 Comparison of flow rates from the electrical and analytical model and experimental data (Heschel et al 1997)

The percentage error increases with the flow rates. The analytical model derived in Section 5.2 shows that resistance is a linear function of pressure and flow rate as can be seen from equation (5-32) above. However from Figure 8-7, the resistance obtained from experimental data, is not a linear function. A quadratic term needs to be added to the equation to give a non-linear function. Energy loss has to be accounted for.

Table 8-8 Percentage difference between flow rates from electrical model to experimental values (Heschel et al 1997) for laminar flow in a microdiffuser

Qanalytical (μl/min)	Qelectrical (μl/min)	Qexpt (μl/min)	% Difference
109.5	109.5	100	8.7
235.8	235.8	200	15.2
421.2	421.2	300	28.8
631.7	631.7	400	36.7

In using the electrical model, the assumptions are that the flow is laminar, there is no turbulence and no flow separation. Laminar flow in a diffuser occurs only for very small diverging angles (less than 10°) and small exit area to throat area ratio. In order to achieve high efficiency, the pressure loss has to be a minimum, and this occurs in what is known as the transitory stall region of the stability map of a diffuser. In this region, the flow pattern is highly unsteady, with large pressure fluctuations, reversed flow and flow separation. (Stemme and Stemme 1993)

8.1.5 COMPARISON OF CPU TIMES

For determining the cpu time for the calculations using the electrical model, a program is written in Matlab, similar to the one carried out for Section 8.1.1.1 for the steady laminar flow in circular microchannels. The program calculates the flow rates of the three-layer flow and also the total flow rates of each of these microchannels, determines the velocities, plots the velocity profile and calculates the percentage difference between the total flow rate using the electrical model with experimental data from (Mala and Li 1999). Each program runs for 50 iterations and the average and the standard deviation for the cpu time in seconds are then calculated.

Another program is written using Ansys, which uses finite element analysis in order to

determine the velocities and total flow rates. Again the program is made to run for 50 iterations and the average and standard deviation are obtained. Table 8-9 below shows the average cpu times, within one standard deviation, for Ansys and the electrical model. The percentage difference between the two sets of data is also shown.

Table 8-9 Comparison of cpu times for the calculation of layered flow rates in circular microchannels.

CIRCULAR MICROCHANNELS				
	Diameter (μm)	CPU TIME (s)		
		ANSYS	Electrical Model	% Difference
1	50.0	1.021 ± 0.084	0.3106 ± 0.12	69.57
2	63.5	1.024 ± 0.120	0.4384 ± 0.21	57.19
3	80.0	1.018 ± 0.094	0.4256 ± 0.12	70.77
4	101.6	1.050 ± 0.094	0.4248 ± 0.18	59.52
AVERAGE OF CPU TIME (s)		1.028 ± 0.094	0.4410 ± 0.16	57.08

Figure 8-9 below shows a chart of the comparison of the average cpu time using Ansys and the electrical model. Each column represents the average cpu time in seconds with the error-bar representing the spread of the data within 1 standard deviation. Table 8-10 below shows the percentage difference obtained by comparing the experimental total flow rates with the flow rates using Ansys and using the electrical model.

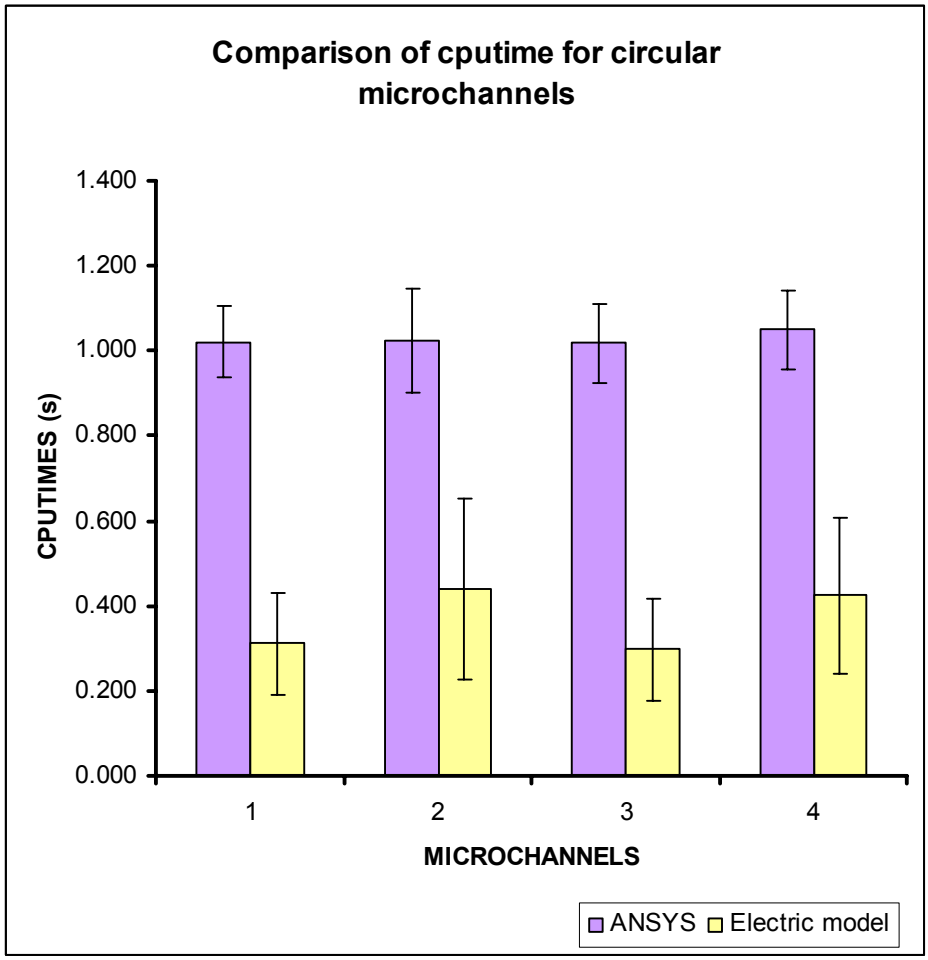

Figure 8-9 Comparison of cputime for several circular microchannels.

Table 8-10 Comparison of experimental total flow rates with Ansys and Electrical Model for circular microchannels

CIRCULAR MICROCHANNELS TOTAL FLOW RATES COMPARISON		
Diameter (μm)	ANSYS (%)	Electrical Model (%)
50.0	1.42	12.34
63.5	6.88	6.10
80.0	2.25	3.11
101.6	1.19	1.31

The same procedure is carried out for the square microchannels and comparison is made with experimental data obtained from (Judy et al 2002). The concept of hydraulic diameters is applied in this case, where the dimensions of the square microchannels are approximated to that of circular ones, as is used in Section 7.2. The hydraulic diameter is defined as in equations (4-22) and (7-2):

$$D_h = \frac{4 * A}{P}$$

where A is the cross-sectional area and P is the perimeter of the cross-section.

Table 8-11 below shows the average cpu times and the spread of the data within 1 standard deviation, each taken out of 50 runs from calculations carried out in Ansys and using the electrical model. The percentage difference between the cpu times obtained by using Ansys and the electric model is shown. Figure 8-10 shows a chart comparing the cpu times and spread of the data within one standard deviation of the average value. Table 8-12 below shows the percentage difference between the flow rates obtained using Ansys with experimental total flow rates and also the percentage difference between the flow rate obtained using the electrical model with experimental data.

Table 8-11 Comparison of cpu times for the calculation of layered flow rates in square microchannels.

SQUARE MICROCHANNELS				
	Hydraulic Diameter (μm)	CPU TIME (s)		
		ANSYS	Electrical Model	% Difference
1	47.1	1.0182 ± 0.098	0.2224 ± 0.067	78.16
2	74.0	1.0045 ± 0.083	0.2164 ± 0.028	78.46
3	74.1	1.0118 ± 0.096	0.2222 ± 0.036	78.04
4	101.0	1.0168 ± 0.100	0.2142 ± 0.033	78.93
5	100.4	1.0326 ± 0.150	0.2264 ± 0.039	78.07
AVERAGE OF CPU TIME (s)		1.0168 ± 0.110	0.2203 ± 0.040	78.33

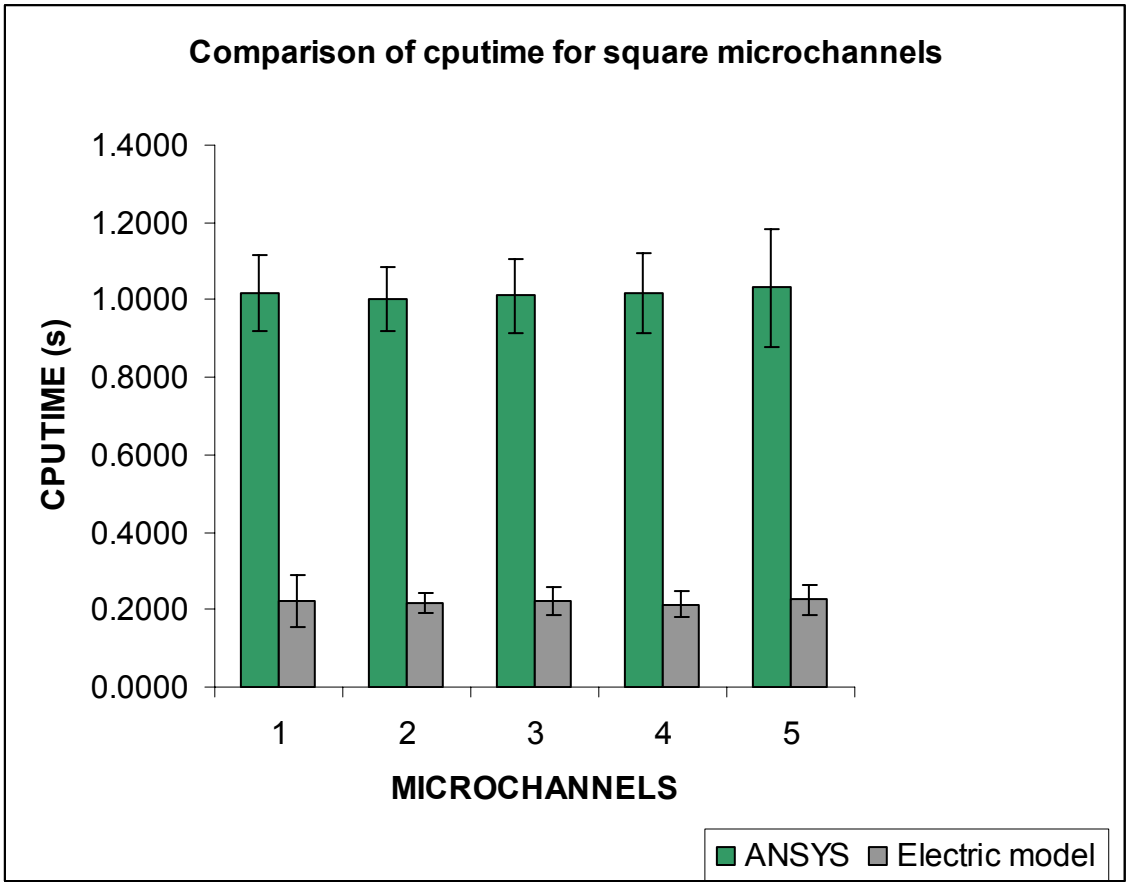

Figure 8-10 Comparison of cputime for several square microchannels.

Table 8-12 Comparison of experimental total flow rates with Ansys and Electrical Model for square microchannels.

SQUARE MICROCHANNELS TOTAL FLOW RATES COMPARISON		
Hydraulic Diameter (μm)	ANSYS (%)	Electrical Model (%)
47.1	30.74	30.16
74.0	30.74	30.16
74.1	30.74	30.16
101.0	30.74	30.16
100.4	30.74	30.16

8.2 DISCUSSION

The results obtained from the steady laminar flow analysis for circular microchannels in Section 8.1.1.1 and rectangular microchannels in Section 8.1.2 show the parabolic velocity profile, as is expected. From Table 8-2, Table 8-5 and Table 8-6 it can be seen that the flow rates for the innermost layer is the fastest while the layers close to the walls are the slowest. This result is in line with the traditional theory of fluid flow in channels.

For circular microchannels, the derived total flow rates differ by an average of 3.2% from experimental data as shown in Table 8-1. The flow rates of the layered steady flow using the electric network model differ by up to 6.6% when compared with values from Ansys (Table 8-2). When compared with Hagen-Poiseuille equation, the electrical model shows a difference of less than 5.22% (Table 8-2). The transient time for the unsteady flow obtained from electrical analysis compares favourably with classical theory, with differences of not more than 11.1% (Table 8-3).

In the analysis of the rectangular microchannel, the total flow rate obtained using the Hagen-Poiseuille, with the concept of hydraulic diameter, gives significant percentage difference of 19.3 % when compared with experimental data. The value obtained from the electrical model differs by 2.2 % (Table 8-4). The values obtained from the ANSYS 2D analysis to determine the layered flow rate are also significantly different from the electrical model implemented in Simulink by up to 46.7 % (Table 8-6). The ANSYS analysis uses the assumption of parallel plates, ignoring the effect of the two side walls.

For starting flow of circular microchannels (Section 8.1.1.2) and square microchannels (Section 8.1.3), the results from the electrical model differ from those obtained theoretically by about 11 %.

For the laminar flow of fluid in diffusers and nozzles (Section 8.1.4), it is not surprising that the values obtained from the electrical model are exactly the same as the analytical model since the former is derived from the latter. However, great differences occur as the pressure difference increases which is due to the fact that the flow is no longer laminar. Turbulence, flow separation and backflow commonly occur in diffusers. This laminar

analysis is applicable only for the limited range of the pressure difference of up to about 100 mbar and also for diffusers of small aperture angles of less than 10°.

In Section 8.1.5, the cpu times of the electrical model is shorter than that of the finite element method by an average of 57 % for the circular microchannels and 78 % for the square microchannels. Comparison of accuracy of calculated values of the total flow rates is made with experimental data. For the circular microchannels, the Ansys analysis gave a better and more consistent accuracy than the values obtained via the electrical model (Table 8-10). The accuracy is better for the circular microchannels than for the square ones. For the square microchannels, both the finite element and electrical analyses did not give good accuracy, since both uses 2D analysis which does not take into account the flow in the sharp, square corners of the channels (Table 8-12). A 3D analysis would be able to give better accuracy.

CHAPTER 9: CONCLUSION

Chapter 1 of this thesis discussed the problem statement and the proposed solution of this research. The main objective was to determine the volumetric flow rate of several microfluidic device components. Calculations were performed for circular, square and rectangular microchannels, microdiffusers and micronozzles. Electrical modeling, a semi-analytical technique, was proposed. This was accomplished by dividing the flow field into layers, then determining the equivalent resistances of the layers from the solution of the Navier-Stokes equation, and finally using simple electrical networks to obtain the flow rates.

The derivation of the layered flow model was demonstrated in Chapter 5. For circular microchannel, the Navier-Stokes equation in cylindrical coordinates was used and an analytical solution for the equivalent resistance was easily obtained. For the rectangular microchannel, the Navier-Stokes equation in cartesian coordinates was used. In this case, a numerical technique is used to determine the equivalent resistance for the layered flow. For the microdiffuser and micronozzle, the region was divided into parts and each solved separately using the solution from the circular channels.

The electrical network modeling was shown in Chapter 6. The layered flow for the microchannels, micronozzles and microdiffusers were represented by simple electrical networks composed of inductors and resistors. The calculations were then carried out in Matlab and Simulink. The simulation results obtained were shown in Chapter 7. Both unsteady starting flow and steady laminar flow analyses were carried out for the circular microchannels. For the square channels, unsteady flow simulation was demonstrated while for diffusers, steady flow simulation.

Validation of the values of the calculated total flow rates was made with experimental data obtained from the literature. For the layered flows, comparison was made using the finite element software Ansys and in the case of unsteady starting flow with values obtained from

classical theory. A comparison of the cpu time used in the calculations of these flow rates was made. These were shown in Chapter 8.

The results obtained in Section 8.1.5 demonstrated that although the accuracy for the electrical model is not as good as or consistent as that for the finite element analysis in Ansys, the former provide a quick first approximation of the flow rates and velocity profiles of the microchannels. The electrical network concept of parallel branches of resistances and inductances does provide a suitable model for the flow rate of a liquid in stead, laminar flow in microchannels.

For the laminar fluid flow in a diffuser in Section 8.1.4, it is divided up into two regions, at the inlet and the diverging sections. The fluid is divided up into three layers with the central two layers parallel to the axis. An electrical network model was derived and implemented in Matlab/Simulink. These results were compared with experimental data from the literature. At low pressure difference, the percentage errors in flow rates are small (less than 10%) but this increases at higher pressure. The electrical network consisting of series and parallel resistances provides a suitable model for the flow rate of a liquid in steady laminar flow in a conical diffuser at low pressure differentials and small aperture angles.

The advantages of the electrical layered flow model developed in this thesis are its simplicity, the ease with which one can apply it and the fast results that it produces. This eliminates the need for repeated meshing and iteration of solution. The results obtained are fairly accurate as compared to experimental data and with FEM software, as long as the flow in the device is laminar and steady with no turbulence or flow separation, although unsteady starting flow can also be modelled successfully using this technique. The results become less accurate at higher pressures where the flow can become turbulent. In the case of microdiffusers, where the channels have expanding cross-sectional area, the model may need to be modified to include second degree terms.

This technique is useful for Microfluidic MEMS devices, which have numerous branches of channels that can be in the thousands. It is suitable at an initial design stage, where

speed of calculation is more important than extreme accuracy. The microchannels themselves are simple structures and using a detailed analysis would be wasting resources, unless there are certain features such as constrictions, additions of grooves in certain parts or other features that are necessary to induce turbulence for mixing, for example. In such circumstances than a detailed analysis using finite element or other numerical technique need to be employed, but only for that small portion of the microchannel.

For future work, the electrical modelling technique may be applied to the modelling of fluid flow in the transition region in which the fluid flow changes from laminar to turbulent and also in the totally turbulent region. The layered flow model may be used to model the flow of several liquids with different densities and also applied to the visualisation of the mixing of these liquids.

PUBLICATIONS ARISING FROM THIS THESIS

[1] Aumeerally, M. and R. Sitte. 2001. "Design and Modeling of Microactuators in MEMS Virtual Reality Prototyping CAD tool." *Electronics and Structures for MEMS II*, *SPIE Proceedings*, vol 4591, pp. 163-171

[2] Aumeerally, M. and R. Sitte. 2003. "Modelling of a Layered Flow in a Circular Microchannel." *Proceedings of The 2003 European Simulation and Modelling Conference (ESMC),* Naples, Italy,pp 458-462.

[3] Aumeerally, M. and R. Sitte. Jan 2004. "Simulation and Modelling of Layered Fluid Flow in a Rectangular Microchannel." *Proceedings of The 2004 Middle East Symposium on Simulation and Modelling (MESM)*, Sharjah, U.A.E., pp 81 – 85.

[4] Aumeerally, M. and R. Sitte. Oct 2004. "Modelling of Layered Microfluidic Flow in Conical Nozzle and Diffusers." *Proceedings of The 2004 European Simulation and Modelling Conference (ESMC)*, Paris, France, pp 306 – 310.

[5] Aumeerally, M. and R. Sitte. 2006. "Layered Fluid Model and Flow Simulation for Microchannels using Electrical Networks." *Simulation Modelling Practice and Theory*, vol. 14, pp. 82-94, Elsevier.

BIBLIOGRAPHY

Anderson, J.D. (author); J.F. Wendt (editor). 1996. "Computational Fluid Dynamics: An Introduction." 2nd Edition. Springer. Berlin, New York.

Andersson, H.; W. van der Wijngaart; P. Nilsson; P. Enoksson; and G. Stemme. 2001. "A Valveless Diffuser Micropump for Microfluidic Analytical Systems." *Sensors and Actuators B: Chemical, v*ol. 72, pp 259-265.

Arik, M.; S.M. Zurn; A. Bar-Cohen; Y. Nam; D. Markus; and D. Polla. 1999. "Development of CAD Model for MEMS Micropumps." *Technical Proceedings 1999 International Conference on Modeling and Simulation of Microsystems*, USA.

Bao, M.; and W. Wang. 1996. "Future of Microelectromechanical systems." *Sensors and Actuators A*, vol. 56, pp. 135-141, Elsevier.

Bardell, R.L.; and F.K. Forster. 1998. "Impedances for Design of Microfluidic Systems." *Proceedings of the Micro-TAS '98 Workshop* (Banff, Oct 13-16), Canada.

Batchelor, G.K. 1967. "An Introduction To Fluid Dynamics." Cambridge University Press, UK.

Brask, A.; G Goranović; and H. Bruus. 2003. "Theoretical Analysis of the Low-voltage Cascade Electro-osmotic Pump." *Sensors and Actuators B*, vol. 92, pp 127-132, Elsevier.

Brask, A.; G. Goranović; M.J. Jensen; and H. Bruus. 2005. "A Novel Electro-osmotic Pump Design for Nonconducting Liquids: Theoretical Analysis of Flow Rate – Pressure Characterisitcs and Stability." *Journal of Micromechanics and Microengineering,* vol.15, pp 883-891, Institute of Physics Publishing.

Bendib, S.; and O. Français. 2001. Analytical Study of Microchannel and Passive Microvalve "Application to Micropump Simulator", *Design, Characterization and Packaging for MEMS and Microelectronics II, Proceedings of SPIE,* pp 17-19, Australia.

Boylestad, R.L. 2000. "Introductory Circuit Analysis, 9th Edition." Prentice Hall, USA.

Bryzek, J. 1996. "Impact of MEMS technology on society." *Sensors and Actuators A*, vol. 56, pp. 1-9, Elsevier.

Büstgens, B.; W. Bacher; W. Menz; and W.K. Schomburg. 1994. "Micropump Manufactured by Thermoplastic Molding." *IEEE Proceedings of MEMS Conference*, pp. 18-21.

Chatterjee, A.N.; and N.R. Aluru. 2005. "Combined Circuit/Device Modeling and Simulation of Integrated Microfluidic Systems." *Journal of Microelectro-mechanical Systems*, vol.14, no.1, IEEE

Chakrabarty, K.; and F. Su. 2005. "Design Automation Challenges for Microfluidics-Based Biochips." *Proceedings of DTIP of MEMS and MOEMS*, 1-3 June 2005, Montreux, Switzerland

CoventorWare™ 2004. 2004. Coventor Inc., Cambridge, MA, http://www.coventor.com/

Day, R.F.; and H.A. Stone. 1999. "Lubrication Analysis and Boundary Integral Simulations of a Viscous Micropump." *Technical Proceedings 1999 International Conference on Modeling and Simulation of Microsystems*, USA.

DeCourtye, D.; M. Sen; and M. Gad-el-Hak. 1988. "Analysis of Viscous Micropumps and Microturbines." *International Journal of Computational Fluid Dynamics*, vol. 10, pp.13-25.

Evans, J.; D. Liepmann; and A.P. Pisano. 1997. "Planar Laminar Mixer." *Proceedings of IEEE Workshop on MEMS*, pp. 96-101, Japan

Fatikow, S.; and U. Rembold. 1997. “Microsystem Technology and Microrobotics.” Springer-Verlag, Germany.

Fay, J.A. “Introduction to Fluid Mechanics.” MIT Press, Cambridge, Massachusetts, 1994

Fedder, G.K. 1999. “Structured Design of Integrated MEMS.” *IEEE Proceedings of MEMS Conference,* pp. 1-8.

Fluitman, J. 1996. “Microsystems Technology: Objectives.” *Sensors and Actuators A*, vol. 56, pp. 151-165, Elsevier.

Français, O.; and I. Dufour. 1998. “Dynamic Simulation of an Electrostatic Micropump with Pull-in and Hysteresis Phenomena.” *Sensors and Actuators A,* vol. 70, pp. 56-60, Elsevier.

Fuhr, G.; R. Hagedorn; T. Muller; W. Benecke; and B. Wagner. 1992. “Microfabricated Electrohydrodynamic Pumps for Liquids of Higher Conductivity.” *Journal of Microelectromechanical Systems*, vol. 1, no. 3, pp. 141-146, Sept 1992

Fujita, H. 1997. “A Decade of MEMS and its Future.” *Proceedings of IEEE Workshop on MEMS*, pp. 1-8, Japan.

Fukuda, T.; and W. Menz. 1998. “Micro Mechanical Systems Principles and Technology.” pp. 6, Elsevier.

Funk, J.M.; J.G. Korvink; M. Bachtold; and H. Baltes. 1997. “SOLIDIS: A Tool for Microactuator Simulation in 3-D.” *Journal of Microelectromechanical Systems,* vol. 6, no. 1, March.

Gad-el-Hak, M. (editor). 2002. “The MEMS Handbook.” CRC Press, USA.

Gamboa, A.R.; C.J. Morris; and F.K. Forster. 2005. “Improvements in Fixed-Valve Micropump Performance Through Shape Optimization of Valves.” *Journal of Fluids Engineering.* vol.127, pp 339-346, Transactions of ASME.

Gerlach, T. 1998. “Microdiffusers as a Dynamic Passive Valves for Micropump Applications.” *Sensors and Actuators A,* vol. 69, 181-191.

Gerlach, T.; and H. Wurmus. 1995. “Working Principle and Performance of The Dynamic Micropump.” *Proceedings of IEEE MEMS Conference,* pp221-226, Netherlands.

Giridharan, M.G.; P. Stout; H.Q. Yang; M. Athavale; P. Dionne; and A. Przekwas. 2001. “Multi-Disciplinary CAD System for MEMS.” *Journal of Modeling and Simulation of Microsystems*, vol. 2, no. 1, pp43-50

Gong, O.; Z. Zhou; Y. Yang; and X. Wang. 2000. “Design, Optimization and Simulation on Microelectromagnetic Pump.” *Sensors and Actuators A*, vol. 83, pp. 200-207, Elsevier.

Guenat, O.T.; D. Ghiglione; W. E. Morf; and N. F. de Rooij. 2001. “Partial electroosmotic pumping in complex capillary systems; Part 2: Fabrication and application of a micro total analysis system (μTAS suited for continuous volumetric nanotitrations.” *Sensors and Actuators B: Chemical,* vol. 72, Issue 3,, pp. 273-282, 10 February 2001

Heschel, M.; M. Müllenborn; and S. Bouwstra. 1997. “Fabrication and Characterization of Truly 3D Diffuser/Nozzle Microstructures in Silicon.” *Journal of Microelectromechanical System, vol. 6, no. 1,* March 1997

Hung, E.S.; and S.D. Senturia. 1999. “Generating Efficient Dynamical Models for Microelectromechanical Systems from a Few Finite-Element Simulation Runs.” *IEEE Journal of Microelectromechanical Systems*, vol. 8, no. 3, Sept 1999.

Hung, E.S.; Y.J. Yang; and S.D. Senturia. 1997. “Low-order models for Fast Dynamical Simulation of MEMS Microstructure.” *Transducers '97, Proceedings of International*

Conference on Solid-State Sensors and Actuators, pp 1101-1104, Chicago.

Ikuta, K.; T. Hasegawa; T. Adachi; and S. Maruo. 2000. "Fluid Drive Chips Containing Multiple Pumps and Switching Valves for Biochemical IC Family." *Proceedings of IEEE Conference on MEMS*, pp. 739-744, Japan.

Jakovljevic, M.; P.A. Fotiu; Z. Mrcarica; and H. Detter. 2000. "A System-level Simulation of Complex Multi-domain Microsystems By Using Analogue Hardware Description Languages." *Sensors and Actuators A*, vol. 82, pp. 30-39, Elsevier.

Jang, J.; and S.S. Lee. 2000. "Theoretical and experimental study of MHD (magnetohydrodynamic) micropump." *Sensors and Actuators A*, vol. 80, pp. 84-89, Elsevier.

Judy, J.; D. Maynes; and B.W. Webb. 2002. "Characterization of frictional pressure drop for liquid flows through microchannels." *International Journal of Heat and Mass Transfer*, vol. 45, pp. 3477-3489, Pergamon.

Kellermann, M.; A. Baer; V. von Hintzenstern; W. Schoor; and C. Steinhauer. 2003. "MEMS Animated Graphics Design Report." Griffith University Report, Griffith University, Gold Coast, Australia.

Kim, J.H.; K.H. Na; C.J. Kang; and Y.S. Kim. 2005. "A Disposable Thermopneumatic-actuated Micropump Stacked with PDMS Layers and ITO-coated Glass." *Sensors and Actuators A*, vol 120, pp 365-369, Elsevier.

Koch, M.; C.G.J. Schabmueller; A.G.R. Evans; and A. Brunnschweiler. 1999. **"**Micromachined chemical reaction system." *Sensors and Actuators A: Physical,* Vol. 74, Issues 1-3, pp 207-210, Elsevier.

Korsmeyer, T.; J. Zeng; and K. Greiner. 2004. "Design Tools for BioMEMS." *Proceedings of the 41st annual Conference on Design Automatio,* pp 622-627, USA.

Leal, L.G. 1992. "Laminar Flow and Convective Transport Processes: Scaling Principles and Asymptotic Analysis." Butterworth-Heinemann, USA.

Lemoff, A.V.; and A.P. Lee. 2000. "An AC Magnetohydrodynamic Micropump." *Sensors and Actuators B*, vol. 63, pp. 178-185, Elsevier.

Linnemann, R.; P. Woias; C.D. Senfft; and D.A. Ditterich. 1998. "A Self-priming and Bubble-tolerant Piezoelectric Silicon Micropump for Liquids and Gases." *IEEE 11th International Workshop on Microelectromechanical Systems (MEMS 98),* pp.532-537, Germany

Makino, E.; T. Mitsuya; and T. Shibata. 2001. "Fabrication of TiNi Shape Memory Micropump." *Sensors and Actuators A*, vol. 88, pp. 256-262.

Mala, G.M.; and D. Li. 1999. "Flow characteristics of water in microtubes." *International Journal of Heat and Fluid Flow,* vol.20, pp. 142-148, Elsevier.

Mathews, J.H.; and K.D. Fink. 1992. "Numerical Methods Using Matlab, 3rd Edition." Prentice Hall, USA.

McCorquodale, M.S.; F.H. Gebara; K.L. Kraver; E.D. Marsman; R.M. Senger; and R.B. Brown. 2003. "A Top-Down Microsystems Design Methodology and Associated Challenges." *Proceedings of the Design, Automation and Test in Europe Conference and Exhibition (DATE '03)*, IEEE

Mehner, J.; S. Kurth; D. Billep; C. Kaufmann; K. Kehr; and W. Dötzel. 1998. "Simulation of Gas Damping in Microstructures with Nontrivial Geometries." *Proceedings of IEEE Conference on MEMS*, pp. 172-177, Germany.

Morris, C.J; and F.K. Forster. 2000. "The Correct Treatment of Harmonic Pressure-Flow Behavior in Microchannels." *Micro-Electro-Mechanical Systems* (MEMS), vol 2, pp. 473-

479, ASME

Mukherjee, T.; G.K. Fedder; D. Ramaswamy; and J. White. 1999. “Emerging Simulation Approaches for Micromachined Devices.” *Technical Proceedings 1999 International Conference on Modeling and Simulation of Microsystems*, USA.

Munson, B.R.; D.F. Young; and T.H. Okiishi. 1998. “Fundamentals of Fluid Mechanics” 3rd edition, John Wiley & Sons, USA.

Nathan, A.; and H. Baltes. 1999. “Microtransducer CAD: Physical and Computational Aspects.” Springer-Verlag Wien, New York.

Nedelcu, O.T.; and V. Moagar-Poladian. 1999. “Modeling of the Piezoelectric Micropump for Improving the Working Parameter.” *Technical Proceedings 1999 International Conference on Modeling and Simulation of Microsystems*, US.

Nguyen, N.T.; and R.M. White. 1999. “Design and Optimization of an Ultrasonic Flexural Plate Wave Micropump using Numerical Simulation.” *Sensors and Actuators A,* vol. 77, pp. 229-236, Elsevier.

Nguyen, N.T.; S. Schubert; S. Richter; and W. Dötzel. 1998. “Hybrid-assembled Micro Dosing System Using Silicon-based Micropump/valve and Mass Flow Sensor.” *Sensors and Actuators A: Physical,* vol. 69, pp 85-91.

Olsson, A. 1998. “Valveless Diffuser Micropumps.” Phd Dissertation, Royal Institute of Technology, Sweden.

Olsson, A.; G. Stemme; and E. Stemme. 1996. “Diffuser-element Design Investigation for Valveless Pumps.” *Sensors and Actuators A,* vol.57, 137-143.

Olsson, A.; G. Stemme; and E. Stemme. 1999. “ The Valveless Diffuser Pump – A Numerical Design Study Using MATLAB.” *Technical Proceedings 1999 International*

Conference on Modeling and Simulation of Microsystems, USA.

Ong, C-M. 1998. "Dynamic Simulation of Electric Machinery using MATLAB^{R}/SIMULINK." Prentice-Hall, New Jersey.

Panton, R.L. 1984. "Incompressible Flow." John Wiley & Sons, USA.

Park, H.; J.J. Pak; S.Y. Son; G. Lim; and I. Song. 2003. "Fabrication of a Microchannel Integrated with Inner Sensors and the Analysis of its Laminar Flow Characteristics." *Sensors and Actuators A,* vol 103, 317-329.

Romanowicz, B.F. 1998. "Methodology For The Modeling and Simulation of Microsystem". Kluwer Academic Publishers, USA.

Richter, M.; R. Linnemann; and P. Woias. 1998. "Robust Design of Gas and Liquid Micropumps." *Sensors and Actuators A,* vol. 68, pp480-486, Elsevier.

Schetz, J.A.; and A.E. Fuhs, editors. 1999. "Fundamentals of Fluid Mechanics." John Wiley & sons, NY.

Schetz, J.A. 1993. "Boundary Layer Analysis." Prentice-Hall, Inc. New Jersey.

Schneider, P.; E. Huck; S. Reitz; S. Parodat; A. Schneider; and P. Schwarz. 2000. "A Modular Approach for Simulation-based Optimization of MEMS." *Design, Modeling and Simulation in Microelectronics,* SPIE Proceedings Series, pp. 71-82, vol. 4228.

Senturia, S.D. 2001. "Microsystem Design." Kluwer Academic Publishers. USA.

Senturia, S.D. 1994. "Feynman Revisited." *Proceedings of IEEE Workshop on MEMS*, pp. 309– 312, Japan.

Shah, R.K.; and A.L. London. 1978. "Laminar Flow Forced Convection in Ducts." In J.P.

Hartnett and T.F.Irvine,Jr,.(eds.), *Advances in Heat Transfer, Supplement 1,* Academic Press. New York.

Shames, I.J. 1998. "Mechanics of Fluids, 2nd Edition." McGraw-Hill Publishing Co. USA.

Shoji, S.; M. Esashi; B. van der Schoot; and N. de Rooij. 1992. "A study of a high-pressure micropump for integrated chemical analysing systems." *Sensors and Actuators A: Physical,* vol. 32, Issues 1-3, pp 335-339, April 1992

Singhal, V.; S.V. Garimella; and J.Y. Murthy. 2004. "Low Reynolds Number Flow Through Nozzle-Diffuser Elements in Valveless Micropumps." *Sensors and Actuators B,* vol. 9, 152-161.

Spurk, J.H. 1997. "Fluid Mechanics." Springer-Verlag, Germany.

Stemme, E.; and G. Stemme. 1993. "A Valveless diffuser/nozzle-based Fluid Pump." *Sensors and Actuators A,* vol. 39, 159-167.

Tang, W.C. 1997. "Overview of Microelectromechanical Systems and Design Processes." *ACM Design Automation Conference*, USA

Teegarden, D.; G. Lorenz; and R. Neul. 1998. "How to Model and Simulate Microgroscope Systems." *IEEE Spectrum*, vol. 35, no. 7, July 1998

Thielick, E.; and E. Obermeier. 2000. "Microactuators and their Technologie." *Mechatronics*, vol. 10, pp. 431-455.

Trimmer, W. 1997. "Grand in Purpose Insignificant in size." *Proceedings of IEEE Workshop on MEMS*, pp. 9– 13, Japan.

Turowski, M.; Z. Chen; and A. Prezekwas. 1999. "High-Fidelity and Behavioral Simulation of Air Damping in MEMS." *Technical Proceedings 1999 International Conference on*

Modeling and Simulation of Microsystems, USA.

Ulrich, J.; and R. Zengerle. 1996. "Static and Dynamic Flow Simulation of a KOH-etched Microvalve Using the Finite-Element Method." *Sensors and Actuators A*, vol. 53, pp. 379-385, Elsevier.

Van de Pol, F.C.M.; H.T.G. Van Lintel.; M. Elwenspoek; and J.H.J. Fluitman. 1990. "A Thermopneumatic Micropump Based on Micro-engineering Techniques." *Sensors and Actuators A,* vol 21pp198-202.

Van der Wijngaart, W.; H. Andersson; P. Enoksson; K. Noren; and G. Stemme. 2000. "The First Self-priming and Bi-directional Valveless Diffuser Micropump for both Liquid and Gas." *Proceedings of IEEE Workshop on MEMS*, pp. 674-679, Japan.

Van Lintel, H.T.G.; F.C.M. Van de Pol; and S. Bouwstra. 1988. "A Piezoelectric Micropump Based on Micromachining of Silicon." *Sensors and Actuators A,* vol. 15, pp 153-167.

Varadan,Vijay; X. Jiang; and Vasundara Varadan. 2001. "Microstereolithography and other Fabrication Techniques for 3D MEMS." Wiley.

Voigt, P.; G. Schrag; and G. Wachutka. 1998. "Microfluidic System Modelling using VHDL-AMS and Circuit Simulation". *Microelectronics Journal 29,* 791-797.

Wang, Y.; Q. Lin; and T. Mukherjee. 2004. "Applications of Behavioral Modeling and Simulation on Lab-on-a-chip: micro-mixer and separation system." *Proceedings of the 2004 IEEE/ACM International Workshop on Behavioral Modeling and Simulation (BMAS '04),* pp.8-13, Oct 21-22, San Jose, California, USA

White, F.M. 1994. "Fluid Mechanics." Mc-Graw Hill, USA.

White, F.M. 1991. "Viscous Fluid Flow." McGraw-Hill Inc., USA.

White, J. 2004. “CAD Challenges in BioMEMS Design.” *Proceedings of the 41st annual Conference on Design Automation*. pp 629-632. USA.

Woias, P. (author); C.H. Mastrangelo; and H. Becker (editors). 2001. “Summarising the First Two Decades, Microfluidics and BioMEMS.” *Proceeding of SPIE,* vol. 4560, pp. 39-52.

Woods, R.L.; and K.L. Lawrence. 1997. “Modeling and Simulation of Dynamic Systems.” Prentice-Hall Inc. USA.

Zeng, S.; C.H. Chen; J.C. Mikkelsen Jr.; and J.G. Santiago. 2001. “Fabrication and Characterization of Electroosmotic Micropumps.” *Sensors and Actuators B*, vol. 79, pp. 107-114, Elsevier.

Zengerle, R.; and M. Richter. 1994. “Simulation of Microfluid Systems.” *Journal of Micromechanical Microengineering*, vol. 4, 192-204.

Zengerle, R.; M. Leitner; S. Kluge; and A. Richter. 1995. “Carbon Dioxide Priming of Micro Liquid Systems.” *Proceedings of IEEE Conference on MEMS,* pp. 340-343, Netherlands.

Zengerle, Z.; S. Kluge; M. Richter; and A. Richter. 1995. “A Bidirectional Silicon Micropump.” *Proceedings of IEEE Conference on MEMS*, pp. 19-24, Netherlands.

Zhong, J.; M. Yi; and H.H. Bau. 2002. “MagnetoHydrodynamic (MHD) Pump Fabricated With Ceramic Tapes.” *Sensors and Actuators A*, vol. 96, pp. 59-66, Elsevier.